

# CHALMERS



## Testing of minerals and industrial by-products as oxygen carriers for chemical-looping combustion in a 300W test reactor

*Master Thesis*

PATRICK MOLDENHAUER

Department of Energy and Environment  
*Division of Energy Technology*  
CHALMERS UNIVERSITY OF TECHNOLOGY  
Göteborg, Sweden 2009  
Report nr: T2009-325





**CHALMERS**

Chalmers University of Technology  
Department of Energy and Environment  
Division of Energy Technology

**Testing of minerals and industrial by-products  
as oxygen carriers for chemical-looping  
combustion in a 300 W test reactor**

Master Thesis

*Author:* Patrick Moldenhauer  
*pmoldenhauer@gmail.com*

*Supervisors:* Dr. Magnus Rydén  
Prof. Dr. Anders Lyngfelt  
Prof. Dr. Bernd Epple

Testing of minerals and industrial by-products as oxygen carriers for chemical-looping combustion in a 300W test reactor

Master Thesis

© PATRICK MOLDENHAUER, 2009

Technical report nr: T2009-325  
Department of Energy and Environment  
Division of Energy Conversion Technology  
Chalmers University of Technology  
SE-412 96 Göteborg  
Sweden  
Telephone: + 46 (0)31-772 1000

Chalmers Reproservice  
Göteborg, Sweden 2009  
Report nr: T2009-325

## **Abstract**

Carbon dioxide emissions have been increasing significantly over the course of the last two hundred years. A higher CO<sub>2</sub> concentration in the atmosphere enhances the greenhouse effect, which is believed to lead to a severe global climate change. Hence, emissions of CO<sub>2</sub> into the atmosphere have to be reduced. The biggest emitter of greenhouse gases is the electricity and heat industry. A reduction of emissions in this sector would have a great impact in terms of reduction of emissions.

Chemical-looping combustion is a rather new technology, where the separation of the CO<sub>2</sub> happens as part of the process and does not implicate an efficiency penalty. An oxygen carrier is circulated between an air and a fuel reactor. In doing so, it transports the necessary combustion oxygen from the air to the fuel. Air and fuel are never mixed and after condensing the water, the stream of flue gases consists of nearly pure CO<sub>2</sub>. The common approach was to synthesize oxygen carrier particles, which made them expensive and only available in small quantities. The employment of alternative sources for oxygen carrier particles would further chemical-looping combustion a great deal.

In this work chemical-looping combustion experiments were performed in a 300 W test reactor with ilmenite (a mineral oxygen carrier) and iron oxide scales (an industrial by-product). Both oxygen carriers were operated for tens of hours, which allowed for a better understanding of the lifetime behavior and other basic characteristics. The gathered data indicates that both oxygen carriers could be an alternative to synthesized particles.

# Contents

<b>List of Figures</b>	<b>iii</b>
<b>List of Tables</b>	<b>iv</b>
<b>Formula Symbols</b>	<b>v</b>
<b>1. Scope</b>	<b>1</b>
<b>2. Introduction</b>	<b>2</b>
2.1. Environmental background . . . . .	2
2.1.1. The uprising of the carbon hunger . . . . .	2
2.1.2. Struggling for the truth . . . . .	2
2.1.3. The meaning of “global change” . . . . .	3
2.2. Technical background . . . . .	4
2.2.1. Carbon capture and storage . . . . .	4
2.2.2. The principle of chemical-looping . . . . .	5
2.2.3. The 300W test reactor . . . . .	8
2.2.4. Downcomer improvements . . . . .	9
<b>3. Experiments</b>	<b>11</b>
3.1. Leakage investigation . . . . .	11
3.1.1. Background . . . . .	11
3.1.2. Experimental procedure . . . . .	12
3.1.3. Analysis . . . . .	13
3.1.4. Results . . . . .	16
3.1.5. Conclusions . . . . .	21
3.2. Ilmenite . . . . .	22
3.2.1. Essentials . . . . .	22
3.2.2. Experimental procedure . . . . .	23
3.2.3. Analysis . . . . .	25
3.2.4. Results . . . . .	29
3.2.5. Conclusions . . . . .	38
3.3. Iron oxide scales . . . . .	39
3.3.1. Background . . . . .	39
3.3.2. Experimental procedure . . . . .	39
3.3.3. Analysis . . . . .	40
3.3.4. Results . . . . .	41

---

CONTENTS

---

3.3.5. Conclusions . . . . .	48
<b>4. Conclusions</b>	<b>49</b>
<b>Bibliography</b>	<b>51</b>
<b>Appendix</b>	<b>I</b>
<b>A. Reactor cross-section with gas inlets and measuring points</b>	<b>I</b>
<b>B. Measured particle levels and properties during and after the experiment sets</b>	<b>III</b>
<b>C. Chemical equilibria of syngas with different amounts of added steam</b>	<b>VII</b>
<b>D. XRD Analysis</b>	<b>X</b>

## List of Figures

2.1. Schematic illustration of the chemical-looping combustion process . . . . .	6
2.2. Schematic three-dimensional illustration of the improved 300 W test reactor .	9
2.3. Schematic and latest downcomer design of the 300 W test reactor . . . . .	10
3.1. Reactor schematic with gas flows and types of gas used for the leakage exper- iments . . . . .	14
3.2. Leakage and dilution for each test of the leakage series . . . . .	19
3.3. Gas flows from the particle locks into air and fuel reactor for each test of the leakage series . . . . .	20
3.4. Measurements during the initial operational phase with ilmenite particles . . .	29
3.5. SEM images of fresh and used ilmenite particles . . . . .	32
3.6. Combustion efficiency for ilmenite experiments at base parameters over 85 h of operation . . . . .	33
3.7. Combustion efficiency for ilmenite experiments with varied fuel flow . . . . .	34
3.8. Combustion efficiency for ilmenite experiments with varied temperature . . . .	35
3.9. Combustion efficiency for ilmenite experiments with varied air flow (only with 135 g of particles) . . . . .	36
3.10. Measurements during the initial operational phase with IOS particles . . . . .	41
3.11. SEM images of fresh, used and agglomerated IOS particles . . . . .	45
3.12. Combustion efficiency for IOS experiments with varied fuel flow . . . . .	46
3.13. Combustion efficiency for IOS experiments with varied temperature . . . . .	47

# List of Tables

2.1. Total amount of bed mass of different oxygen carrier materials for real size CLC reactors . . . . .	7
3.1. Base parameters for the leakage test series . . . . .	13
3.2. Settings and parameters for each test of the leakage test series . . . . .	13
3.3. Description of the unknown internal gas flows . . . . .	15
3.4. Approximations for leakage and dilution . . . . .	21
3.5. Fluidization gases used at the different locations in the reactor . . . . .	23
3.6. Base parameters for the test series with fresh ilmenite particles . . . . .	23
3.7. Settings and parameters for each test of the test series with fresh ilmenite particles . . . . .	24
3.8. Base parameters for the test series with used ilmenite particles . . . . .	24
3.9. Settings and parameters for each test of the test series with used ilmenite particles	25
3.10. Oxygen transfer capacities for different oxygen carrier materials . . . . .	28
3.11. Ilmenite particle properties of fresh material and after 31 h of operation . . . .	30
3.12. Ilmenite particle properties of used particles after 31 h and 85 h of operation .	31
3.13. XRD analysis of ilmenite particles . . . . .	32
3.14. Base parameters for experiments with IOS particles . . . . .	40
3.15. Settings and parameters for each test of the test series with IOS particles . . .	40
3.16. Reduction reference numbers $\omega$ and $X$ for the IOS experiments . . . . .	42
3.17. IOS particle properties of fresh material and after 17 h of operation . . . . .	43
3.18. Used IOS particle properties after 17 h and 37 h of operation . . . . .	44
3.19. XRD analysis of IOS particles . . . . .	44

# Formula Symbols

## Latin symbols

<b>Formula symbol</b>	<b>Unit</b>	<b>Definition</b>
$m$	[kg]	mass
$x$	[vol%]	dry-gas concentration
$y$	[vol%]	wet-gas concentration
$D$	[-]	dilution from air reactor only
$D_{\text{PL}}$	[-]	dilution from particle locks only
$D_{\text{tot}}$	[-]	total dilution (from air reactor and particle locks)
$H_{i1}$	[kJ/kg]	lower heating value I
$H_{i2}$	[kJ/m <sup>3</sup> ]	lower heating value II (normalized to 25 °C)
$H/C$	[-]	hydrogen to carbon ratio
$K_{\text{wgs}}$	[-]	equilibrium constant for the water-gas shift reaction
$L$	[-]	leakage
$R$	[J/mol K]	universal gas constant
$R_o$	[wt%]	oxygen transfer capacity
$T$	[°C] or [K]	temperature
$U$	[L <sub>n</sub> /min]	volume flow (normalized to 25 °C)
$\dot{V}$	[m <sup>3</sup> /s]	volume flow
$X$	[%]	degree of oxidization

## Greek symbols

<b>Formula symbol</b>	<b>Unit</b>	<b>Definition</b>
$\gamma_{\text{CO}_2}$	[%]	CO <sub>2</sub> gas yield
$\gamma_{\text{eff}}$	[%]	combustion efficiency
$\mu$	varies	mean value
$\sigma$	[-]	standard deviation
$\omega$	[%]	degree of mass-based conversion

## Indices

<b>Index</b>	<b>Definition</b>
$( )_{\text{fm}}$	fuel mix
$( )_{\text{in}}$	at the inlet
$( )_{\text{out}}$	at the outlet
$( )_{\text{ox}}$	most oxidized state
$( )_{\text{red}}$	most reduced state
$( )_{\text{tot}}$	total
$( )_{\text{AR}}$	air reactor
$( )_{\text{D}}$	dilution
$( )_{\text{DC}}$	downcomer
$( )_{\text{DCI}}$	main downcomer fluidization inlet
$( )_{\text{DCII}}$	additional downcomer fluidization inlet
$( )_{\text{FR}}$	fuel reactor
$( )_{\text{L}}$	leakage
$( )_{\text{OC}}$	oxygen carrier
$( )_{\text{PL}}$	particle lock(s)
$( )_{\text{SL}}$	slot
$( )^*$	initial value

## Abbreviations

<b>Abbreviation</b>	<b>Definition</b>
AR	air reactor
ASU	air separation unit
CCS	carbon capture and storage (sometimes also: carbon capture and sequestration)
CLC	chemical-looping combustion
DC	downcomer
FR	fuel reactor
GC	gas chromatograph
HiPL	higher particle lock; alternative name: downcomer
IOS	iron oxide scales (glödskal)
IPCC	Intergovernmental Panel on Climate Change
LoPL	lower particle lock; alternative name: slot
PL	particle lock(s); alternative name: loop seal(s)
SEM	scanning electron microscope/microscopy
SL	slot
XRD	X-ray powder diffraction

### Chemical Abbreviations

<b>Molecular formula</b>	<b>Name</b>
Ar	argon
CO	carbon monoxide
CO <sub>2</sub>	carbon dioxide
CO/H <sub>2</sub>	syngas
H <sub>2</sub>	hydrogen
H <sub>2</sub> O	water, steam
Fe	iron
FeO	wüstite
Fe <sub>2</sub> O <sub>3</sub>	hematite
Fe <sub>3</sub> O <sub>4</sub>	magnetite
FeTiO <sub>3</sub>	ilmenite
Fe <sub>2</sub> TiO <sub>5</sub>	pseudobrookite
Me <sub>x</sub> O <sub>y</sub>	metal oxide
Me <sub>x</sub> O <sub>y-1</sub>	reduced metal oxide
N <sub>2</sub>	nitrogen
N <sub>2</sub> O	nitrous oxide
O <sub>2</sub>	oxygen
O <sub>3</sub>	ozone
TiO <sub>2</sub>	titanium dioxide

# 1. Scope

Chemical-looping combustion (CLC) is a promising technology for future energy production with inherent carbon dioxide (CO<sub>2</sub>) separation. High efficiency, very high CO<sub>2</sub> capture rate and the possibility to use different kinds of fuels suggests that CLC could be economically feasible and thus competitive.

One important factor in the system is the oxygen carrier. It circulates between two fluidized-bed reactors, transporting oxygen from the air reactor to the fuel reactor. Since it is chemically active and undergoes permanent mechanic stress due to abrasion, it eventually needs to be replaced. Finding a cheap and durable oxygen carrier is a key factor, which has a significant impact on the overall plant properties. A good oxygen carrier needs to have high reduction and oxidation reaction rates, be non-toxic, available and cheap. A recent approach is to use industrial by-products, natural ores or minerals instead of synthesizing the oxygen carrier particles. Such particles need less preparation and are therefore cheaper.

This work will focus on the investigation of iron-based minerals, which are tested in a 300 W test reactor. The experiments in this reactor are part of a logical investigation chain and succeed experiments in a batch reactor, in which only a few grams of oxygen carrier particles are used. The experiments in the 300 W test reactor are the first to test a new oxygen carrier in a continuous process, thereby determining whether an oxygen carrier is suitable for scale-up CLC experiments or not.

## 2. Introduction

### 2.1. Environmental background

#### 2.1.1. The uprising of the carbon hunger

Since the beginning of the industrialization (around 1800), fossil fuels have become the main source of energy. Unlike wood, which had been the main fuel until then, fossil fuels were still widely available and cheap and thus granted a fast industrial growth to a few countries. More industrial power meant an increasing need for resources, which could be gotten by trade or, as often was the case, by exploiting colonies [1].

Fossil fuels mainly consist of hydrocarbons which have been taken out of the natural carbon cycle over the last hundreds of million years. With the beginning of the so called “industrial revolution” the fossil fuels were started to be used intensely and were thus added anew to the natural carbon cycle (mostly as atmospheric  $\text{CO}_2$ ). Our environment is basically flooded with a substance in one millionth of the time that it took to separate it out.

As the biggest secondary carbon dioxide sources, deforestation and land clearing are to be mentioned. During photosynthesis plants absorb  $\text{CO}_2$ . If this absorption is retarded by reducing the amount of plants on the planet, more  $\text{CO}_2$  will remain in the atmosphere. Those secondary sources are also referred to as natural  $\text{CO}_2$  sinks.

Due to this “ $\text{CO}_2$  shock” and the destruction of the natural sinks, the natural equilibrium is threatened and could lead to a severe global climate change if not stopped [2].

#### 2.1.2. Struggling for the truth

During the combustion of hydrocarbons two main substances are created. One of them is water, which is neither toxic nor hazardous in any other sense. The more harmful resulting compound, that is released in vast quantities, is the gas carbon dioxide ( $\text{CO}_2$ ). Just as water, it is not hazardous or toxic. It is even one of the few gases in the food industry that does not require any permission in order to be used. Its downside is that it contributes to the greenhouse effect and has a long residence time in the atmosphere (water vapor has actually the biggest contribution to the natural greenhouse effect, but its atmospheric concentration is rather stable due to the natural hydrological cycle).

The greenhouse effect describes the phenomenon of selective absorption: Incoming solar radiation (short wavelength) passes through the earth’s atmosphere and is absorbed by the earth’s surface, which then in turn emits infrared radiation (longer wavelength). A great part

of this heat radiation is then absorbed by the atmosphere before it can leave into space. The gases that contribute most to the natural greenhouse effect are water vapor ( $\text{H}_2\text{O}$ ), carbon dioxide ( $\text{CO}_2$ ), ozone ( $\text{O}_3$ ), nitrous oxide ( $\text{N}_2\text{O}$ ) and methane ( $\text{CH}_4$ ). The greenhouse effect is essential for the life on earth as we know it. Without the greenhouse effect the average surface temperature of the earth would be  $-18^\circ\text{C}$  instead of  $+15^\circ\text{C}$ . The existence of the greenhouse effect had been known before, but it was not until the experiments of Charles Keeling, starting in 1958, that the atmospheric greenhouse effect was proven to be linked to human actions (the theoretic possibility was pointed out by Svante Arrhenius as early as 1893). Keeling could show an annual increase of the  $\text{CO}_2$  concentration in the atmosphere. This “man-made” part of the greenhouse effect is called the anthropogenic greenhouse effect.

The probably most important institution monitoring climate changes nowadays is the Intergovernmental Panel on Climate Change (IPCC). This UN founded organization mainly gathers scientific findings about the climate change, derives effects on humanity and suggests countermeasures. Its findings are summarized in the so called “Assessment Reports”, which were published in 1990, 1995, 2001 and 2007 [2–4]. In the first of those publications the existence of a global warming was not considered as clearly evident, not to mention anthropogenic. During the years, observations and findings have become more convincing though, that humans are responsible for a global climate change. In the latest Assessment Report, it is seen as “very likely” that global warming can be linked to increasing  $\text{CO}_2$  concentrations and thus to human actions [3]. “Very likely” in terms of the IPCC means a probability of more than 90 %. Hence, the careful phrasings from the earlier reports have been replaced by conclusions that explicitly state that “business as usual” is not an option.

It needs to be said though that there is still a small scientific opposition that claims other effects than human caused ones to be responsible for the global climate change respectively the global warming.

One spin-off result of the Assessment Reports is an international agreement, the Kyoto Protocol, from 1997. All ratifying countries agree to pursue the objective of the United Nations Framework Convention on Climate Change. It basically states the “stabilization of greenhouse gas concentrations in the atmosphere at a level that would prevent dangerous anthropogenic interference with the climate system” [5].

### 2.1.3. The meaning of “global change”

A throughout explanation of all the known climate change mechanisms, secondary effects and the discussion to what degree they are anthropogenic is very complex and certainly not the aim of this work. However, in order to understand the seriousness of the current situation, the main points and dangers will be highlighted here.

To name just a few, the results of a global climate change might occur as (with different probabilities of occurrence) heat waves, heavy rainfalls, droughts, tropical cyclones, high tides, the melting of glaciers, sea and polar ice and a general rise of the sea water level. When talking about different forecast scenarios, the characteristics of each scenario are usually reduced to an increase of the average surface air temperature of the earth and the corresponding estimated

rise of the sea level (sometimes CO<sub>2</sub> concentrations are mentioned as well). Most of the above mentioned consequences occur rather locally and cause a subtle but continuous deterioration of a country's situation. A general rise of the sea water is different though, for it occurs simultaneously around the globe. In addition it calls extra attention, because most of the world's biggest cities are situated next to the oceans (about three out of four of the so called "megacities" in 2009 are situated next to the sea).

As explained above, the general belief nowadays is, that increased CO<sub>2</sub> concentrations in the atmosphere cause an amplification of the natural greenhouse effect. The moral dilemma about this situation is that the industrialized countries (with high CO<sub>2</sub> emissions) have a low vulnerability towards climate change, whereas the developing countries with low CO<sub>2</sub> emissions have a great vulnerability [1, 2, 6]. The industrialized countries therefore have the moral obligation to take responsibility and to start making changes.

The fate of the island states in the south Pacific (e.g. Tuvalu, Niue, the Marshall Islands or Kiribati) can be seen as an early harbinger of an increasing rise of the sea water level. These small islands are located between Australia and Hawaii and their highest elevations are only a few meters above sea level. The erosion of the shorelines and the slow but steady rise of the sea water level (about 20 cm in the last hundred years [7] and currently about 3 mm per year [8]) will cause at least severe changes for the islands. One estimation for example says that Tuvalu will vanish from the maps by the middle of the century. Other smaller islands and atolls will become uninhabitable by the 2030s [1, 9]. Already, there are suggestions and plans to evacuate some of the islands. The questions where the islanders will find asylum and who will pay for the evacuation remain unanswered.

With a reduction of the CO<sub>2</sub> emissions, as being the gas with the highest share of the anthropogenic greenhouse effect, much can be accomplished. This is why we have a strong need for new energy conversion technologies that do not emit carbon dioxide.

## 2.2. Technical background

### 2.2.1. Carbon capture and storage

CO<sub>2</sub> emissions from electricity and heat generation account for about one-third of the global CO<sub>2</sub> emissions, respectively 25 % of all greenhouse gas emissions (data from 2005; [10, 11]). Carbon capture and storage (CCS; sometimes also: carbon capture and sequestration) is a possibility to reduce those CO<sub>2</sub> emissions drastically while still being able to use fossil fuels for electricity production. It involves the steps sequestration, transportation and storage of CO<sub>2</sub>. Whereas sequestration and transportation are chemical and process engineering challenges, storage is more a geological issue. Underground storages are required to separate CO<sub>2</sub> from the natural carbon cycle for the next millennia (and possibly absorb the CO<sub>2</sub> permanently).

Fossil fuels are well established in the world's energy production. The energy sources coal, oil and gas combined account for about 66 % of the worldwide net electricity generation (data

from 2006; [12]). This figure makes it clear that even if a complete transition from fossil fuels to other energy sources was pursued, the process would take a considerable amount of time. Abandoning fossil fuels completely does not seem to be a realistic option in the near future. If the global climate goal of reducing the CO<sub>2</sub> emissions shall be reached, CCS seems to be the only realistic option at the moment.

There are three different CCS strategies, which are presently pursued by different research groups (universities and companies):

- **Pre-combustion** is a combustion method, where the carbon is separated from the rest of the fuel *before* the combustion. The typical ways are either steam reforming or partial oxidation (depending on the fuel type) of the fossil fuel to syngas (CO and H<sub>2</sub>). During the succeeding water-gas shift reaction, CO is shifted to CO<sub>2</sub> and more H<sub>2</sub> is formed. Now, the only remaining species are CO<sub>2</sub> and H<sub>2</sub>. If those gases are separated (e.g. by CO<sub>2</sub> absorption processes), the remaining H<sub>2</sub> can be used as carbon-free fuel. Since the gasification process typically requires significant amounts of process steam, pre-combustion CCS will only be able to play out its strengths in highly integrated processes. Thus, retrofitting of existing power plants does not seem to be a realistic option.
- **Post-combustion** describes a process, where the produced CO<sub>2</sub> is separated from the rest of the flue gases and captured *after* the combustion. Therefore, post-combustion is generally suited for retrofitting existing power plants or other industrial plants without much change to the original design, even though the integration of the process will achieve higher efficiencies.
- **Oxy-fuel combustion** characterizes a process where oxygen mixed with steam and carbon dioxide – instead of air – is used to combust the fuel. Thereby, the flue gases do not contain nitrogen, which would otherwise be the main component, and CO<sub>2</sub> and H<sub>2</sub>O will be the only combustion products. Those can then be separated relatively easy by condensing the water. Pure oxygen can for instance be obtained from a cryogenic air separation unit (ASU), which has to be installed on the plant site. Retrofitting could be possible, although difficult, since the process parameters would change considerably. The topic of this work – chemical-looping combustion (CLC) – is sometimes considered as an oxy-fuel process. Since the plant design differs quite a lot from existing combustion methods, retrofitting is not an option.

### 2.2.2. The principle of chemical-looping

Chemical-looping combustion (CLC) is a method of combusting fuels with inherent sequestration of carbon dioxide. The main technical challenge, that all CCS processes have in common, is the separation of gases. Gas separation is difficult to perform and involves a high level of technical challenges. CLC overcomes this by selectively binding one gas type to solid particles. The separation of solids and gases is a lot less complex and requires a simpler technical setup. After the separation, the gas bound to the particles is released again in a gaseous form.

The reactions take place in two interconnected fluidized beds with particles that continuously circulate between the two reactors. This idea of having two adjacent fluidized beds with an exchange of solids but no gas mixing has first been published academically by Richter and Knoche in 1983 [13] and in 1986 by Chong et al. [14] (the general idea was first mentioned in the 1950s). The general idea has been picked up again in 2001 by Lyngfelt et al. [15] and has been developed and brought forward ever since.

The whole concept is based on the process of fluidizing particles. This is a process where a steady gas flow is conducted through a column of particles thus forming a two-phase mixture (solid and gas). Depending on the magnitude of the gas flow, the process can be stationary (bubbling bed) or circulating [16]. Solids in a fluidized two-phase mixture can be processed nearly like regular fluids.

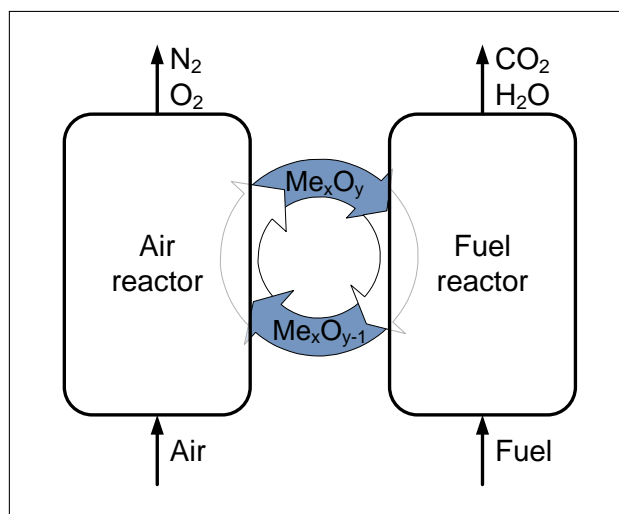


**Figure 2.1.:** Schematic illustration of the chemical-looping combustion process

Figure 2.1 shows the basic design of a CLC system and illustrates the working principle. The reduced metal oxide particles ( $\text{Me}_x\text{O}_{y-1}$ ) get into the air reactor, where they are fluidized by regular air. During the fluidization the reduced metal oxide particles become oxidized according to equation 2.1.



The fluidization velocity in the air reactor is high enough to create a circulating fluidized bed: While new particles are constantly fed to the bottom of the particle bed, particles at the top are accelerated upwards and leave the bed. The particle-gas mixture is then separated: the oxygen depleted air is returned to the ambience, whereas the metal oxide particles are transported via a particle lock to the fuel reactor. There, the metal is reduced anew by the fuel, which is usually also used to fluidize the particles. If the fuel only consists of hydrocarbons,

there will be no other reaction products besides water vapor ( $\text{H}_2\text{O}$ ) and carbon dioxide ( $\text{CO}_2$ ). The reaction in the fuel reactor is expressed by equation 2.2.



If the product gas is then cooled below the condensation temperature of the water, the remaining gas flow consists of pure  $\text{CO}_2$ . The reduced particles are returned via another particle lock to the air reactor, where the whole cycle starts over again.

In the majority of cases the reaction is exothermic in the air reactor (Eq. 2.1) and endothermic in the fuel reactor (Eq. 2.2). That depends on the oxygen carrier particle though. The oxygen carrier determines a major part of the CLC characteristics:

- **The reduction rate**, i.e. the amount of oxygen that is carried from air to fuel reactor per cycle, needs to be sufficiently high in order to avoid both large circulation rates and bed inventories. Both would make the reactor system bigger and more expensive.
- High **mechanical integrity** is also advantageous. Particle agglomeration, fragmentation or attrition cause either fouling in the reactor or pollution of the tail gases. The more particles become unusable, the higher the necessary make-up feed and therefore the operating expenses.
- Other important characteristics of a good oxygen carrier particle are **costs, availability and its environmental impact**. Well suited would be for example a by- or waste product from another process, that can be obtained with little or no expenses. Since it is very likely that particle fines are transported into the ambience with the tail gas, they should not be toxic, poisonous or hazardous in any way. Otherwise filters or other cleaning devices would have to be used.

In order to get a better understanding for the quantities of oxygen carrier needed in real size reactor systems, some estimated values are displayed in table 2.1.

**Table 2.1.:** Total amount of bed mass of different oxygen carrier materials for real size CLC reactors

Oxygen carrier	Fuel type	Bed mass ( $\text{kg}/\text{MW}_{th}$ )
Nickel oxide <sup>1</sup>	gas	80
Copper oxide <sup>1</sup>	gas	200
Iron-based <sup>1</sup>	gas	330
Ilmenite <sup>2</sup>	solid	250-1300
Mt Wright iron ore <sup>2</sup>	solid	350-2000
Iron oxide scales <sup>2</sup>	solid	350-2000
<sup>1</sup> ... from [17]		
<sup>2</sup> ... from [18]		

The part of the reactor where the exothermic reaction happens can be used to heat and evaporate water. The produced steam can then drive a steam turbine thus generating electricity. The alternative application would be the integration of the chemical-looping process in a combined cycle. The process in the air reactor would then be pressurized and be succeeded by an expansion turbine (the AR would thus act as the combustion chamber of a gas turbine). The remaining heat content of the flue gas is then used to evaporate the water of a steam cycle. Besides power generation there are other possible applications for chemical-looping, e.g. gasification of biofuels or reforming of fossil fuels (known as CLR: chemical-looping reforming [19]).

A detailed overview of the development of the different fields within CLC until 2008 can be found in [20].

### 2.2.3. The 300W test reactor

The purpose of the 300 W test reactor of Chalmers' division of Energy Conversion Technology is to make a general assessment of the suitability of oxygen carrier particles for a CLC process. Only a few hundred grams of the oxygen carrier particles are needed in order to run experiments. Especially if an oxygen carrier needs to be synthesized, the cost per mass can be quite high.

The 300 W reactor is integrated in a logical analysis chain:

1. Batch reactor experiments at the division of Environmental Inorganic Chemistry (ca. 15–25 g of oxygen carrier needed)
2. 300 W reactor experiments at the division of Energy Conversion Technology (ca. 100–300 g of oxygen carrier needed)
3. 10 kW reactor at the division of Energy Conversion Technology (ca. 15–20 kg of oxygen carrier needed)
4. 100 kW reactor at the division of Energy Conversion Technology (approx. 50–100 kg of oxygen carrier needed); the reactor has been designed but not yet constructed

The 300 W reactor is designed for the use of gaseous fuels. As of the present day, experiments can be run with methane ( $\text{CH}_4$ ), natural gas (different combinations of alkanes) or syngas ( $\text{CO}/\text{H}_2$ ). Steam addition to any of the gases is possible. The measuring equipment is set up in a way that prohibits the continuous measurement of high carbon monoxide ( $\text{CO}$ ) concentrations. This limits the extent to which syngas experiments can be run.

After the development of a cold model [21], the first hot version of the 300 W reactor was manufactured and put into use [22–24]. Due to the small thermal output, the heat of reaction is not enough to grant a sufficiently high temperature (typically 750–950 °C). The reactor is therefore encased in an electric furnace. The design was focused on compactness rather than on ideal fluid flow conditions. Due to high leakages between the two reactor parts (air and fuel reactor), the design was improved. Those improvements concerned basically the downcomer and are described in detail in the next section (Chap. 2.2.4). An illustration of the latest

reactor design can be seen figure 2.2. A cross-section of the reactor with all the measuring points can be found in appendix A.

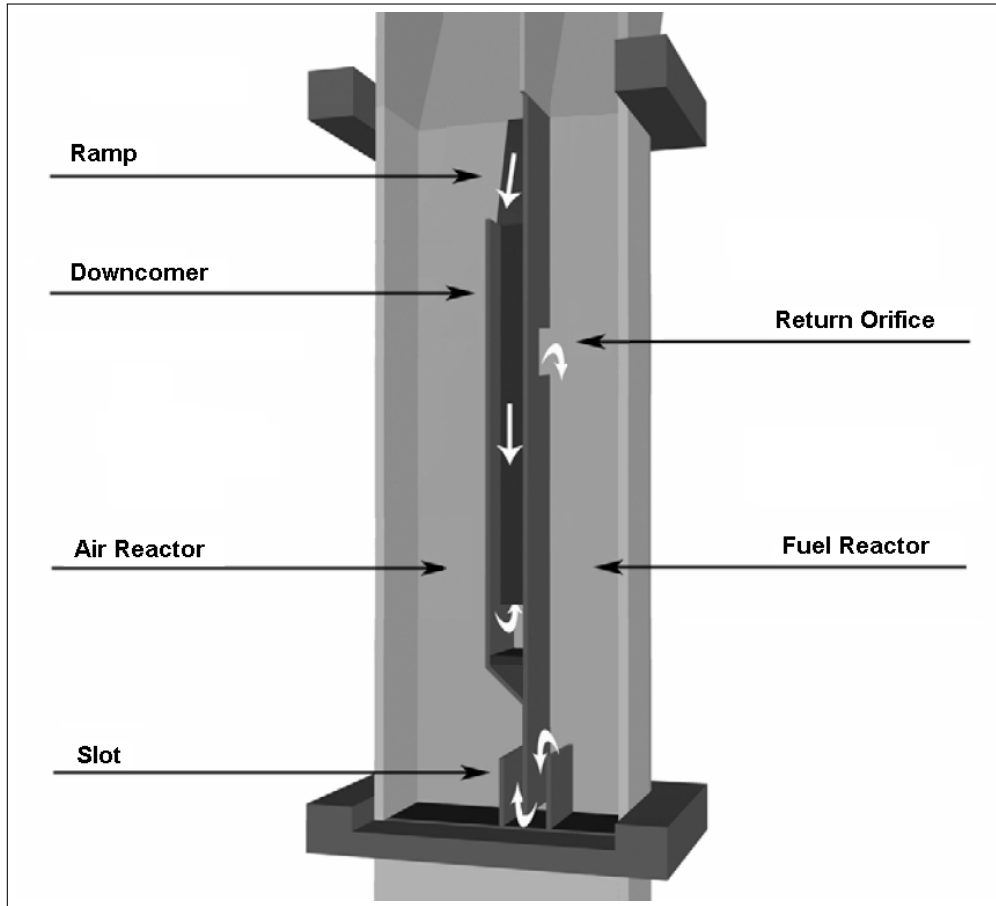
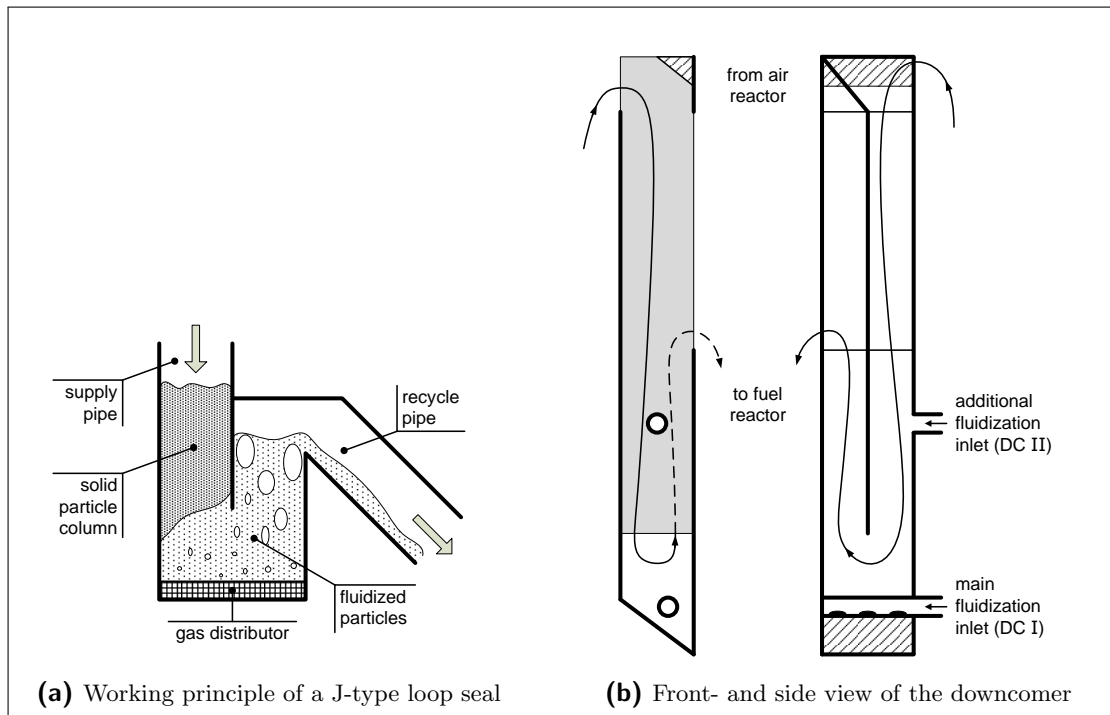


Figure 2.2.: Schematic three-dimensional illustration of the improved 300 W test reactor

#### 2.2.4. Downcomer improvements

The downcomer is one of the two particle locks in the reactor (downcomer and slot). Particle locks allow particles to pass, but hinder gases from flowing directly from one reactor to the other. They should be completely gas tight but in reality they allow small amounts of gas to pass. The old reactor design of the 300 W unit has been altered twice in the past in order to further reduce a gas leakage through the downcomer. In the original version the downcomer had an open design causing less resistance for the circulating particles. The downside however was quite a high leakage between the two reactors. This open downcomer design was then changed into a J-type loop seal. Leakages could thereby be reduced significantly (leakage: from as much as 35 % to 5 %; dilution: from 25 % to 2 % [25]). The changes are described more in detail in [25, 26]. Schematics of the old reactor design can be seen in [22–24, 27].



**Figure 2.3.:** Schematic and latest downcomer design of the 300 W test reactor

A schematic working principle of a J-type loop seal can be seen in figure 2.3a. As the particles first get into the loop seal they become part of a solid (non-fluidized) particle column. This compact column is the main reason why gas cannot pass through the loop seal. The particles at the bottom of the loop seal on the other hand get fluidized and eventually spill into the recycle pipe. The height difference between the solid and the fluidized bed is due to friction within the loop seal and, as in the case of the 300 W reactor, due to a pressure difference between the reactors (higher absolute pressure in the FR).

One problem that occurred with this design, was that the particles from the solid column did not flow freely into the fluidized part but somehow got stuck. This did not happen with all particle types but most often with particle that did not have a spherical shape. This plugging stopped the circulation and prevented successful experiments from being run. In order to avoid the particles from getting stuck in the supply pipe, an additional fluidization inlet was installed to the downcomer. This has been done just before the experiments that are described in this work were carried out. Thus, the effectiveness of the new downcomer design had to be tested, before the actual experiments could be run. Figure 2.3b shows the latest downcomer design used in the 300 W test reactor.

# 3. Experiments

## 3.1. Leakage investigation

### 3.1.1. Background

In a small-scale system, like the 300 W reactor, leakages between air and fuel reactor occur almost continuously and are very hard to control. Since there are not a lot of parameters that can be used to control the leakages, their magnitude is mainly fixed by the chosen design.

As has been described in the introduction (cf. Chap. 2.2.4), the design of the downcomer has been changed just before this work was started. To make sure that everything works as it should on one hand and to get a better understanding for the magnitudes of the leakages on the other hand, some preliminary leakage experiments need to be carried out. This will allow for interpreting the main experiments with a higher level of confidence.

There are two main kinds of leakages that have been used to describe the carbon capture efficiency of a CLC process during various continuous circulation experiments [19, 21, 22, 24, 27].

- **Leakage** describes the gas flow from the fuel reactor to the air reactor. If *leakage* occurs, fuel reacts directly with air and carbon dioxide is formed in the air reactor. This carbon dioxide is not captured and thus reduces the carbon capture efficiency.
- **Dilution** describes the gas flow from the air reactor to the fuel reactor. If *dilution* occurs, air is transported into the fuel reactor. The oxygen in the air reacts with the fuel, forming carbon dioxide and water (amongst others). The nitrogen in the air dilutes the outlet flow of the fuel reactor and is further processed with the carbon dioxide (after the water is condensed). This raises the costs of the carbon sequestration process, since more gas needs to be processed and stored.

The quantities of leakage and dilution are usually described as the ratio of the cross-flows  $\dot{V}_L$  (from FR to AR) respectively  $\dot{V}_D$  (from AR to FR) to the fuel inlet flow  $\dot{V}_{FR,in}$ .

$$L = \frac{\dot{V}_L}{\dot{V}_{FR,in}} \quad (3.1)$$

$$D = \frac{\dot{V}_D}{\dot{V}_{FR,in}} \quad (3.2)$$

The flow of the fluidization gases in the two particle locks can have a dilution or a leakage character. Leaking, if carbon dioxide is used as a fluidization gas and dilution, if anything but carbon dioxide is used. Equations 3.1 and 3.2 are not considering those flows. The reason for that is that with the old reactor design the amount of fluidization gas was small in comparison to the cross-flows from one reactor to the other. Depending on the results of the leakage experiments, those equations should be reconsidered.

For operating large-scale reactor systems, steam could be used to fluidize the particle locks. It would neither dilute the fuel reactor gases (water is condensed after the FR) nor cause a CO<sub>2</sub> leak into the air reactor (which would reduce the CO<sub>2</sub> capture rate).

In order to keep the dilution in the 300 W at a low level, the fuel reactor is operated under slight overpressure: At the reactor exit the exhaust gases have to overcome a water column of 2 cm height (corresponds to about 0.2 kPa or 2 mbar) thus increasing the absolute pressure in the fuel reactor. The average pressure in the air reactor corresponds to atmospheric pressure. The pressure difference needs to be sufficiently high to create a pressure gradient that hinders flows into the fuel reactor, but low enough so that the fuel reactor gases do not overcome the pressure drop of the particle seals and leave the reactor through the air reactor instead.

As has been stated in other publications before [21, 22, 24], low magnitudes of leaking and dilution flows are not of crucial importance for laboratory reactor systems. Of course, unwanted cross-flows might cause equally unwanted reactions that could even distort the results. However, as long as the magnitudes are known, the results can be analyzed sufficiently well. Furthermore, the magnitude of leakage and dilution mainly depends on the reactor design. As laboratory reactors are scaled up, more space is available and the particle locks can be designed in a way that minimizes gas leakages.

### 3.1.2. Experimental procedure

A fundamental investigation of the leaking behavior of the different reactor parts is being carried out. In order to be able to detect the different leakage volume flows, different gases are used for the air reactor (air), the fuel reactor (argon) and the two particle locks (carbon dioxide). Since no fuel gas is added to the system all other species are inert and no reaction is expected to happen. This means that no other gases will form and only the gases that enter the reactor will leave it.

During this experiment different parameters will be varied to investigate how they each influence the leakage. The main parameters are the volume flows into the fuel reactor, into the air reactor, to the downcomer and to the slot. The experiments are carried out in a hot reactor, because the gas volume (and thus the flow velocity) increases if a gas is heated (a temperature change from room temperature to 900 °C corresponds to an expansion factor of 4).

Table 3.1 shows the base parameters for the leakage experiments. They were chosen as base parameters, because they are expected to match the real conditions in the reactor (with a

fuel flow). For the leakage tests (Tab. 3.1 and 3.2) only the lower downcomer nozzle was used for fluidizing the particles in the downcomer.

**Table 3.1.:** Base parameters for the leakage test series

$U_{\text{FR}}$ (L <sub>n</sub> /min)	$U_{\text{AR}}$ (L <sub>n</sub> /min)	$U_{\text{DC}}$ (L <sub>n</sub> /min)	$U_{\text{SL}}$ (L <sub>n</sub> /min)	$T_{\text{FR}}$ (°C)	Corresponding power (W)	
					CO/H <sub>2</sub>	CH <sub>4</sub>
1.4	7.2	0.3	0.1	900	270	900

The parameters in table 3.1 are each varied in order to create a set of leakage experiments that form a test series. Table 3.2 gives an overview of the different test settings within the test series.

**Table 3.2.:** Settings and parameters for each test of the leakage test series

Test number	$U_{\text{FR}}$ (L <sub>n</sub> /min)	$U_{\text{AR}}$ (L <sub>n</sub> /min)	$U_{\text{DC}}$ (L <sub>n</sub> /min)	$U_{\text{SL}}$ (L <sub>n</sub> /min)	$T_{\text{FR}}$ (°C)	Corresponding power (W)	
						CO/H <sub>2</sub>	CH <sub>4</sub>
L1	0.7–1.4	7.2	0.3	0.1	900	140–270	450–900
L2	1.4	4.1–10.3	0.3	0.1	900	270	900
L3	0.7–1.4	3.6–7.2	0.3	0.1	900	140–270	450–900
L4	1.4	7.2	0.1–0.5	0.05–0.2	900	270	900
L5	1.4	7.2	0.3	0.1	900	270	900

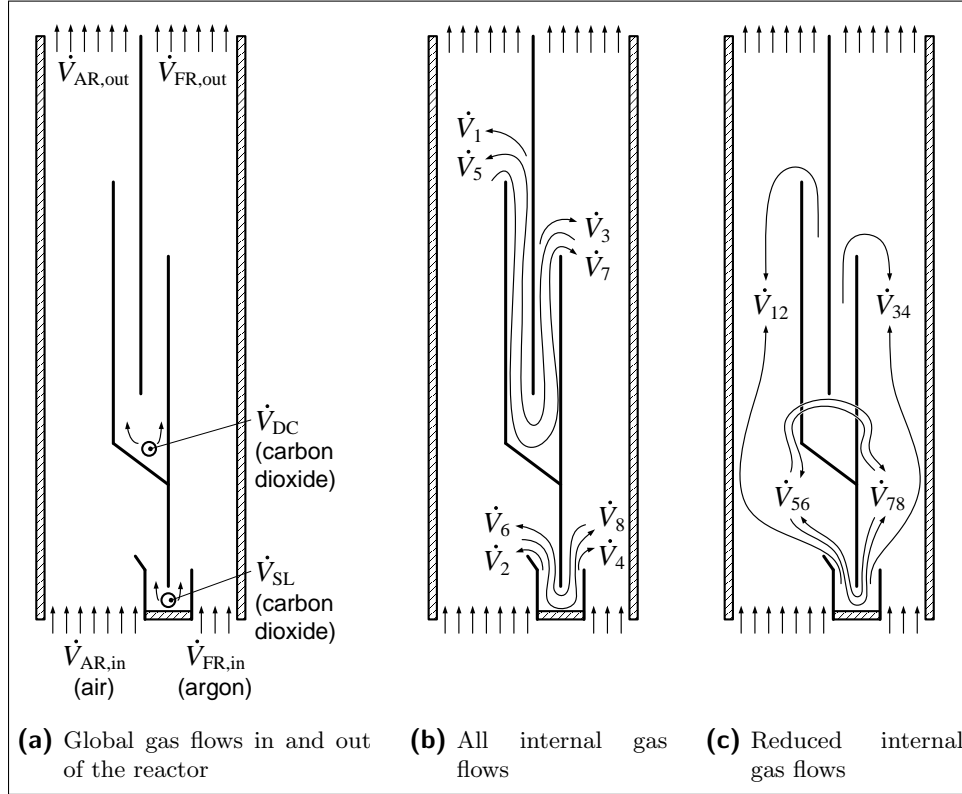
### 3.1.3. Analysis

Figure 3.1 shows a schematic drawing of the reactor to illustrate the different gas flows. Figure 3.1b shows all possible internal flows: the flows from the particle locks and the leakage flows from one reactor into the other. Since the same fluidization gas is used for both particle locks, it cannot be distinguished from which of the two the gas originates. The same is true for the flows from one reactor into the other: it cannot be distinguished whether the flow went through the downcomer or through the slot. This is the reason why the different flows can be combined. The amount of unknown flows is thus reduced from eight to four (Fig. 3.1c; cf. Tab. 3.3).

In table 3.3 the different internal gas flows are summarized and explained. The alternative names use the subscript notation at full length. The shorter versions were used to make the illustrations and equations clearer.

All incoming volume flows ( $\dot{V}_{\text{FR,in}}$ ,  $\dot{V}_{\text{AR,in}}$ ,  $\dot{V}_{\text{DC}}$  and  $\dot{V}_{\text{SL}}$ ) are parameters that are known and can be adjusted. The (dry-)gas concentrations of carbon dioxide and oxygen at each reactor outlet ( $x_{\text{CO}_2,\text{FR}}$ ,  $x_{\text{O}_2,\text{FR}}$ ,  $x_{\text{CO}_2,\text{AR}}$  and  $x_{\text{O}_2,\text{AR}}$ ) are measured with gas analyzers and are therefore known as well.

The concentrations of argon and nitrogen at each reactor outlet ( $x_{\text{N}_2,\text{FR}}$ ,  $x_{\text{Ar,FR}}$ ,  $x_{\text{N}_2,\text{AR}}$  and  $x_{\text{Ar,AR}}$ ) are not measured. The oxygen and nitrogen flows respectively concentrations are connected though. Both species enter the system as part of the air and thus occur in a fixed ratio. Hence the nitrogen concentration can be calculated as follows:



**Figure 3.1.:** Reactor schematic with gas flows and types of gas used for the leakage experiments

$$x_{N2,AR} = \frac{78}{21} \cdot x_{O2,AR} \quad (3.3)$$

$$x_{N2,FR} = \frac{78}{21} \cdot x_{O2,FR} \quad (3.4)$$

The last unknown concentration (of argon) can be calculated due to the fact that the sum of all concentrations at each outlet must be 100 % respectively 1:

$$x_{Ar,AR} = 1 - x_{CO2,AR} - x_{O2,AR} - x_{N2,AR} \quad (3.5)$$

$$x_{Ar,FR} = 1 - x_{CO2,FR} - x_{O2,FR} - x_{N2,FR} \quad (3.6)$$

If the two outgoing volume flows ( $\dot{V}_{FR,out}$  and  $\dot{V}_{AR,out}$ ) were known, the internal (leakage) flows in the reactor ( $\dot{V}_{12}$ ,  $\dot{V}_{34}$ ,  $\dot{V}_{56}$  and  $\dot{V}_{78}$ ) could be calculated. However, they are not. Therefore the solution is derived in an iterative loop. First, the outgoing flow of

**Table 3.3.:** Description of the unknown internal gas flows

<b>all internal flows</b>		
unknown flow	alternative name	description
$\dot{V}_1$	$\dot{V}_{DC-AR}$	gas flow from downcomer to air reactor
$\dot{V}_2$	$\dot{V}_{SL-AR}$	gas flow from slot to air reactor
$\dot{V}_3$	$\dot{V}_{DC-FR}$	gas flow from downcomer to fuel reactor
$\dot{V}_4$	$\dot{V}_{SL-FR}$	gas flow from slot to fuel reactor
$\dot{V}_5$	$\dot{V}_{FR-AR,DC}$	gas flow from fuel reactor to air reactor (leakage) via the downcomer
$\dot{V}_6$	$\dot{V}_{FR-AR,SL}$	gas flow from fuel reactor to air reactor (leakage) via the slot
$\dot{V}_7$	$\dot{V}_{AR-FR,DC}$	gas flow from air reactor to fuel reactor (dilution) via the downcomer
$\dot{V}_8$	$\dot{V}_{AR-FR,SL}$	gas flow from air reactor to fuel reactor (dilution) via the slot
<b>reduced internal flows</b>		
unknown flow	alternative name	description
$\dot{V}_{12}$	$\dot{V}_{PL-AR}$	combined gas flow from both particle locks into the air reactor
$\dot{V}_{34}$	$\dot{V}_{PL-FR}$	combined gas flow from both particle locks into the fuel reactor
$\dot{V}_{56}$	$\dot{V}_{FR-AR}$	combined gas flow via both particle locks from fuel reactor to air reactor (leakage)
$\dot{V}_{78}$	$\dot{V}_{AR-FR}$	combined gas flow via both particle locks from air reactor to fuel reactor (dilution)

the fuel reactor is guessed (the incoming flow plus half the flow to each of the particle locks):

$$\dot{V}_{FR,out}^* = \dot{V}_{FR,in} + 0.5 \cdot (\dot{V}_{DC} + \dot{V}_{SL})$$

With that information, all other values can be calculated.

$$\dot{V}_{\text{AR,out}} = \dot{V}_{\text{AR,in}} + \dot{V}_{\text{FR,in}} + \dot{V}_{\text{DC}} + \dot{V}_{\text{SL}} - \dot{V}_{\text{FR,out}}^* \quad (3.7)$$

$$\dot{V}_{12} = \dot{V}_{\text{AR,out}} \cdot x_{\text{CO}_2,\text{AR}} \quad (3.8)$$

$$\dot{V}_{34} = \dot{V}_{\text{DC}} + \dot{V}_{\text{SL}} - \dot{V}_{12} \quad (3.9)$$

$$\dot{V}_{56} = \dot{V}_{\text{AR,out}} \cdot \left( x_{\text{Ar,AR}} - 0.01 \cdot x_{\text{O}_2,\text{AR}} \cdot \frac{100}{21} \right) \quad (3.10)$$

$$\dot{V}_{78} = \dot{V}_{\text{AR,in}} - \dot{V}_{\text{AR,out}} \cdot x_{\text{O}_2,\text{AR}} \cdot \frac{100}{21} \quad (3.11)$$

$$\dot{V}_{\text{FR,out}} = \dot{V}_{\text{FR,in}} + \dot{V}_{78} - \dot{V}_{56} + \dot{V}_{34} \quad (3.12)$$

At last, the calculated volume flow  $\dot{V}_{\text{FR,out}}$  in equation 3.12 is used as the new initial value:

$$\Rightarrow \dot{V}_{\text{FR,out}}^* = \dot{V}_{\text{FR,out}} \quad (3.13)$$

After the initial guess of the outgoing fuel reactor flow, equations 3.7 – 3.13 are being run through several times. Stopping criteria could be a sufficient small difference between the initial value of the outgoing fuel reactor flow and the calculated value at the end of the loop or simply a fixed numbers of loops. Due to the smaller numeric complexity, a fixed number of cycles was chosen and the difference between the initial and the calculated value for the outgoing fuel reactor flow was plotted to show whether the system is converging.

### 3.1.4. Results

As a result from the computations, the leakage and dilution could be calculated. Those values were quantified according to equations 3.1 and 3.2. Additionally, a new dilution value was used. This new definition of the dilution takes into account the inflow into the fuel reactor from the air reactor and the two particle locks. It was calculated according to the following equation:

$$D_{\text{tot}} = \frac{\dot{V}_{\text{AR-FR}} + \dot{V}_{\text{PL-FR}}}{\dot{V}_{\text{FR,in}}} \quad (3.14)$$

As can be seen in figure 3.2, this new definition of the dilution makes much more sense for the new reactor design, since the share of the diluting inflow from the particle locks is much greater than from the air reactor. This new definition of the dilution is from now on referred to as the *total dilution* ( $D_{\text{tot}}$ ).

A further differentiation will be made by introducing the dilution of the fuel reactor gas by the combined flow from both particle locks:

$$D_{\text{PL}} = \frac{\dot{V}_{\text{PL-FR}}}{\dot{V}_{\text{PL}}} \quad (3.15)$$

The main difference between the two dilutions  $D$  and  $D_{\text{PL}}$  is, that the gas from the air reactor (expressed through  $D$ ) will partly react in the fuel reactor but amounts to only a minute fraction of the total dilution  $D_{\text{tot}}$ . The dilution from the particle locks ( $D_{\text{PL}}$ ) on the other hand amounts to nearly the whole of the total dilution but will not cause any reaction in the fuel reactor (if an inert gas is used to fluidize the PLs).

That lines of best fit that are displayed in figure 3.2 and 3.3 are second degree polynomials (adjusted by applying the method of least squares). They match the data from most measurements reasonably well. Only the variation of the slot-flow seems to cause a rather linear leakage and dilution behavior (Fig.3.2e and 3.3e).

All the leakage tests L1 – L5 have one setting in common: The setting with the base parameters (cf. Tab. 3.1). Since this setting has been run and measured five times, it can be used to determine the deviation of the data. For the data shown in figure 3.2 it amounts to about  $\pm 4\%$  points for the total dilution (corresponds up to  $\pm 50\%$  of the total) respectively  $\pm 0.5\%$  points for the leakage. The two flows from the particle locks in figure 3.3 deviate by  $\pm 0.05 \text{ L}_n/\text{min}$  each (corresponds up to  $\pm 50\%$  of the total). This shows that even if the reactor runs stable, it does not run in a fixed condition.

Another kind of error can be seen in figures 3.2b and 3.2e. The setting with the lowest volume flow to the air reactor ( $U_{\text{AR}}$ ) respectively to the slot ( $U_{\text{SL}}$ ) show slightly negative dilution values (graph “+” in Fig. 3.2: Dilution of FR;  $-0.04\%$  respectively  $-0.02\%$ ). Of course, this does not make sense physically. However, those were the only points where the gas analyzer measured slightly negative oxygen concentrations. Thus the negative dilution values originate from measuring errors.

The leakage (graph “▼” in Fig. 3.2) is constant most of the times (Fig. 3.2a, 3.2d and 3.2e) and has an average value of  $3.0\%$  (maximum  $6.7\%$ ). Variations of the air reactor flow ( $U_{\text{AR}}$  in Fig. 3.2b) have the strongest impact. This could be due to the fluid mechanics principle that states, the faster a fluid flows, the lower its static pressure (Venturi effect). The air reactor flow is the highest flow in the whole reactor and its increase amplifies the pressure difference between fuel and air reactor even more. This could explain why more of the fuel reactor gas leaks into the air reactor.

The same circumstance can be seen in figure 3.2c. The effect is damped though, because the fuel reactor flow is increased as well: Higher air reactor flows cause a higher absolute leakage, whereas higher fuel reactor flows lower the relative value (as in Eq. 3.1). The fuel flow hence dampens the stronger influence of the air flow.

The dilution according to the old definition (graph “+” in Fig. 3.2 according to Eq. 3.2; only taking into account the flow from AR to FR) seems to be constant most of the times and never exceeds 1.7% (average 0.7%). Variations of the slot-flow seem to have the greatest effect. The dilution is even suppressed completely when the slot-flow is reduced far enough (Fig. 3.2e). A variation of the downcomer-flow on the other hand hardly causes any effect at all (Fig. 3.2d).

The dependency of the dilution on the fuel reactor flow, which can be seen in figure 3.2a, is strictly linear (doubling the FR flow causes a halving of the dilution). This means that the amount of dilutional flow (in volume per time) is constant. The percentile value changes only, due to the alteration of the reference value ( $U_{FR}$ ).

This leads to the conclusion that the main part of the dilution – which is very small anyway – passes through the slot. The downcomer only lets insignificant amounts of gas pass from air to fuel reactor, if any at all.

The major amount of gas flowing into the fuel reactor and thus diluting the gas there, originates from the particle locks. This can be seen when looking at figure 3.2 and comparing the great offset between the two different dilution values (graph “+”: dilution vs. graph “•”: total dilution). The difference between the two curves corresponds to the share of the particle locks in the total dilution.

As can be seen in figure 3.3, the amount of gas that flows from the two particle locks into each reactor is not constant. A further analysis showed that typically about 30–50% of the combined flow from the two particle locks goes to the fuel reactor. Due to its design most of the downcomer fluidization gas is expected to flow into the fuel reactor. The pressure difference between air and fuel reactor probably forces most of the slot-flow into the air reactor. The amounts and ratios seem to vary under different parameters though.

The following observations can be made when analyzing the graphs in figure 3.2 and 3.3:

- The dilutional shares from each the air reactor (Fig. 3.2a) and the particle locks (Fig. 3.3a) stay nearly constant, when the fuel flow ( $U_{FR}$ ) is varied. The fact that the total dilution decreases with an increasing fuel flow in figure 3.2a is mainly due to the fact that the dilution is calculated relatively to the fuel flow (cf. Eq. 3.2).
- In figure 3.2b the total dilution increases with higher air reactor flows, while the fuel reactor flow was held constant. The dilution from the air reactor is negligible. Thus, the total dilution corresponds to the dilution from the particle locks (Fig. 3.3b).
- When increasing the gas flows in the air and the fuel reactor while maintaining a constant flow ratio, the gas flow from the particle locks into fuel reactor (Fig. 3.3c) stays approximately constant (the visible variance is only  $\pm 0.02 L_n/\text{min}$ ). The dilutional flow from the air reactor is insignificant compared to the influence of the particle locks.
- When varying the downcomer-flow, as was done in leakage test L4, the combined flow from both particle locks is divided nearly evenly between air and fuel reactor, with a slightly higher share going to the air reactor (Fig. 3.3d).
- Varying the slot-flow shows that a greater share of the slot gas flows towards the air reactor (Fig 3.3e). This share becomes even higher as the slot-flow is increased.

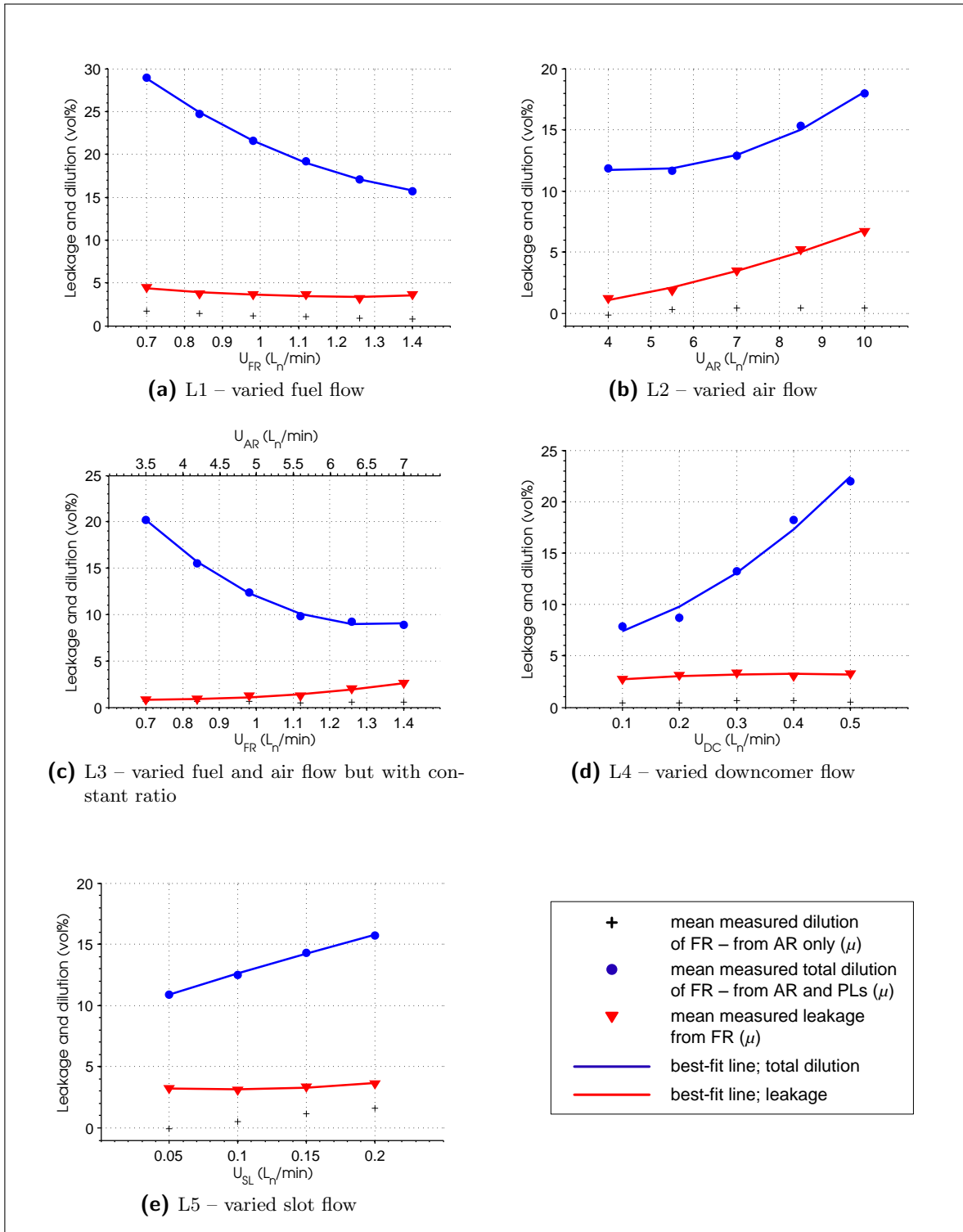


Figure 3.2.: Leakage and dilution for each test of the leakage series

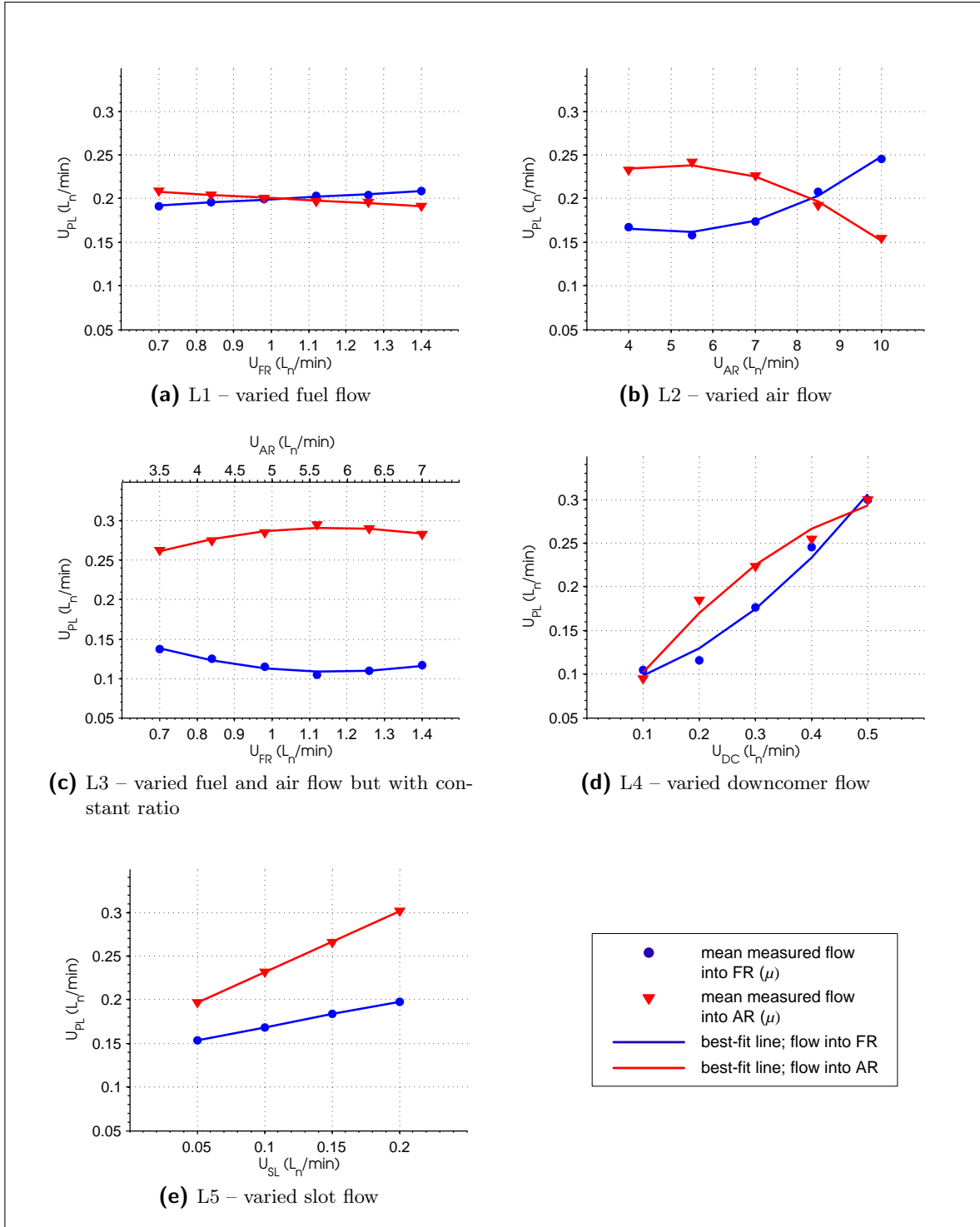


Figure 3.3.: Gas flows from the particle locks into air and fuel reactor for each test of the leakage series

### 3.1.5. Conclusions

The cross-flows between the reactors amount on average to 0.7 % for the dilution and 3.0 % for the leakage respectively. Most of the gas exchange seems to happen via the slot. The improvements of the downcomer were hence successful.

Almost the whole of the total dilution originates from the fluidization gas of particle locks. Even though the value of dilution is quite high (up to 30 %), no impact in the outcome of the experiments is expected, if inert gases are used to fluidize the particle locks. For an operating large-scale power plant this magnitude of dilution would mean a significant economic disadvantage – leakages between air and fuel reactor however, would be nearly non-existent.

In order to estimate leakages and dilutions during later experiments, the following assumptions can be applied<sup>1</sup> (summarized in Tab. 3.4):

1. The leakage ( $L$ ) can be approximated as a function of the air reactor flow ( $U_{AR}$ ).
2. The dilution from the air reactor only ( $D$ ) can be approximated as a constant 1 % of the fuel reactor gas flow ( $U_{FR}$ ).
3. The dilution from the particle locks only ( $D_{PL}$ ) can be approximated as a constant 45 % of the combined gas flows from both particle locks ( $U_{PL}$ ).

**Table 3.4.:** Approximations for leakage and dilution

Term	Correlation	Relative value (%)	Absolute value ( $L_n/\text{min}$ )
$L$	$L = f(U_{AR})$	$L \approx 0.95 \cdot U_{AR}^\dagger - 2.9$	$\dot{V}_{56}^\ddagger \approx (0.95 \cdot U_{AR}^\dagger - 2.9) \cdot U_{FR}$
$D$	$D \approx \text{const.}$	$D \approx 1\% \text{ (of } U_{FR}\text{)}$	$\dot{V}_{78}^\ddagger \approx 0.01 \cdot U_{FR}$
$D_{PL}$	$D_{PL} \approx \text{const.}$	$D_{PL} \approx 45\% \text{ (of } U_{PL}\text{)}$	$\dot{V}_{34}^\ddagger \approx 0.45 \cdot U_{PL}$

<sup>†</sup> ... in ( $L_n/\text{min}$ )

<sup>‡</sup> ... cf. figure 3.1c and table 3.3

<sup>1</sup>They can be applied if the reactor settings stay within reasonable limits, so to say roughly the spectrum of variations that have been investigated during the leakage experiments (cf. Tab. 3.2).

## 3.2. Ilmenite

### 3.2.1. Essentials

Ilmenite ( $\text{FeTiO}_3$ ) is a naturally occurring mineral that consists of iron titanium oxides. The term ilmenite is also used for ores that contain more or less of said mineral. It is mined at several sites around the globe. The here used particles originate from Norway and were supplied by *Titania A/S*. They consist mainly of ilmenite ( $\text{FeTiO}_3$ ) but also contain hematite ( $\text{Fe}_2\text{O}_3$ ). The particles were delivered as ground particles that only needed to be sieved in order to achieve suitable size ranges.

Ilmenite is not toxic, radioactive or hazardous in any known way. Its only environmental impact is due to the fact that it is mined, thus causing environmental damage by the mining in itself.

Apart from grinding and enrichment, ilmenite is an unprocessed mineral and rather cheap. For comparison: The price per metric ton of bulk material is comparable to the one of hard coal [28]. Its main application is the conversion into titanium dioxide ( $\text{TiO}_2$ ). In 2007 the world's total mine production of ilmenite amounted to 5.72 million tons and the world's reserve was about 680 million tons [28]. If CLC processes were used for electricity production with coal as fuel and ilmenite as oxygen carrier, today's mine production of ilmenite would suffice for an electric power of about  $2860 \text{ GW}_{\text{el}}$ <sup>2</sup>. This value is not a realistic claim, but rather meant to show dimensions. If compared to the world's installed capacity of conventional thermal electricity generation, which was about  $2750 \text{ GW}_{\text{el}}$  in 2006 [12], it can be seen that a CLC process with ilmenite as oxygen carrier is probably not suited to replace the whole conventional thermal generation overnight. However, a complete transition is not expected during the next few decades, which means that the CLC process will most probably be further improved or that other replacement technologies might be found. It seems like ilmenite is very well suited for CLC processes.

A characteristic of ilmenite is that fresh particles are not fully oxidized. This changes during the initial operation period when fresh particles are first used. As a result of the oxidization the particles gain mass. At the same time they become more porous and their reactivity increases. The reason for the increasing reactivity is most likely due to the fact that the BET surface area more than doubles. This process leads to an increase of the particle size and a decrease of the bulk density. Those processes have been experienced before [29] and are responsible for a highly non-stationary behavior of fresh particles during the initial operational period. It is therefore suggested to use relatively low temperatures and fuel flows during the initial phase.

One fact that is unknown about ilmenite is whether the particles ever reach a steady state where their properties do not change any more.

---

<sup>2</sup>It is assumed that about  $800 \text{ kg}/\text{MW}_{\text{th}}$  of ilmenite are needed when coal is combusted (average; as indicated in table 2.1) and that the CLC power plants will have an efficiency of about 40%. The lifetime of the particles is assumed to be one year. Other make-up feeds are not taken into account.

Ilmenite particles have been investigated thoroughly in a batch fluidized-bed reactor with methane ( $\text{CH}_4$ ), syngas ( $\text{CO}/\text{H}_2$ ) and solid fuels [18, 29, 30]. Those experiments were followed by continuous cycle experiments in the 300 W test reactor (new design) with natural gas (mostly methane  $\text{CH}_4$  and ethane  $\text{C}_2\text{H}_6$ ) as fuel gas [31]. The experiments described here were all run with syngas.

### 3.2.2. Experimental procedure

The reactor was initially filled with 270 g of ilmenite particles in the size range of 125–180  $\mu\text{m}$ . This amount was derived from the bed volume. The volume has to be within certain limits in order to have bed heights that allow for the reactor to operate. The amount is thus primarily a function of the particle density, which can then be adjusted (within a certain range) to the reactivity.

Table 3.5 shows which gases were used to fluidize the different parts of the reactor.

**Table 3.5.:** Fluidization gases used at the different locations in the reactor

Location	Gas	Gas composition
Fuel reactor	syngas (+steam <sup>1</sup> )	50% $\text{CO}$ + 50% $\text{H}_2$ (41.67% $\text{CO}$ + 41.67% $\text{H}_2$ + 16.67% $\text{H}_2\text{O}$ )
Air reactor	air	78% $\text{N}_2$ + 21% $\text{O}_2$ + 1% $\text{Ar}$
Downcomer (main)	argon	100% $\text{Ar}$
Downcomer (additional)	argon	100% $\text{Ar}$
Slot	argon	100% $\text{Ar}$

<sup>1</sup>. . .  $\frac{5}{6}$  syngas +  $\frac{1}{6}$  steam

The particles were heated up stepwise to 750, 800 and finally 900°C. After a temperature was reached, it was upheld for about 30 minutes before changing to the next temperature level.

First, it was investigated whether the particles showed a stable behavior in an extended time test with constant settings. Those settings have been determined by adjusting the design conditions with the “trial & error” method. The main obstacle was defluidization of the particles in the downcomer, which happened quite often – even after running stable for longer time periods like 30 minutes. After suitable flows for both downcomer nozzles had been found, the fuel flow was set to a level where full conversion of the fuel was just not reached anymore. The settings that were thus determined are shown in table 3.6.

**Table 3.6.:** Base parameters for the test series with fresh ilmenite particles

$U_{\text{FR}}$ ( $\text{L}_n/\text{min}$ )	$U_{\text{AR}}$ ( $\text{L}_n/\text{min}$ )	$U_{\text{DCI}}$ ( $\text{L}_n/\text{min}$ )	$U_{\text{DCII}}$ ( $\text{L}_n/\text{min}$ )	$U_{\text{SL}}$ ( $\text{L}_n/\text{min}$ )	$T_{\text{FR}}$ (°C)	Corresponding power (W)
1.7	7.2	0.14	0.21	0.10	900	330

The first series of experiments consisted of 31 hours of operation with fuel and is summarized in table 3.7. During this time the particle properties changed significantly. As expected, the initial period where the particles were fully oxidized, was followed by a period where the reactivity of the particles increased drastically.

**Table 3.7.:** Settings and parameters for each test of the test series with fresh ilmenite particles

Test number	$U_{FR}$ ( $L_n/min$ )	$U_{AR}$ ( $L_n/min$ )	$U_{DCI}$ ( $L_n/min$ )	$U_{DCII}$ ( $L_n/min$ )	$U_{SL}$ ( $L_n/min$ )	$T_{FR}$ ( $^{\circ}C$ )	Corresponding power (W)
I1.1	0.8–1.8	7.2	0.14	0.21	0.1	900	160–350
I1.2	0.8–1.6	7.2	0.14	0.21	0.1	750	160–310
I1.3	0.8–1.6	7.2	0.14	0.21	0.1	800	160–310
I1.4	0.8–1.6	7.2	0.14	0.21	0.1	850	160–310
I1.5	0.8–1.6	7.2	0.14	0.21	0.1	950	160–310

In order to judge the suitability of oxygen carrier particles, looking exclusively at the chemical properties is not enough. The particles could have excellent chemical properties, but if they broke down into fines after a short time, they would be blown out of the system and therefore be no good for a CLC process. Hence, the other criterion that has to be met is a sufficient structural stability of the particles.

After this first series of experiments the reactor was opened and the particles were optically examined, weighted and sieved. The results are summarized in table 3.11 (Chap. 3.2.4). The density of the particles was reduced to half that of fresh particles, and the particles had grown in size.

A decrease in particle density causes an increase of the bed heights in the reactor, i.e. the reactor did not operate within design conditions any more (see App. B for a visualization). Hence, half the bed mass as before (135 g instead of 270 g) with particles in the size range of 90–250  $\mu m$  was selected and put back into the reactor. The new base parameters are summarized in table 3.8.

**Table 3.8.:** Base parameters for the test series with used ilmenite particles

$U_{FR}$ ( $L_n/min$ )	$U_{AR}$ ( $L_n/min$ )	$U_{DCI}$ ( $L_n/min$ )	$U_{DCII}$ ( $L_n/min$ )	$U_{SL}$ ( $L_n/min$ )	$T_{FR}$ ( $^{\circ}C$ )	Corresponding power (W)
0.55	7.2	0.14	0.21	0.1	900	100

Experiments at those setting were conducted for about 27 hours. During that time, problems concerning defluidization were encountered regularly. Simultaneously, some indications in the measurements suggested that solid carbon was forming in the hot part of the fuel line, close to the reactor. Both problems were solved by adding steam to the fuel. Another 27 hours of experiments were then run with steam addition.

At first, experiments with different amounts of steam were performed. After a stable steam setting has been found (as high as necessary but as low as possible), a variation of the parameters fuel flow, temperature and air flow has been investigated. The setup of those experiments is shown in table 3.9.

**Table 3.9.:** Settings and parameters for each test of the test series with used ilmenite particles

Test number	$U_{FR}^1$ ( $L_n/\text{min}$ )	$U_{AR}$ ( $L_n/\text{min}$ )	$U_{DCI}$ ( $L_n/\text{min}$ )	$U_{DCII}$ ( $L_n/\text{min}$ )	$U_{SL}$ ( $L_n/\text{min}$ )	$T_{FR}$ ( $^{\circ}\text{C}$ )	Corresponding power (W)
I2.1	0.55–0.83	7.2	0.28	0.14	0.1	750	110–160
I2.2	0.55–0.69	7.2	0.28	0.14	0.1	800	110–135
I2.3	0.55–0.69	7.2	0.28	0.14	0.1	850	110–135
I2.4	0.55–1.10	7.2	0.28	0.14	0.1	900	110–215
I2.5	0.55	6.2–10.3	0.28	0.14	0.1	900	110

<sup>1</sup>... additionally:  $1/6$  steam ( $5/6$  syngas +  $1/6$  steam)

Altogether, about 85 hours of experiments were conducted with the same ilmenite particles. The particle properties at the end of the ilmenite series of experiments are shown in table 3.12 (Chap. 3.2.4). A collective overview of particle properties and bed heights upon reactor openings can be found in appendix B.

### 3.2.3. Analysis

During operation, the dry-gas concentrations of carbon monoxide (CO), carbon dioxide (CO<sub>2</sub>) and oxygen (O<sub>2</sub>) were measured and recorded continuously by a set of gas analyzers. Additionally, the dry-gas concentration of carbon monoxide (CO), nitrogen (N<sub>2</sub>) and hydrogen (H<sub>2</sub>) could be measured with a gas chromatograph (GC). The working principle of the GC only allows one measurement every few minutes (with the here chosen settings, the latency was about 4 minutes). Furthermore, the GC measurements were not recorded automatically. Hence, the GC measurements are rather suited for checking purposes (e.g. calculated gas concentrations and leakages) than for continuous data processing (which is needed to measure the highly non-stationary conditions in the reactor).

As indicated in appendix A the pressure is continuously recorded at various locations. Due to gas bubbles, the pressure drop over a fluidized bed alternates strongly around an average value and is generally higher than over a static non-fluidized particle column. The readings from the pressure measurements thus allow drawing conclusions about particle levels in the whole reactor and whether or not the particles are fluidized.

The inlet flows are controlled by individual mass flow controllers (MFCs) for each gas line. While the different flows into the reactor system are precisely known (volume flows and concentrations), the amount of measured data about flows that leave fuel and air reactor is quite limited. Not all gas concentrations can be measured and precise volume flows are unknown. However, chemical calculations and the applied findings from the previous leakage experiments (Chap. 3.1) allow the unknown figures to be calculated or reliably estimated.

An established method of rating the combustion process is through the *combustion efficiency*  $\gamma_{\text{eff}}$ . The *CO<sub>2</sub> gas yield*  $\gamma_{\text{CO}_2}$  is used to describe how much of the carbon containing species are converted into carbon dioxide.

The combustion efficiency is more suited though for rating the overall combustion process, which gets more important as the CLC process is scaled up. It requires the calculation of the hydrogen concentration, thus making the results a bit more uncertain as if only measured values were used.

The gas yield on the other hand is suitable for rating the conversion of the different gas components. This makes sense when looking at the process from a chemical point of view. Using the gas yield also has the advantage that it can be calculated from measured values only.

CLC in the 300 W reactor is an intermediate step between a lab-scale analysis and real world combustion. This is why both combustion efficiency and gas yield are used here. But since the main focus is the combustion, the combustion efficiency is the more practical value.

$$\gamma_{\text{eff}} = 1 - \frac{U_{\text{CO,FR,out}} \cdot H_{\text{i2,CO}} + U_{\text{CO}_2,\text{FR,out}} \cdot H_{\text{i2,CO}_2} + U_{\text{H}_2,\text{FR,out}} \cdot H_{\text{i2,H}_2}}{U_{\text{FR,in}} \cdot H_{\text{i2,fm}}} \quad (3.16)$$

$$\gamma_{\text{CO}_2} = \frac{x_{\text{CO}_2,\text{FR}}}{x_{\text{CO,FR}} + x_{\text{CO}_2,\text{FR}}} \quad (3.17)$$

The volume flow for each component  $i$  is calculated as follows:

$$U_{i,\text{FR,out}} = U_{\text{FR,out}} \cdot y_{i,\text{FR}} \quad (3.18)$$

$$\text{with: } U_{\text{FR,out}} = U_{\text{FR,in}} \cdot (1 - L + D) + U_{\text{PL}} \cdot D_{\text{PL}} \quad (3.19)$$

$$\begin{aligned} \text{and: } y_{i,\text{FR}} &= \frac{x_{i,\text{FR}}}{x_{\text{CO,FR}} + x_{\text{CO}_2,\text{FR}} + x_{\text{O}_2,\text{FR}} + x_{\text{H}_2,\text{FR}} + x_{\text{N}_2/\text{Ar,FR}} + x_{\text{H}_2\text{Oeq,FR}}} \\ &= \frac{x_{i,\text{FR}}}{1 + x_{\text{H}_2\text{Oeq,FR}}} \end{aligned} \quad (3.20)$$

The values for  $L$ ,  $D$  and  $D_{\text{PL}}$  in equation 3.19 are calculated according to the suggestions given in table 3.4<sup>3</sup>.

In order to obtain all wet-gas concentrations  $y_i$ , the concentrations of hydrogen, the inert gases nitrogen and argon and the steam content need to be found first.

The dry-gas equilibrium concentration of steam  $x_{\text{H}_2\text{Oeq,FR}}$  in equation 3.20 is an auxiliary variable that expresses the amount of steam, that was condensed prior to the gas analysis, as a fraction of the total amount of dry gases. The denominator in equation 3.20 – containing all dry-gas species plus steam – is therefore greater than 1.

---

<sup>3</sup> $L = f(U_{\text{AR}})$ ,  $D = 0.01$  and  $D_{\text{PL}} = 0.45$

The hydrogen content can be estimated if it is assumed that the gas inside the fuel reactor is at thermodynamical equilibrium<sup>4</sup>. Under that assumption equations 3.21 is valid.

$$K_{\text{wgs}} = \frac{y_{\text{CO}_2,\text{FR}} \cdot y_{\text{H}_2,\text{FR}}}{y_{\text{CO},\text{FR}} \cdot y_{\text{H}_2\text{O},\text{FR}}} = \frac{x_{\text{CO}_2,\text{FR}} \cdot x_{\text{H}_2,\text{FR}}}{x_{\text{CO},\text{FR}} \cdot x_{\text{H}_2\text{Oeq},\text{FR}}} \quad (3.21)$$

The equilibrium constant  $K$  is defined as the ratio of reaction products and educts for the state where the change of Gibbs free energy for a reaction is zero. In other words, the concentrations of all species stay constant if the driving force for reactions becomes zero. The equilibrium constant is known for any given temperature.

In the fuel mix the amount of hydrogen and carbon atoms appear in a fixed ratio  $(\text{H}/\text{C})_{\text{fm}}$ . If no solid carbon is formed in the fuel line or in the reactor, this ratio applies for the whole system. For pure syngas (50 %  $\text{H}_2$  + 50 %  $\text{CO}$ ) this ratio is 2. If 20 % of steam are added to the syngas (as described in Chap. 3.2.2),  $(\text{H}/\text{C})_{\text{fm}}$  is 2.8. The hydrogen to carbon ratio at the outlet of the fuel reactor is calculated according to equation 3.22.

$$(\text{H}/\text{C})_{\text{fm}} = (\text{H}/\text{C})_{\text{FR}} = \frac{2 \cdot x_{\text{H}_2\text{Oeq},\text{FR}} + 2 \cdot x_{\text{H}_2,\text{FR}}}{x_{\text{CO},\text{FR}} + x_{\text{CO}_2,\text{FR}}} \quad (3.22)$$

The two equations 3.21 and 3.22 can now be solved for  $x_{\text{H}_2,\text{FR}}$  and  $x_{\text{H}_2\text{Oeq},\text{FR}}$ . The concentration of the combined inert gases nitrogen (through dilution) and argon (from the PLs) is calculated according to equation 3.23.

$$x_{\text{N}_2/\text{Ar},\text{FR}} = 1 - x_{\text{CO},\text{FR}} - x_{\text{CO}_2,\text{FR}} - x_{\text{O}_2,\text{FR}} - x_{\text{H}_2,\text{FR}} \quad (3.23)$$

This allows for the calculation of the combustion efficiency (Eq. 3.16). Through equations 3.18–3.23 all flows and concentrations inside the fuel reactor can be expressed. This is necessary in order to analyze and understand the processes in the reactor. Nevertheless, the conclusions that can be drawn are not always clear and distinct.

Another possibility to rate an oxygen carrier is through the *oxygen transfer capacity*  $R_o$ . It expresses the highest theoretic mass change between the state of complete oxidization ( $m_{\text{OC,ox}}$ ) and full reduction is ( $m_{\text{OS,red}}$ ).

---

<sup>4</sup>The conditions for a thermodynamic equilibrium are that the gases are well mixed and that the residence time is much bigger than the reaction rate. A state of sufficient mixture can be generally assumed for gases. The residence time of the combustion gases in the reactor is about 4 s. It is calculated from the reactor volume above the particle bed ( $\approx 0.53 \text{ dm}^3$ ) and the fuel flow at 900 °C ( $2 \text{ L}_n/\text{min}$  corresponds to about  $8.6 \text{ l}/\text{min}$  at 900 °C). This number seems sufficient to assume equilibrium conditions.

$$R_o = \frac{m_{OC,ox} - m_{OC,red}}{m_{OC,ox}} \quad (3.24)$$

The difference between the reduced form of ilmenite ( $\text{FeTiO}_3$ ) and its most oxidized form ( $\text{Fe}_2\text{TiO}_5 + \text{TiO}_2$ ) corresponds to an oxygen transfer capacity of 5%. In order to have a comparison, values for other oxygen carriers are shown in table 3.10.

**Table 3.10.:** Oxygen transfer capacities for different oxygen carrier materials

Oxygen carrier (oxidized / reduced)	Oxygen transfer capacity
Iron ( $\text{Fe}_2\text{O}_3$ / $\text{Fe}_3\text{O}_4$ ) <sup>1</sup>	3.3 %
Nickel ( $\text{NiO}$ / $\text{Ni}$ ) <sup>1</sup>	21.4 %
Copper ( $\text{CuO}$ / $\text{Cu}$ ) <sup>1</sup>	20.1 %
Iron based (F6A, F6AS, F6K, F6KS) <sup>2</sup>	2 %
Nickel based (N6AN) <sup>2</sup>	16 %
Copper based (C6AC) <sup>2</sup>	16 %
Ilmenite ( $\text{Fe}_2\text{TiO}_5 + \text{TiO}_2$ / $\text{FeTiO}_3$ ) <sup>3</sup>	5 %
Iron oxide scales ( $\text{Fe}_2\text{O}_3$ / $\text{Fe}_3\text{O}_4$ ) <sup>3</sup>	3.3 %

<sup>1</sup>... from [32]      <sup>2</sup>... only 60% active material; from [17]  
<sup>3</sup>... from [18]

The oxygen transfer capacity permits the evaluation of the basic suitability of an oxygen carrier. However, that does not mean that it is not always possible or even recommendable to reach that value. Previous experiments have shown that if the oxygen carrier gets reduced until almost reaching the maximum reduction, the combustion efficiency deteriorates significantly [17, 18]. To describe the actual reduction rate, two terms are usually used in the CLC literature: The *degree of oxidation*  $X$  and the *degree of mass-based conversion*  $\omega$ . They are defined according to equations 3.25 and 3.26.

$$X = \frac{m_{OC} - m_{OC,red}}{m_{OC,ox} - m_{OC,red}} \quad (3.25)$$

$$\omega = \frac{m_{OC}}{m_{OC,ox}} \quad (3.26)$$

The current mass of the oxygen carrier ( $m_{OC}$ ) cannot be determined during the operation of the 300 W reactor. Hence, the only way to ascertain the actual reduction is to indirectly infer it from how much oxygen is needed to oxidize the oxygen carrier when the fuel flow is shut off (at the end of each experiment).

### 3.2.4. Results

The processing of data is explained by using the first 160 minutes of operation as an example. During this initial phase ilmenite was reduced for the first time (by a fuel gas). This phase is especially interesting since the reactivity of the ilmenite particles increased considerably. Figure 3.4 shows this phase.

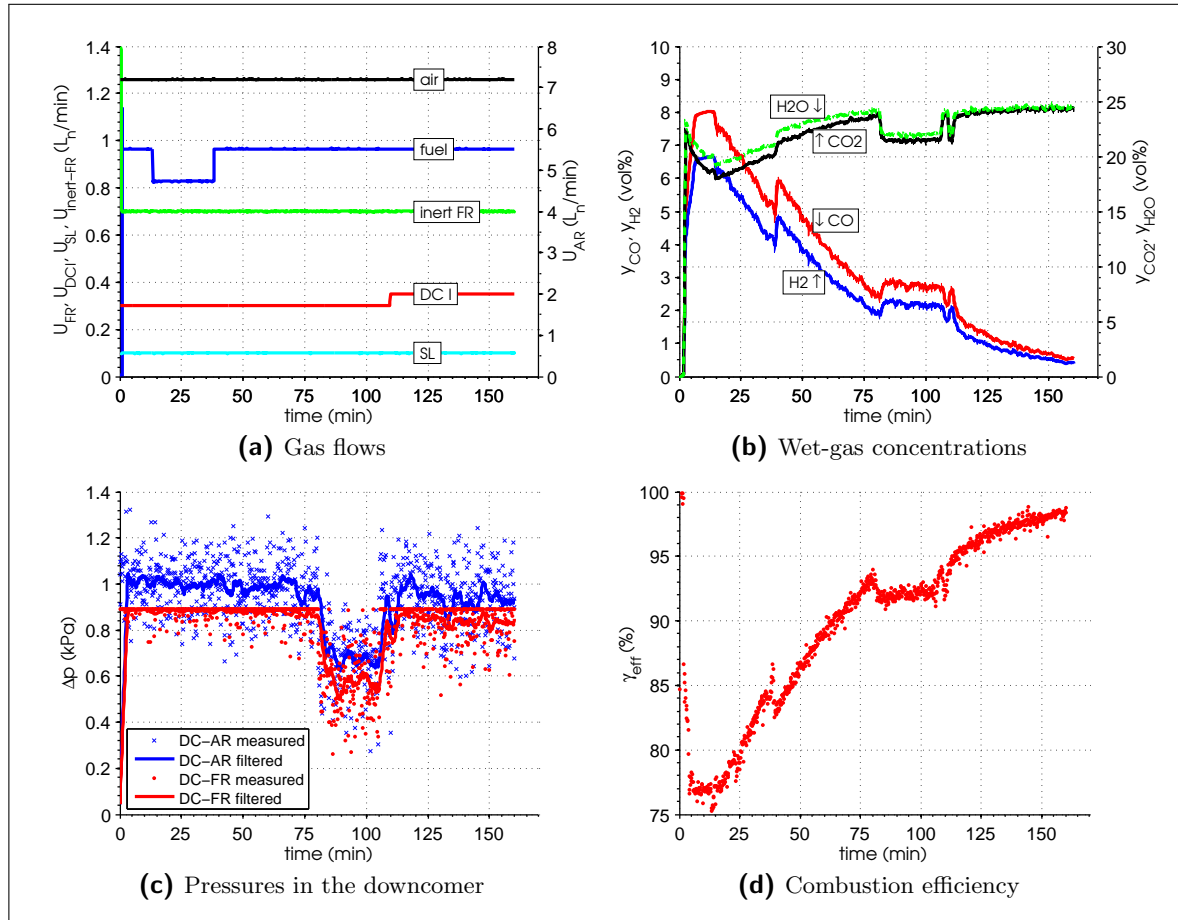


**Figure 3.4.:** Measurements during the initial operational phase with ilmenite particles

It takes a few minutes until the first usable data is obtained. That is due to the fact that the particle circulation and the reactions need a certain time to be established and to become stable. Furthermore, there is a time delay for the gases until they reach the gas analyzers. This time delay effect also occurs when changes to the gas flows are being made: The gas flows are recorded instantaneously, whereas the gases need to pass through the reactor first and then travel through the gas lines to the gas analyzers. This delay is about 2 minutes. During this initial phase not only the fuel gas is led to the fuel reactor, but also a flow of inert gas (“inert FR” in Fig. 3.4a). This was done during the first experimental phase for two reasons. Firstly, the additional flow ensures that, despite the low fuel flow, a sufficient amount of gas gets into the fuel reactor to fluidize the particles there. Secondly, the additional flow of

inert gas dilutes the fuel gas, reducing its partial pressure, which in turn reduces the degree of reduction of the particles and the chemical stress on the particles.

After about 13 minutes the fuel flow was reduced. This was done, because the CO concentration went beyond the measuring range of the instrument. As the particles became more reactive, the CO concentration fell back into the measurable range and the fuel flow was switched back to the original level. This caused a slight drop of the combustion efficiency, since temporarily more fuel gas passed through the reactor without reacting. Henceforward, the efficiency increased continuously until the circulation partly collapsed at about 80 minutes. The pressure drop from the downcomer to both, air and fuel reactor turned out to be good indicators for such break downs (Fig. 3.4c<sup>5</sup>). After the circulation was re-established (by mechanical stimulation and an increase of the downcomer flow DCI), increasingly more fuel was converted into carbon dioxide and water (Fig. 3.4b), and the combustion efficiency increased steadily.

Table 3.11 illustrates what happened to the structure of the particles on a microscopic level. Even though the properties were determined after the first 31 hours, most of the changes are believed to have happened during the first few hours of CLC operation (the particles had been used for 8 h at 900°C for the preliminary leakage experiments), when the reactivity increased considerably.

**Table 3.11.:** Ilmenite particle properties of fresh material and after 31 h of operation

		Fresh particles <sup>1</sup>	Recovered particles <sup>2</sup>
Color		dark gray	brown
Total bed mass (g)		270	264
Bulk density (g/cm <sup>3</sup> )		2.40	1.22
Relative size distribution (—)	45–90 μm	0	0.002
	90–125 μm	0	0.030
	125–180 μm	1	0.433
	180–212 μm	0	0.324
	212–250 μm	0	0.204
	250–355 μm	0	0.004
	> 355 μm	0	0.002

<sup>1</sup>... particles not fully oxidized (⇒ lighter)

<sup>2</sup>... particles fully oxidized (⇒ heavier)

As was being said before, the most drastic change was the reduction of the density of the particles. Most of the particles grew in size and only a minor amount decayed into fines. It cannot be said with certainty how high the amount of particles was, that left the system, because the fresh mineral particles were not fully oxidized and thus were gaining mass during oxidization. The particles that are blown out of the system with the gases are usually mostly fines (< 45 μm). It is believed that 2–7% of the particles escaped from the system in that

<sup>5</sup>The pressure gauge that measures the pressure drop “DC-FR” has a limited measurement range. Hence, the data appears to be constant most of the time.

way.

Even though the properties of the particles changed significantly, they neither formed big agglomerations nor did they decay into fines or dust. This is a positive finding, because it suggests that the particles are structurally stable – at least during the first 31 hours.

Table 3.12 illustrates what happened to the particles during the subsequent 54 hours of operation. About 19% of the particles was lost this time. This share is more than twice as high as before. But then, the total operational time was almost tripled and more longer lasting experiments were performed, which put the particles under a constant stress.

As before, the range of the size distribution of the particles was widened out during the operational time. The main amount of particles was still in the size range of 125–180  $\mu\text{m}$  though. The increasing bulk density can be explained by the fact that the share of smaller particles increased over the experiments. Smaller particles fill out the gaps between the bigger particles and thus increase the bulk density.

**Table 3.12.:** Ilmenite particle properties of used particles after 31 h and 85 h of operation

		Inserted particles <sup>1</sup>	Recovered particles <sup>2</sup>
Color		brown	brown
Total bed mass (g)		135	110
Bulk density ( $\text{g}/\text{cm}^3$ )		1.22	1.54
Relative size distribution (–)	45 – 90 $\mu\text{m}$	0	0.005
	90 – 125 $\mu\text{m}$	0.030	0.104
	125 – 180 $\mu\text{m}$	0.437	0.672
	180 – 212 $\mu\text{m}$	0.327	0.158
	212 – 250 $\mu\text{m}$	0.206	0.046
	250 – 355 $\mu\text{m}$	0	0.005
	> 355 $\mu\text{m}$	0	0.011

<sup>1</sup>... after 31 h of operation

<sup>2</sup>... after 85 h of operation

Figure 3.5 shows scanning electron microscope (SEM) images of the ilmenite particles at different points of the experiments. The structural changes of the particles during the initial operation time can be seen clearly.

The X-ray powder diffraction (XRD) analysis shows the different phases the particles consist of but does not give any information about quantities. As expected, the fresh particles are in a reduced state ( $\text{FeTiO}_3$ ) and there is some hematite ( $\text{Fe}_2\text{O}_3$ ) present. There is no visible difference between the particles after 31 and 85 hours. The oxidized particles consist of pseudobrookite ( $\text{Fe}_2\text{TiO}_5$ ) and titanium dioxide ( $\text{TiO}_2$ ).

The mechanism that is believed to be responsible for the degrading of the particles is that the iron phases become separated from the titanium phases. As can be seen in table 3.10, the relative amount of oxygen that can be carried and released by iron based materials corresponds only to 2 respectively 3.3% of their mass. Ilmenite on the other hand has the ability to carry and release 5%. It has been found that the particles obtain better properties

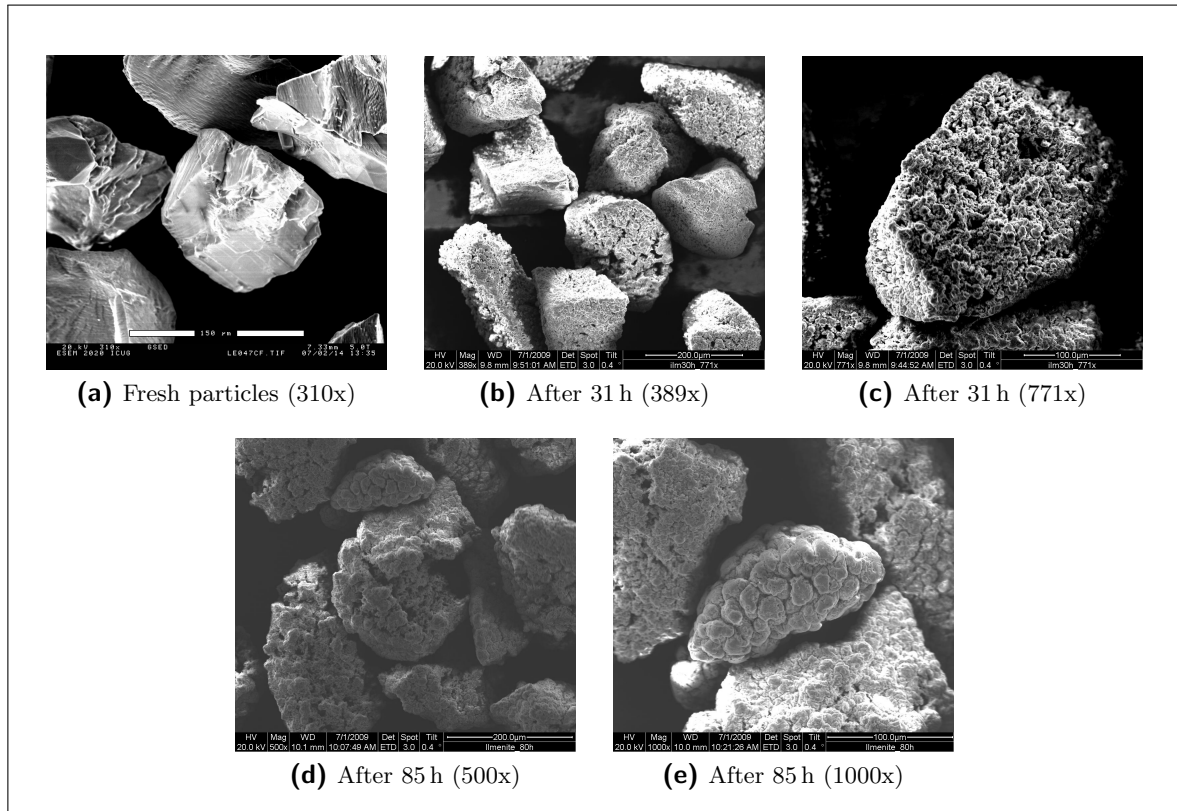


**Figure 3.5.:** SEM images of fresh and used ilmenite particles

if the actual active metal oxides are stabilized by an inert matrix (e.g.  $\text{Al}_2\text{O}_3$ ,  $\text{ZrO}_2$ ,  $\text{TiO}_2$  or  $\text{SiO}_2$ ; [24, 33]). This is believed to be the case naturally for the ilmenite mineral. A separation of phases would mean that this synergy effect is lost and the particles degrade noticeably. The recorded XRD response curves are shown in appendix D.

**Table 3.13.:** XRD analysis of ilmenite particles

Operational phase	Indicated phases
Fresh particles <sup>1</sup>	$\text{FeTiO}_3$ , $\text{Fe}_2\text{O}_3$
After 31 h	$\text{Fe}_2\text{TiO}_5$ , $\text{Fe}_2\text{O}_3$ , $\text{TiO}_2$
After 85 h	$\text{Fe}_2\text{TiO}_5$ , $\text{Fe}_2\text{O}_3$ , $\text{TiO}_2$

<sup>1</sup>. . . from [18]

One of the aims of this work was an investigation of the lifetime behavior of the particles. It would have been desired to determine a set of base parameters in the beginning and to run one long experiment with those settings. However, this was not possible, mainly for three reasons. Firstly, the particle properties changes significantly and using the same settings would not have been suitable or even possible. Secondly, an investigation of how the different parameters influence the process was at least as important as the long term run. And lastly, the degradation of the particles goes along with a lower fuel conversion and thus higher carbon

monoxide concentrations, which could not have been measured with the used gas analyzers. Despite of all the changes, the methodical determination of the base parameters still allows for the different stages of the experiments to be compared – at least to a certain extent.

Figure 3.6 shows all measurements with the base settings for temperature, and air and fuel flow. These base parameters differ in the experiments with 270 g and with 135 g of ilmenite particles. They are described in table 3.6 and 3.8 respectively (Chap. 3.2.2).

Figure 3.6 gives a general overview of the lifetime behavior of the ilmenite particles. At the same time it shows the basic pattern of the different experimental phases: In the first time period (from 0–31 hrs.) the experiments were performed with 270 g of ilmenite particles. The subsequent phase, when only half of those particles were continued to be used, lasted from the 31<sup>st</sup> hour until the end of the experiments (85<sup>th</sup> hr.). Apart from the 58<sup>th</sup> hour, steam was added to the fuel.

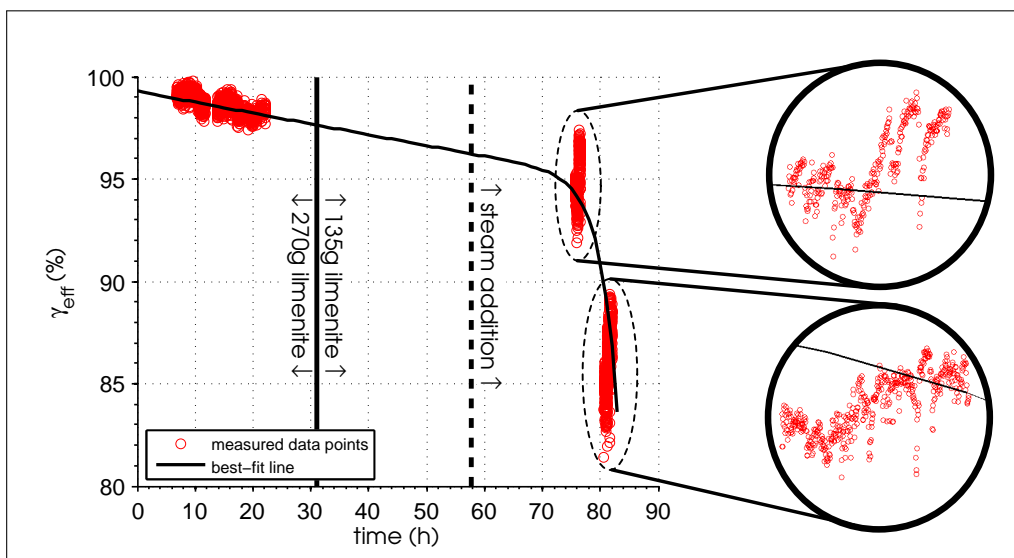


**Figure 3.6.:** Combustion efficiency for ilmenite experiments at base parameters over 85 h of operation

The two most evident changes between the initial period (270 g ilmenite) and the phase in the end (135 g ilmenite with steam addition) are that the conversion got significantly worse and that the variance of the data points increased. The increased variance for the lower bed mass can be explained by the fact that a process with a higher bed mass carries a higher chemical momentum, i.e. it is more robust and not as easily unbalanced as a process with less particles. The worsened conversion simply shows that the particles are somehow “depleted” or “worn out”. The best-fit line, that is drawn through the relatively few data clusters, declines rather constantly throughout the first 70 hours of operation and then drops quite sharply. This suggests that the properties of ilmenite as an oxygen carrier are only good during the first 70 hours of operation (even though the structural integrity is still retained as can be seen in Tab. 3.12 and Fig. 3.5).

Figure 3.7 shows the experimental series when the fuel flow was varied while all other parameters were held constant. It was run from the 17<sup>th</sup> until the 22<sup>nd</sup> hour with 270 g of particles and between hours 68 and 77 with 135 g of particles.

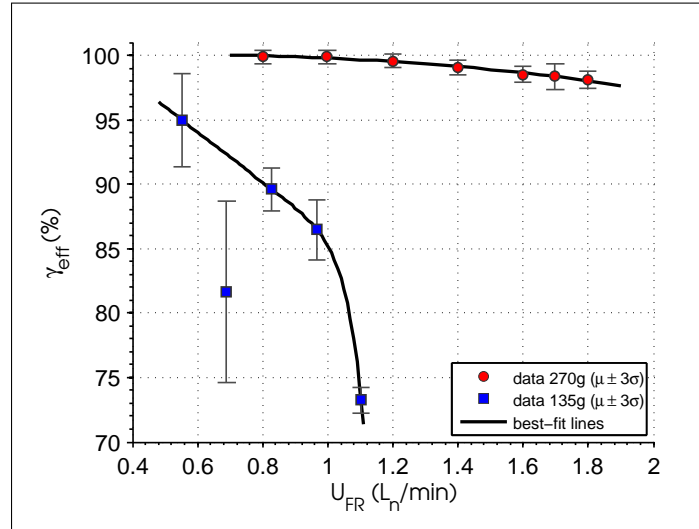


**Figure 3.7.:** Combustion efficiency for ilmenite experiments with varied fuel flow

When the fuel flow is increased, the combustion efficiency for the CLC process with 135 g of ilmenite particles deteriorates sharper than for the process with 270 g. The efficiencies with 270 g of particles lie generally above the ones with fewer particles. The lower efficiency has to be seen with reservations: The experiments with 135 g of ilmenite were performed about 60 operational hours later than the ones with 270 g of particles. The aging process of the ilmenite particles is thus far more advanced and the efficiency is generally deteriorated. The sharper decline of the combustion efficiency though reflects an increased sensitivity towards a change of the fuel flow. More particles make the process more robust against changes of the fuel flow.

The measured data for  $0.69 L_n/\text{min}$  and 135 g of particles does not seem to fit into the pattern of the other measurements. It could be that this specific setting causes a considerable impairment of the process. However, it is more probable that the circulation and/or the reactions were somehow not fully established, even though the pressure measurements did not indicate any anomalies. This would also explain the relatively high variance of that setting.

The experimental series with the temperature being the main parameter is shown in two different ways. In figure 3.8a, the temperature is varied while the other parameters are kept at the base settings (equivalent to Fig. 3.7). Figure 3.8b on the other hand, shows the combustion efficiency over the temperature as well but for a high and a low fuel flow<sup>6</sup>. The experiments were performed between the 20<sup>th</sup> and the 31<sup>st</sup> hour of operation with 270 g of particles and high fuel flow, 17<sup>th</sup> – 29<sup>th</sup> hour for 270 g and low fuel flow and finally 68<sup>th</sup> – 77<sup>th</sup> hour with 135 g at high and low fuel flow.

The two basic findings from the experiments with a varied fuel flow apply also when the temperature is varied: The combustion efficiencies have deteriorated significantly from the

<sup>6</sup>The high fuel flows are  $1.6 L_n/\text{min}$  (270 g of ilmenite) and  $0.69 L_n/\text{min}$  (135 g). The low flows are  $0.8 L_n/\text{min}$  (270 g) and  $0.55 L_n/\text{min}$  (135 g; corresponds to the base value).

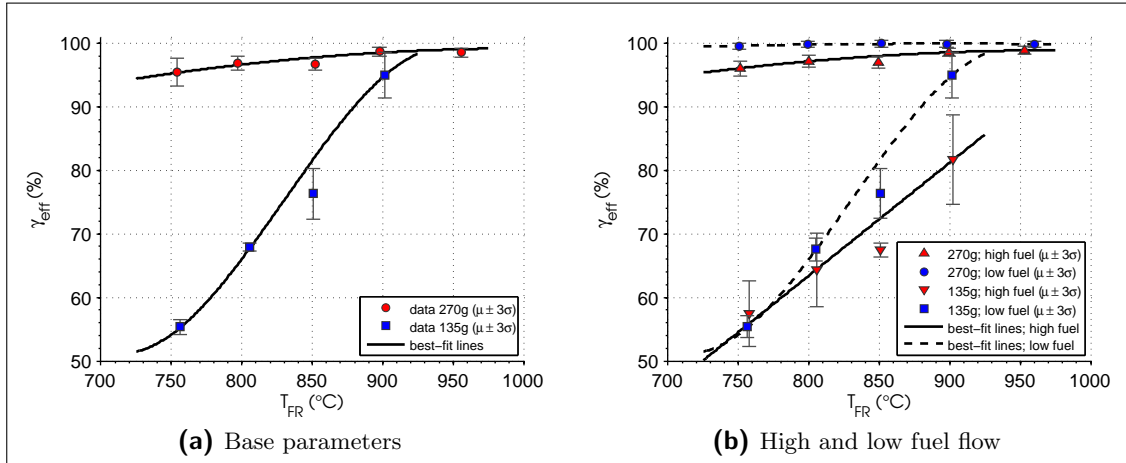


**Figure 3.8.:** Combustion efficiency for ilmenite experiments with varied temperature

experiments with 270 g of ilmenite particles to the ones with 135 g and the process behaves more sensitive towards a change of parameters (here: the temperature).

Over the curve shape of the best-fit lines can be argued, but one detail stands out too regularly to be a random error: In all data series there is a visible deviation of the combustion efficiency at 850°C from the trendline (except for the one with 270 g at a low fuel flow, where the differences between the data points are too marginal to be seen). The experiments series were performed and recorded in a way that makes the possibility of the deviation being a methodical error very improbable<sup>7</sup>. Hence, it can be concluded that most probably something peculiar happens to the process at 850 °C. The reasons are widely unclear though.

A variation of the air flow in the air reactor was only investigated during the last part of the experiments with ilmenite, thus when 135 g of particles were circulated in the reactor (Fig. 3.9). This was the last experiment with ilmenite particles and was performed between the operational hours 77 and 85.

Even though performed when the chemical properties of the ilmenite particles were nearly depleted, the data series with a varied air flow shows a rather regular behavior. The only indication of the well advanced employment of the particles can be seen in the rather large deviations (in comparison to the other test series). The air flow is believed to affect the circulation rate of the particles. A higher circulation means that the average amount of oxidized oxygen carrier particles in the fuel reactor is increased respectively that more oxygen gets into the fuel reactor. Increasing the degree of the mass based conversion  $\omega$  by increasing the air flow means boosting the combustion process.

During the initial part of the experiments (until steam was added to the fuel flow), the phenomenon occurred that the pressure drop over the fuel inlet line increased exponentially

<sup>7</sup>The data series for 135 g and base parameters was recorded consecutively in one day, whereas the series for 270 g was recorded on different days. Between the measurements of the experiments with 270 g and 135 g lie about 60 operational hours respectively 40 days.

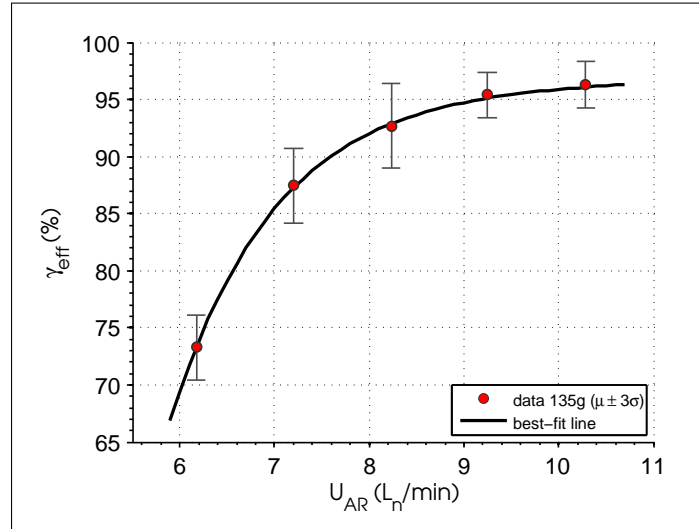


**Figure 3.9.:** Combustion efficiency for ilmenite experiments with varied air flow (only with 135 g of particles)

until the maximum of the pressure sensor was reached (8.2 kPa)<sup>8</sup>. Sometimes the pressure did not increase immediately after the fuel flow was started. The longest it took until the pressure started to increase was about 30 minutes. During the reoxidation of the particles (at the end of each experiment) when air was added to the fuel reactor instead of syngas, significant amounts of carbon dioxide and some minor amounts of carbon monoxide were measured. That led to the conclusion, that solid carbon was formed in the fuel line. The reaction that is believed to be responsible is the Boudouard reaction:



The equilibrium lies on the side of  $\text{CO}_2$  and  $\text{C}$  for low temperatures. However, at low temperatures the reaction kinetics is too slow for the reaction to be significant. From experience the Boudouard reaction is believed to have the strongest impact at around 600 °C. This temperature is reached somewhere in the fuel line, when the fuel is heated from ambient temperature to the reactor temperature (750–950 °C).

The formation of solid carbon is known to be autocatalytic. This means that once the reaction starts, it happens with an increasing rate. This explains the exponential pressure build-up and why it sometimes occurs delayed.

The formation of solid carbon is unwanted for several reasons: It distorts the oxygen consumption during the reoxidation phase and thus prohibits conclusions about the degree of oxidation  $X$  (Eq. 3.25) respectively the degree of mass based conversion  $\omega$  (Eq. 3.26). Fur-

<sup>8</sup>Two pressure sensors were measuring the pressure drop over the fuel inlet: “PT1-dp\_low” and “PT5-FR1”; cf. App. A

thermore, it changes the hydrogen to carbon ratio in the fuel reactor  $(H/C)_{FR}$  (in Eq. 3.22) which in turn causes an error in the calculation of hydrogen and the combustion efficiency. Further, the reaction of carbon and oxygen during the reoxidation phase when air is led to the fuel reactor, is exothermic and could cause thermal damage to certain parts of the fuel inlet.

The amount of carbon that was accumulated in the fuel line (during one representative experiment) was about 0.88 % of the incoming fuel flow<sup>9</sup>. The hydrogen to carbon ratio would thus change from 2.00 to 2.02. This error of 1 % occurred during the first 53 hours of operation until steam was added to the fuel thereby preventing carbon formation and deposition.

Steam is known to have the property of restraining carbon formation. The theoretic equilibrium calculations are shown in appendix C and the effect of the added steam can be seen quite clearly: Apart from about 33 vol% of steam addition (corresponds to about 44 kmol of added steam in App. C.5), the formation of solid carbon should be suspended completely. However, during the first experiments with steam addition it was found that no more carbon was accumulated (i.e. the pressure over the fuel line did not increase anymore and no major amounts of CO<sub>2</sub> were formed during reoxidation) when 20 vol% of steam were added to the fuel.

The degree to what the particles were reduced (degree of mass based conversion  $\omega$ , Eq. 3.26) can only be estimated if the following values are known: The bed mass of the fuel reactor and the amount of oxygen that is consumed in the fuel reactor during the reoxidation. Useful data could only be obtained during the last experiment that was done with ilmenite particles, thus when the particles were noticeably degraded. Despite the advanced degradation, the very last setting before the reoxidation (an increased air flow of 8.2 L<sub>n</sub>/min; cf. Fig. 3.9) boosted the combustion efficiency to 92.5 % – a value that could not be reached at this point anymore with the base parameters. In order to obtain a representative value for the level of reduction, the process should have been run with the base settings.

The bed mass in the fuel reactor was measured indirectly when the reactor was opened (see App. B.2) and amounted to about 21 g. The consumed oxygen can be derived from the data during the reoxidation phase and was about 0.53 g. The resulting degree of mass based conversion  $\omega$  is thus 97.5 % ( $X = 50.5$  %). This number lies well within the expected range of 95–100 %, but the uncertainty is quite high and the data was obtained when the process was boosted and thus running better than would have been normal after this amount of operational hours. Hence, it can be concluded that the degree of mass based conversion is quite high respectively that the oxygen transfer capacity is not fully utilized anymore. This does not explain why the particles become degraded but shows how the degradation occurs.

---

<sup>9</sup>Experiment on 03/19/2009 (pressure build-up occurred right from the beginning): During the combustion phase of the experiment, which lasted a total time of 332 min, about 554 L<sub>n</sub> of syngas passed into the fuel reactor. This corresponds to about 136 g of solid carbon. During the subsequent reoxidation phase, about 2.21 L<sub>n</sub> of CO<sub>2</sub> (and no CO) were formed in the fuel reactor, which corresponds to about 1.19 g of solid carbon.

### 3.2.5. Conclusions

During the initial first few hours, the ilmenite particles became more porous, grew noticeably in size and experienced a reduction in bulk density. This led to an increase of the surface, which in turn increased the reactivity of the particles. This trend was then reversed during the following tens of hours when the particles slowly became smaller and less reactive again. Responsible for that could be attrition or shrinking of the particles. The decay was most likely caused by both, mechanical friction and continuous chemical stress.

The theoretically needed bed mass for complete combustion is probably lower than both bed masses that were investigated in this work (270 g and 135 g). However, the amount of bed mass in the reactor is rather derived from circulation properties than from chemical requirements. It was found that a higher bed mass makes the process more stable and not as sensitive to a change of parameters.

The combustion efficiency can be improved by raising the reactor temperature, decreasing the fuel flow and/or increasing the air flow. For all these parameters there exists an upper point though where the efficiency levels out.

By adjusting different parameters, the process can still be boosted to high efficiencies, even when the particles are noticeably degraded. But although high efficiencies are reached, the initial mass based conversion is not reached anymore. That means that the degradation of the particles occurs as a noticeable loss of the oxygen transfer capacity.

As a continuation of this investigation, the particles should be analyzed further. The assumption that the particles properties degraded significantly could be checked by comparing the reaction rates of the used particles to the ones of “fresh” particles. The “fresh” particles should not be completely fresh though, but have undergone a few hours of operation so that the initial structural change already took place.

## 3.3. Iron oxide scales

### 3.3.1. Background

Iron oxide scales (IOS) is a waste product from the steel industry, which is produced during the rolling of steel sheets. Just as ilmenite, this material is available in large amounts and cheap. Detailed calculations or reliable estimations of available quantities are rather complex to carry out and have not been done in this work.

An X-ray powder diffraction (XRD) analysis that has been done earlier to analyze the particle phases [30], showed that “fresh” and used IOS basically consist of hematite ( $\text{Fe}_2\text{O}_3$ ). This is the oxidized form of the material, which in the CLC process is reduced to magnetite ( $\text{Fe}_3\text{O}_4$ ). Further reduction to wüstite ( $\text{FeO}$ ) or even metallic iron ( $\text{Fe}$ ) is possible, but inadvisable for two reasons: Firstly, because full conversion to carbon dioxide can thermodynamically not be reached anymore [32, 34]. Secondly, because those reduced phases are known to have a high tendency to form agglomerations [35–37].

Iron oxide scales come as small scales in undefined size ranges. It is fully oxidized but contaminated with oil. The first step to make this material usable as oxygen carrier is heat treatment to get rid of the oil: The material is heated to 950 °C and kept at this temperature for about six hours. That way all the oil is burnt away. The downside to this procedure is that the particles partially agglomerate. In order to obtain particles in a suitable size range, it is necessary to grind the particles, sieve them and make a selection. The term *fresh* in the context of IOS particles means that the particles underwent this treatment but have not been in operation in any reducing/oxidizing process.

The initial particle batch is a mix of fresh and used particles. The particle properties are summarized in table 3.17.

IOS particles have been investigated thoroughly in a batch fluidized-bed reactor with methane ( $\text{CH}_4$ ) and syngas ( $\text{CO}/\text{H}_2$ ) as fuels [30]. During those experiments IOS particles proved to have good conversion rates for both fuel types but failed to reach stable reactivity. Overall, they looked promising though. As a continuation to those investigations, there have been some unpublished experiments in the 300 W reactor with IOS particles and methane as fuel. Those experiments did not turn out to be very successful. The problems were initially suspected to be due to an unsuitable reactor design. But even a change in the design did not lead to satisfactory results. Some of the difficulties are expected to be overcome when syngas is used as fuel gas.

### 3.3.2. Experimental procedure

The experimental procedure resembles that of the ilmenite particles to a large extent. The gases that are used in the reactor are the same as before with the only exception that steam has been used from the very beginning (cf. Tab. 3.5 in Chap. 3.2.2).

The base parameters for the IOS experiments have been found in the same way as has been done for the preceding ilmenite experiments. They are summarized in table 3.14.

**Table 3.14.:** Base parameters for experiments with IOS particles

$U_{FR}$ ( $L_n/min$ )	$U_{AR}$ ( $L_n/min$ )	$U_{DCI}$ ( $L_n/min$ )	$U_{DCII}$ ( $L_n/min$ )	$U_{SL}$ ( $L_n/min$ )	$T_{FR}$ ( $^{\circ}C$ )	Corresponding power (W)
1.10	7.2	0.14	0.21	0.1	900	210

The main problem that occurred with the IOS particles was that they formed big hard agglomerations in the fuel reactor. Those agglomeration typically covered the whole area of the fuel reactor and had a few gas canals that still allowed the fuel gas to enter the reactor. When those agglomeration were formed however, the process got significantly worse and grew unstable. The reactor then had to be opened and the agglomeration to be removed mechanically. Since the agglomerated particles could not be used any further, they had to be replaced by fresh material. This circumstance inhibited a life time study of the particles to a large extent.

During the first 17 hours of operation (two charges of IOS particles), no usable data could be obtained at all. Only with the third charge of particles, a series of tests with varying parameters could be performed. And even after running the whole test series successfully, some minor agglomeration was found in the fuel reactor: covering the whole area, but only a few millimeters high and below the edge of the slot wall. Hence, it is believed that this agglomeration – regardless of when it formed – did not affect the CLC process significantly.

The series of experiments, that is summarized in table 3.15, was performed when part of the IOS particles had been in operation for 17 hours. The whole test series lasted about 14 hours. After that the influence of the steam addition was investigated for another 6 hours.

**Table 3.15.:** Settings and parameters for each test of the test series with IOS particles

Test number	$U_{FR}$ ( $L_n/min$ )	$U_{AR}$ ( $L_n/min$ )	$U_{DCI}$ ( $L_n/min$ )	$U_{DCII}$ ( $L_n/min$ )	$U_{SL}$ ( $L_n/min$ )	$T_{FR}$ ( $^{\circ}C$ )	Corresponding power (W)
G1	0.55 – 1.93	7.2	0.14	0.21	0.1	900	110 – 380
G2	1.10	4.1 – 10.3	0.14	0.21	0.1	900	210
G3	0.55 – 1.65	7.2	0.14	0.21	0.1	800	110 – 320
G4	0.55 – 1.65	7.2	0.14	0.21	0.1	850	110 – 320
G5	0.55 – 1.65	7.2	0.14	0.21	0.1	950	110 – 320

“G” stands for the Swedish term of IOS: Glödskal

### 3.3.3. Analysis

The analysis has been performed exactly the same way as for the experiments with ilmenite as oxygen carrier (Chap. 3.2.3). No further calculations were necessary.

### 3.3.4. Results

IOS particles show an increase of reactivity during the initial operating period. This increase is displayed in figure 3.10. However, this “initial” phase was not recorded during the very first experiments with the IOS particles, but after they had been in operation for 17 hours already. Prior to this phase, the reactor had been opened due to an agglomeration of particles in the fuel reactor (see App. B.4). The agglomerated piece was no longer utilizable and thus had to be replaced by fresh particles (about 28 % of the whole fill was replaced). It was those particles that caused this initiation effect.

Figure 3.10 shows a steady increase of the reactivity without any noteworthy disturbances. If this effect is extrapolated to 100 % of fresh particles, the magnitude of the reactivity increase should be quite comparable to that of fresh ilmenite particles.

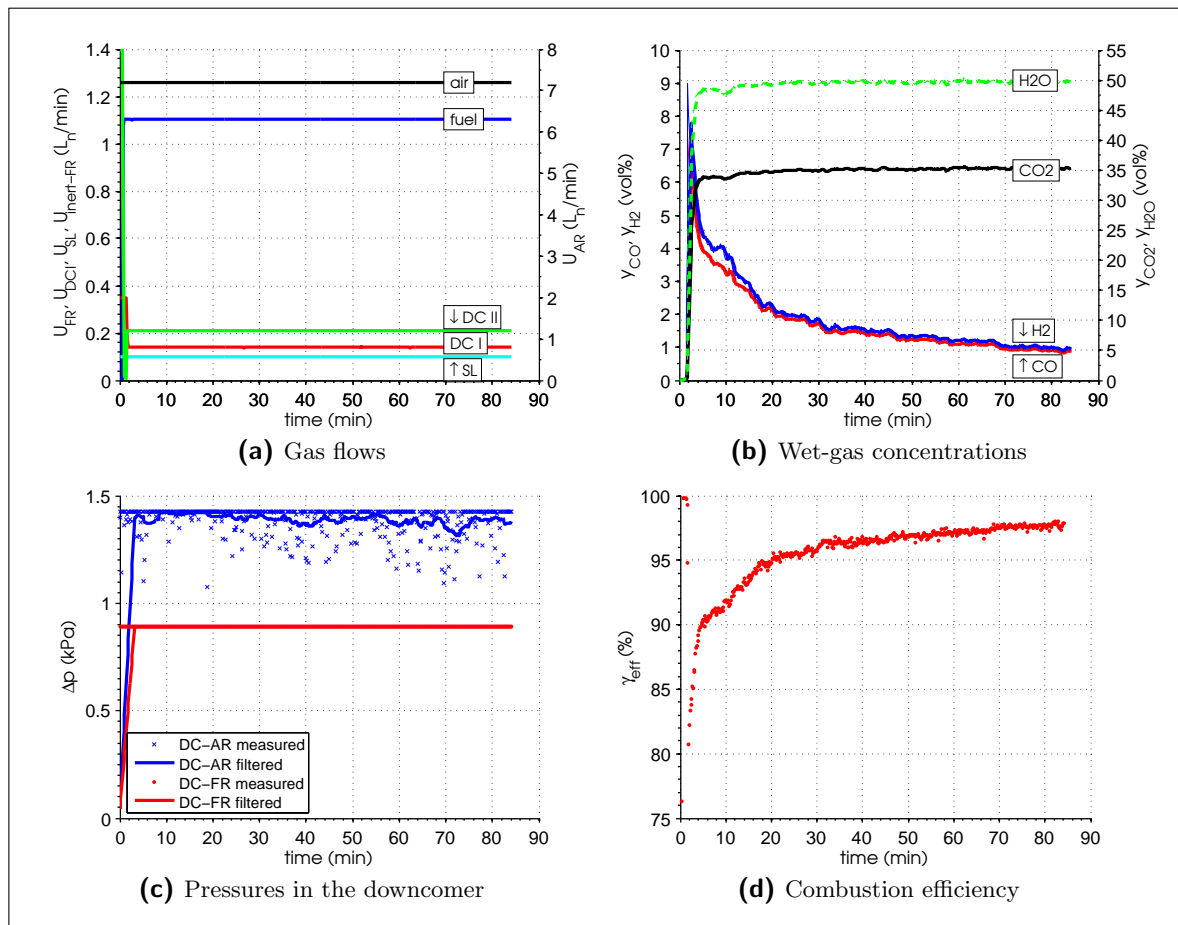


**Figure 3.10.:** Measurements during the initial operational phase with IOS particles

After this first experiment, about 0.53 g of oxygen were consumed to reoxidize the particles. The mass of the particle bed in the fuel reactor at this time is estimated to be 161 g (the bed height in App. B.5 is taken as a reference, because it is closest to a non-agglomerated state). The resulting degree of mass based conversion  $\omega$  is 99.7 % ( $X = 90.0$  %). Table 3.16 shows

the reference numbers of the reduction  $\omega$  and  $X$  after different numbers of operational hours. The level of reduction does not change significantly and is generally quite low. The only captured exception – when the particles were reduced slightly further – was the reduction of the particles at 950°C. The recorded degrees of mass based conversion stay well below the theoretical maximum reduction of 96.7% ( $R_o = 3.3\%$ ). A low degree of reduction indicates that particles in the reactor were circulating at a fast rate.

**Table 3.16.:** Reduction reference numbers  $\omega$  and  $X$  for the IOS experiments

Operational phase	Consumed oxygen <sup>1</sup>	Bed mass	$\omega$	$X$	Previous setting <sup>2</sup>
@ 18.5 h	0.53 g	161 g	99.7 %	90.0 %	–
@ 22 h	0.75 g	161 g	99.5 %	85.9 %	–
@ 26 h	0.53 g	161 g	99.7 %	90.0 %	$U_{AR} = 4.1 \text{ L}_n/\text{min}$
@ 30.5 h	1.03 g	161 g	99.4 %	80.6 %	$T_{FR} = 950^\circ\text{C}$
@ 33 h	0.71 g	161 g	99.6 %	86.4 %	no steam addition
@ 37 h	0.48 g	161 g	99.7 %	90.8 %	$U_{FR} = 1.65 \text{ L}_n/\text{min}$ ; no steam addition

<sup>1</sup>... during the reoxidation phase

<sup>2</sup>... only if differing from base parameters

As indicated in table 3.17, about 6% of the particles escaped the system as fines and the particle size distribution shifted slightly towards smaller diameters. This shifting could be the reason for the slight increase of the density as smaller particles would fill out the gaps between the bigger ones.

During the last part of the experiments (the last 20 hrs.), the changes to the particles became more noticeable. As can be seen in table 3.18, the density was significantly reduced and the ratio of smaller particles increased considerably: 9% of the initial particles charge left the system as fines and a total of 34% was ground to sizes below 90  $\mu\text{m}$ . Particularly interesting about the change of density is that it happened after most of the particles had been in use for a considerable amount of operational hours. Two possibilities seem plausible to explain this circumstance: It could either be that the reduction and oxidization during the first 17 hours did not happen consequently enough to cause an initiation process to the particles whatsoever (no major structural change at all during the first period). The alternative explanation is that the increase of reactivity happens uncoupled from the decrease of density or is heavily distorted by severe attrition. Even though thinkable, the second possibility is more unlikely though, because usually an increase of reactivity is attributed to an increase of the reactive surface. That on the other hand happens as the particles swell and/or grow porous. However, the available results do not allow for drawing unequivocal conclusion.

The experiments still show clearly that the IOS particles are not only likely to form agglomerations, but also have a rather low structural integrity and become pulverized after a quite limited operational period.

Figure 3.11 shows some selected SEM images of IOS particles at different states. It can clearly be seen that the particles change from a solid bulky form (Fig. 3.11a) to a thin flaky one (Fig. 3.11b and 3.11c). It does not require much imagination to believe that those flakes have a greater reactive surface but are quite fragile. This supports the earlier observation in

**Table 3.17.:** IOS particle properties of fresh material and after 17 h of operation

		Fresh particles	Recovered particles
Color		dark gray with a touch of red	dark gray
Total bed mass (g)		270	198.9 <sup>1</sup>
Bulk density (g/cm <sup>3</sup> )		2.40	2.48
Relative size distribution (—)	45–90 μm	0	0.010
	90–125 μm	0.149	0.193
	125–180 μm	0.468	0.517
	180–212 μm	0.383	0.265
	212–250 μm	0	0.013
	250–355 μm	0	0.002
	> 355 μm	0	0.001

<sup>1</sup>... additionally: 54.2 g agglomerations

table 3.18, that a major amount of the particles has decayed into fines. The XRD analysis shows that there is no visible difference in the chemical structure between fresh material and the used particles: The main component is hematite ( $\text{Fe}_2\text{O}_3$ ) with some minor amounts of quartz ( $\text{SiO}_2$ ), which is suspected to be an impurity from the steel making process (it was also found in minor amounts in [30]).

The structural change of the IOS particles is quite comparable to the one of ilmenite particles, whereas the ilmenite particles have a higher stability. Unlike the ilmenite particles, the IOS particles were heat-treated prior to the CLC experiments. However, the structural change of the ilmenite particles is strongly believed to be connected to the continuous reduction/oxidization of the CLC process rather than to thermal exposure. A distinct change of the density of the IOS particles during the initial oxidation/reduction cycles did either not happen at all or it happened, but the particles decayed in such a short time span (which cause the density to increase again) that it was not noticed. This second scenario seems more likely, for it would explain the peculiarities of IOS particles more throughout.

Some very interesting results can be obtained from the analysis of a piece of agglomerated particles, since agglomeration was a constant problem during the experiments. Figure 3.11e shows the edge of one of the gas canals that were formed (on the left side of the image). Closest to that canal the surface has a very smooth structure, almost like the particles there completely melted on and then solidified again. The shape of individual particles can no longer be recognized. A little further away from the gas canal (Fig. 3.11f), the structure looks slightly different: It is still possible to make out the shapes of individual particles, but it seems like they are covered by a layer of something that bound them together. The XRD analysis shows that all known oxidation states of iron are present. From reduced to oxidized, those are:  $\text{Fe} \rightarrow \text{FeO} \rightarrow \text{Fe}_3\text{O}_4 \rightarrow \text{Fe}_2\text{O}_3$ .

The agglomeration of particles might have been triggered by a partly defluidization in the fuel reactor: Being defluidized, they could have become too far reduced and thus agglomerated.

**Table 3.18.:** Used IOS particle properties after 17 h and 37 h of operation

		Inserted particles	Recovered particles
Color		dark gray	dark gray
Total bed mass (g)		270	237.8 <sup>1</sup>
Bulk density (g/cm <sup>3</sup> )		2.51	1.60 (1.40) <sup>2</sup>
Relative size distribution (–)	45–90 μm	0	0.280
	90–125 μm	0.189	0.141
	125–180 μm	0.471	0.317
	180–212 μm	0.340	0.168
	212–250 μm	0	0.087
	250–355 μm	0	0.007
	> 355 μm	0	0

<sup>1</sup>... additionally: 7.6 g agglomerations

<sup>2</sup>... with (without) fines (< 90 μm)

Agglomerated pieces are even harder to fluidize than regular particles which might have catalyzed the process even more. That would explain how and why such big agglomerations were formed.

**Table 3.19.:** XRD analysis of IOS particles

Operational phase	Indicated phases
Fresh particles <sup>1</sup>	Fe <sub>2</sub> O <sub>3</sub>
After 37 h	Fe <sub>2</sub> O <sub>3</sub> (+ SiO <sub>2</sub> )
Agglomeration	Fe, FeO, Fe <sub>3</sub> O <sub>4</sub> , Fe <sub>2</sub> O <sub>3</sub>

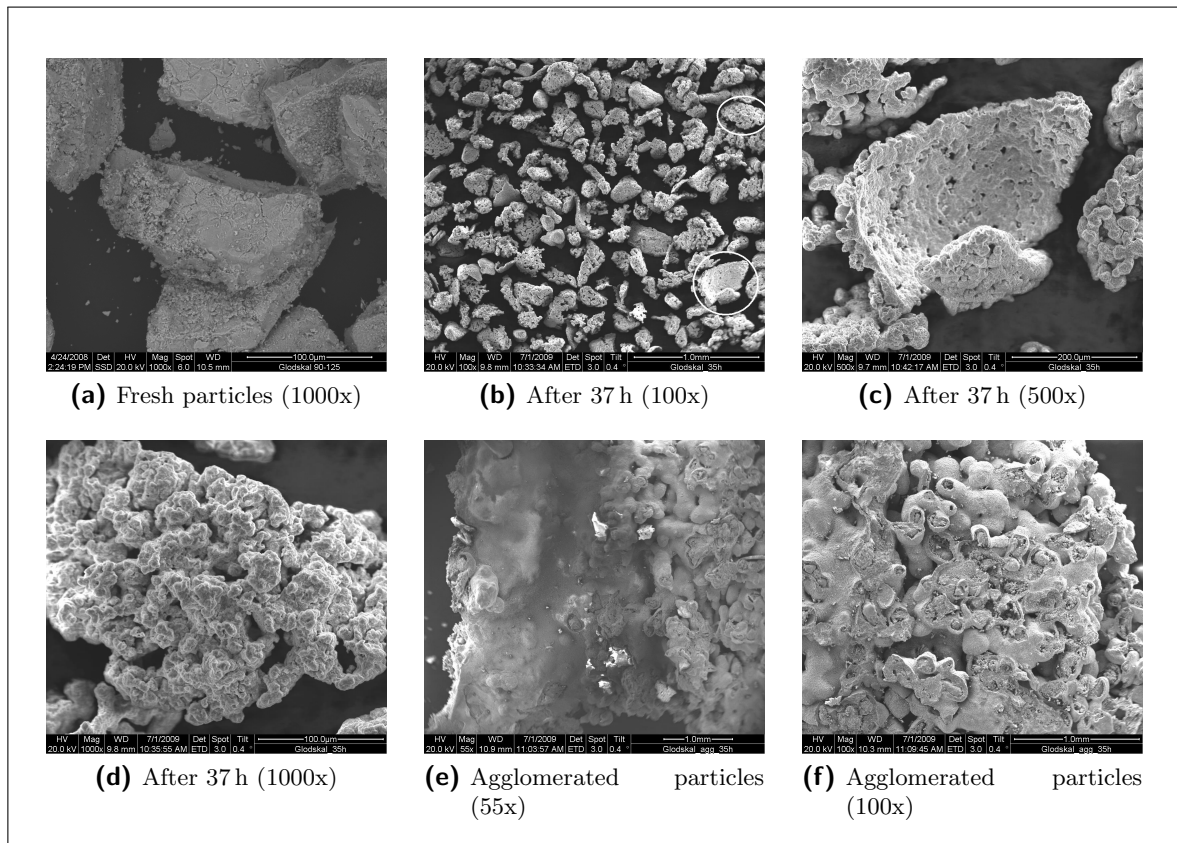
<sup>1</sup>... from [18]

Figure 3.12 shows the experiments where the fuel flow was varied. The general tendency is that the more fuel is used, the higher the share of unconverted fuel gets. Hence, the combustion efficiency drops.

What can be seen in figure 3.13 is a variation of the temperature in the reactor. It was varied from the base setting of 900 °C between the limits of 800 °C and 950 °C.

The expected behavior – that the process improves with higher temperatures – cannot be seen very clearly. Three factors distort the picture: First, the fuel flow was generally too low which caused a nearly complete fuel conversion most of the time (the horizontal parts of the graphs in Fig. 3.13). A generally higher flow would have reduced the fuel conversion (the resulting higher CO concentrations might not have been measurable though) and shown the sensitivity of the process toward a change of temperature more clearly.

Secondly, a dip of the efficiency can be observed at 850 °C for all flow levels in figure 3.13. This has been observed earlier during the discussion of the results of the experiments with ilmenite particles (cf. Chap. 3.2.4). Now, that this effect has occurred with different oxygen carrier materials at different gas flows, the effect stands out more clearly. However, a distinct



**Figure 3.11.:** SEM images of fresh, used and agglomerated IOS particles

interpretation cannot be made at the moment.

The third peculiarity, that strikes out clearly, is the decline of the combustion efficiency above 900 °C. One explanation for that could simply be that the circulation was not completely established during the experiments at 950 °C. As can be seen in table 3.15, the experiments at 950 °C (G5) were the last of the test series and they were all performed consecutively. The agglomeration in the fuel reactor could have formed just before those particular experiments and thus distorted the whole test. An argument against this scenario is the fact that experiments with a varied steam addition were performed subsequently (on a different day though), with results that are comparable to earlier experiments.

Despite the fact that the graphs in figure 3.13 do not seem to show a clear picture, it can be concluded that a higher temperature increases the fuel conversion up to 900 °C. It cannot be said with certainty though, whether the lower fuel conversion at 950 °C was due to a retarded circulation or was caused by characteristic behavior of the particles. The latter is more probable but in order to be certain, further investigation is necessary.

The variation of the airflow that has been performed with the IOS particles (G2 in Tab. 3.15) did not produce much valuable information. The fuel conversion seemed to have reached a maximum, so that a variation of the airflow did not boost or degrade the process. A higher

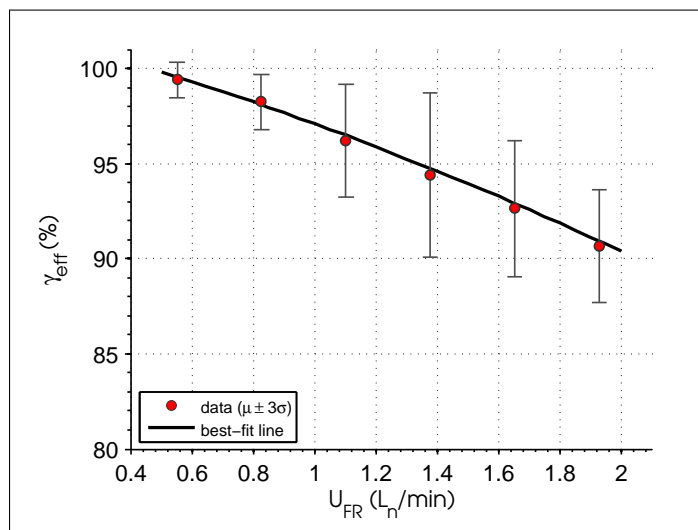


**Figure 3.12.:** Combustion efficiency for IOS experiments with varied fuel flow

fuel flow would have implicated a higher share of unconverted fuel and hence given a clearer picture.

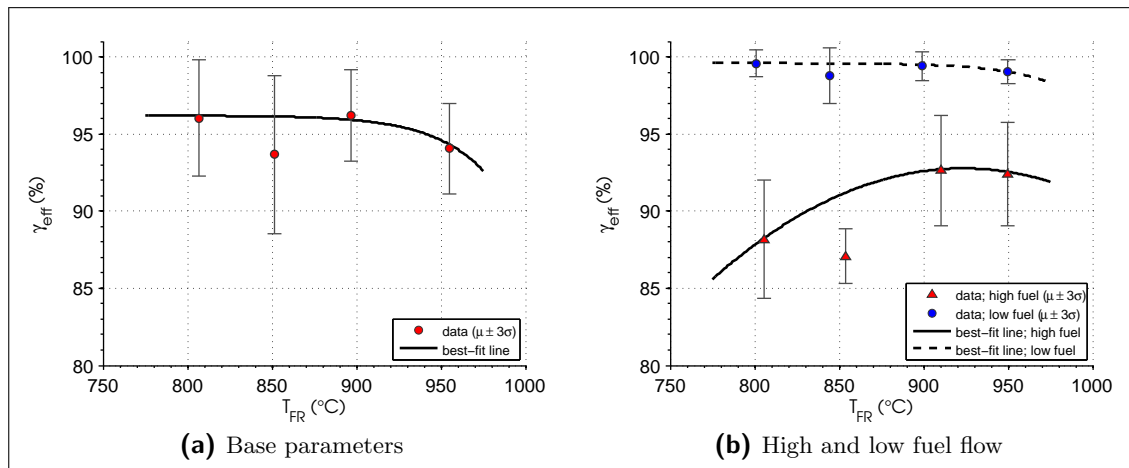


Figure 3.13.: Combustion efficiency for IOS experiments with varied temperature

### 3.3.5. Conclusions

Running CLC experiments with IOS particles is possible, but its employment remains a delicate matter and is accompanied by severe problems. The nature of the problems was different from the ones during earlier experiments in the batch reactor though. The tendency to agglomerate is expected not to have such fatal consequences in bigger reactor systems. The high level of attrition on the other hand will persist. If scaled-up CLC reactor systems are to be operated with IOS particles for longer time spans, the necessary amount of make-up feed will be rather high in comparison to other oxygen carrier materials.

The life time of IOS particles is relatively short and limited rather by a structural decay than by a chemical depletion. It remains unknown whether the particles become significantly bigger during the initial operational phase (accompanied with a density reduction) and then break down very fast or whether the reactive particle surface is increased without any effect on size and density. Further investigations would be needed in order to bring more clarity.

One factor that could be responsible for the initial problems with the IOS particles could be the use of an unsuitable fluidization velocity during the determination of the base parameters. This could have caused improper fluidization and poor mixing, thus reducing certain particles further which eventually caused agglomerations. The fluidization properties only became better after the structure of the particles changed partly. This speculation could be checked by comparing the fluidization velocities of fresh and used particles.

It cannot be said with certainty what caused the lower fuel conversion at 950 °C. If IOS particles are to be used for further experiments – possibly in bigger reactor systems – this effect should be kept in mind and its origins should be investigated.

Furthermore it was found that a lower fuel flow and a higher temperature generally have a positive effect on the fuel conversion. Even though the same could not be shown explicitly for an increased air flow, it is assumed to have the same effect as could be shown for the experiments with ilmenite particles: Increasing the airflow has a direct influence on the circulation which in turn delivers more oxygen to the fuel reactor. Thus the conversion can be increased until a maximum is reached.

## 4. Conclusions

Ilmenite particles generally worked quite well over a long operating period. They are structurally stable and have good fluidization properties. Overall, ilmenite particles produced very promising results.

Initially the particles underwent a considerable alteration process during which they grew bigger, more porous and as a result became more reactive. After this initiation period they were stable in matters of structural stability and reactivity for tens of hours. After about 70 hours of operation, the reactivity of the particles decreased sharply. However, a corresponding drastic structural change was not noticed.

During the course of the experiments it happened a few times that the particles were reduced very far over significant time periods. Those were the only incidents when ilmenite was found to form agglomerations. However, those agglomerations were rather soft and are believed to be of negligible significance - especially when the process is scaled up.

In order to affirm the deterioration of the reactivity of the ilmenite particles, it should be analyzed again with a more sophisticated method. The reactivity of the used ilmenite particles should be compared directly the one of fresh particles (such that already have undergone the initiation phase). This could for instance be done in a batch reactor with more defined reducing/oxidization conditions.

Employing iron oxide scales as an oxygen carrier for chemical-looping combustion, turned out to be possible but implicated some difficulties.

The biggest problem that was encountered during the experiments was that the particles formed agglomerated chunks in the fuel reactor and thus deteriorated or even inhibited fluidization and circulation conditions. The agglomerations are believed to originate from particles that are reduced too far. That could either be the case if the residence times in the fuel reactor is generally too long (too low global circulation), if particles are trapped in zones of poor circulation (wall or corner effects) or if the general mixing level in the fuel reactor is not sufficient. All three error sources can be controlled in bigger reactor systems. Furthermore, the possibility that agglomerations can form which cover the whole reactor area is quite low. Agglomeration as an error source should be possible to control or suppress as the reactor systems get bigger.

The rate of attrition is noticeably higher than for other materials. This requires a higher make-up feed and counteracts the reduction of the running costs. On the other hand iron oxide scales are a by-product from the steel rolling industry and thus are rather cheap - much cheaper than synthesized oxygen carriers.

There are still circumstances which remain unknown and can only be speculated about. Most of the unknown concerns the structural changes of the particles, the fluidizing conditions and the structural decay. Identifying those facts and narrowing down the possibilities is the first

step towards understanding the behavior of the particles and thus make processes more predictable.

The conclusion regarding iron oxide scales particles is that it is generally possible to use them for a chemical-looping process.

With comparable settings and about the same bed mass, the fuel conversion with ilmenite particles was clearly better than with IOS particles. The full oxygen transfer capacity of both materials was far from being reached though.

When syngas was used as a fuel, it was found that it caused a deposition of solid carbon in the hot part of the fuel line. This could be overcome by adding steam to the fuel.

Another effect whose origins could not be made out was that the general tendency towards higher levels of fuel conversion at higher temperatures was locally reversed at 850 °C. This peculiarity has not been observed before and its origin is unknown at this point.

The ability to only measure rather low carbon monoxide concentrations is very constraining when experiments are to be run with syngas. As a consequence, the parameters can only be varied in a limited bandwidth, which makes the results hard or impossible to interpret.

It could be shown that a chemical-looping combustion process with the materials ilmenite and iron oxide scales is possible. Employing minerals and by-product materials as oxygen carriers is a considerable step towards reducing the running costs of a power plant with chemical-looping technology and thus making it more competitive against the existing energy producing technologies. Using syngas as a fuel is an indirect step towards the combustion of solid fuels, for syngas is the main product from the gasification of solid fuels (e.g. coal or biomass).

Even though both materials were found to be feasible oxygen carriers, they have different characteristics that result in different applications.

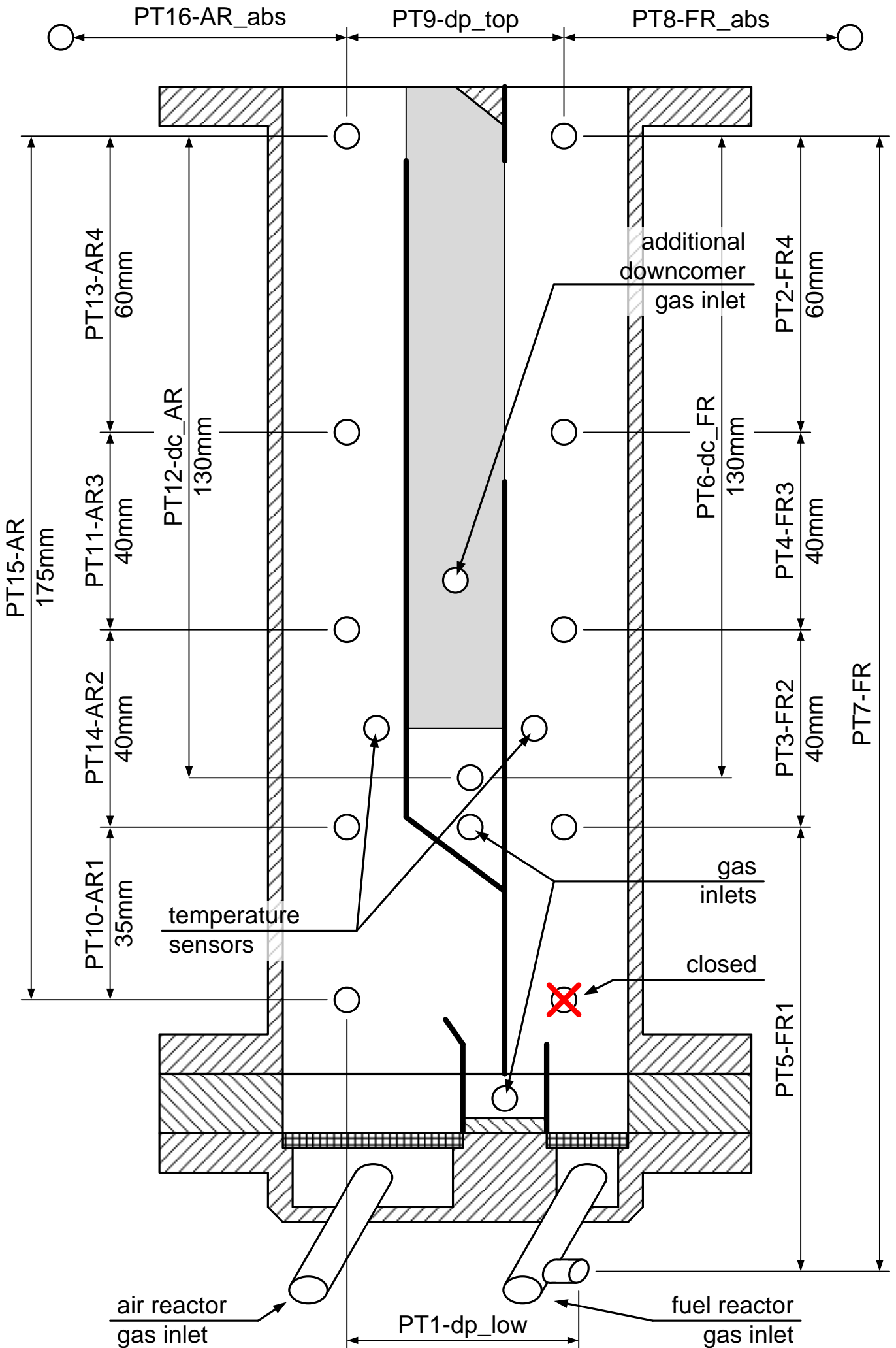
# Bibliography

- [1] Clive Ponting. *A New Green History of the World: The Environment and the Collapse of Great Civilisations*. Penguin Books, London, UK and New York, NY, USA, 2007.
- [2] IPCC. *Climate Change 2007 - Impacts, Adaptation and Vulnerability: Working Group II contribution to the Fourth Assessment Report of the IPCC*. Cambridge University Press, Cambridge, UK and New York, NY, USA, September 2007.
- [3] IPCC. *Climate Change 2007 - The Physical Science Basis: Working Group I Contribution to the Fourth Assessment Report of the IPCC*. Cambridge University Press, Cambridge, UK and New York, NY, USA, September 2007.
- [4] IPCC. *Climate Change 2007 - Mitigation of Climate Change: Working Group III contribution to the Fourth Assessment Report of the IPCC*. Cambridge University Press, Cambridge, UK and New York, NY, USA, September 2007.
- [5] United Nations Conference on Environment and Development. Article 2. In *United Nations Framework Convention on Climate Change*, June 1992. URL [http://unfccc.int/essential\\_background/convention/background/items/1353.php](http://unfccc.int/essential_background/convention/background/items/1353.php).
- [6] Ottmar Edenhofer. Minderung und Anpassung: Kosten und Strategien des globalen Klimaschutzes - Sustainable Solutions: Research Domain III of the Potsdam Institute for Climate Impact Research. Lecture, April 2008. Global Challenges – Klimawandel.
- [7] Bruce C. Douglas. Chapter 3 Sea level change in the era of the recording tide gauge. In Bruce C. Douglas, Michael S. Kearney, and Stephen P. Leatherman, editors, *Sea Level Rise - History and Consequences*, volume 75 of *International Geophysics*, pages 37–64. Academic Press, 2001. doi: 10.1016/S0074-6142(01)80006-1.
- [8] Robert Steven Nerem, Éric Leuliette, and Anny Cazenave. Present-day sea-level change: A review. *Comptes Rendus Geoscience*, 338(14-15):1077–1083, 2006. doi: 10.1016/j.crte.2006.09.001. La Terre observée depuis l’espace.
- [9] Gerhard Fischer and Urs Wälterlin. Angst vor dem Untergang. *Süddeutsche Zeitung*, October 25, 2006. URL <http://www.sueddeutsche.de/wissen/384/325249/text/>.
- [10] Kevin A. Baumert, Timothy Herzog, and Jonathan Pershing. *Navigating the Numbers: Greenhouse Gas Data and International Climate Policy*. World Resources Institute, Washington DC, USA, 2005. URL <http://www.wri.org/publication/navigating-the-numbers>. WRI Working Paper.

- [11] Timothy Herzog. *Navigating the Numbers: Greenhouse Gas Data and International Climate Policy*. World Resources Institute, Washington DC, USA, July 2009. URL <http://www.wri.org/chart/world-greenhouse-gas-emissions-2005>. WRI Working Paper; updated version of the chart "World Greenhouse Gas Emissions in 2005".
- [12] Energy Information Administration - Official Energy Statistics from the U.S. Government. International Energy Annual 2006, 2009. URL <http://www.eia.doe.gov/emeu/international/contents.html>. [Online; accessed: 06-July-2009].
- [13] H. J. Richter and K. F. Knoche. Reversibility of combustion processes. *ACS Symposium Series*, 235:71–85, 1983.
- [14] Y.-O. Chong, D. J. Nicklin, and P. J. Tait. Solids exchange between adjacent fluid beds without gas mixing. *Powder Technology*, 47:151–156, 1986.
- [15] Anders Lyngfelt, Bo Leckner, and Tobias Mattisson. A fluidized-bed combustion process with inherent CO<sub>2</sub> separation; application of chemical-looping combustion. *Chemical Engineering Science*, 56:3101–3113, 2001.
- [16] D. Kunii and O. Levenspiel. *Fluidization engineering*. Butterworth–Heinemann, Boston, MA, USA, 2<sup>nd</sup> edition, 1991.
- [17] Paul Cho, Tobias Mattisson, and Anders Lyngfelt. Comparison of iron-, nickel-, copper-, and manganese-based oxygen carriers for chemical-looping combustion. *Fuel*, 83:1215–1225, 2004.
- [18] Henrik Leion. *Capture of CO<sub>2</sub> from solid fuels using Chemical-Looping Combustion and Chemical-Looping Oxygen Uncoupling*. PhD thesis, Chalmers University of Technology, Göteborg, Sweden, 2008.
- [19] Magnus Rydén, Anders Lyngfelt, and Tobias Mattisson. Chemical-looping combustion and chemical-looping reforming in a circulating fluidized-bed reactor using Ni-based oxygen carriers. *Energy & Fuels*, 22:2585–2597, 2008.
- [20] Anders Lyngfelt, Marcus Johansson, and Tobias Mattisson. Chemical-Looping Combustion – Status of Development. In *9th International Conference on Circulating Fluidized Beds (CFB-9)*, Hamburg, Germany, May 2008.
- [21] B. Kronberger, E. Johansson, G. Löffler, T. Mattisson, A. Lyngfelt, and H. Hofbauer. A two-compartment fluidized bed reactor for CO<sub>2</sub> capture by chemical-looping combustion. *Chemical Engineering & Technology*, 27(12):1318–1326, 2004. doi: 10.1002/ceat.200402137.
- [22] A. Abad, T. Mattisson, A. Lyngfelt, and M. Rydén. Chemical-looping combustion in a 300 W continuously operating reactor system using a manganese-based oxygen carrier. *Fuel*, 85:1174–1185, 2006.
- [23] E. Johansson, T. Mattisson, A. Lyngfelt, and H. Thunman. Combustion of syngas and natural gas in a 300 W chemical-looping combustor. *Chemical Engineering Research and Design*, 84(A9):819–827, 2006.

- [24] A. Abad, T. Mattisson, A. Lyngfelt, and M. Johansson. The use of iron oxide as oxygen carrier in a chemical-looping reactor. *Fuel*, 86:1021–1035, 2007.
- [25] *Improved construction of 300 W unit*. Chalmers University of Technology, Göteborg, Sweden, 2007. Cachet deliverable 1.2.3, revision 1.
- [26] Magnus Rydén. *Ny mellanbit till 300 W CLC-reaktor*. Chalmers University of Technology, Göteborg, Sweden, 2007.
- [27] Eva Johansson, Tobias Mattisson, Anders Lyngfelt, and Hilmer Thunman. A 300 W laboratory reactor system for chemical-looping combustion with particle circulation. *Fuel*, 85:1428–1438, 2006.
- [28] U.S. Geological Survey. Mineral Commodity Summary 2009 - Titanium mineral concentrates, 2009. URL <http://minerals.usgs.gov/minerals/pubs/mcs/>. [Online; accessed: 17-July-2009].
- [29] Henrik Leion, Anders Lyngfelt, Marcus Johansson, and Erik Jerndal Tobias Mattisson. The use of ilmenite as an oxygen carrier in chemical-looping combustion. *Chemical Engineering Research and Design*, 86:1017–1026, 2008.
- [30] Henrik Leion, Tobias Mattisson, and Anders Lyngfelt. Use of Ores and Industrial Products As Oxygen Carriers in Chemical-Looping Combustion. *Energy & Fuels*, 23:2307–2315, 2009.
- [31] Magnus Rydén, Marcus Johansson, Eric Cleverstam, Anders Lyngfelt, and Tobias Mattisson. Ilmenite with addition of NiO as oxygen carrier for chemical-looping combustion. submitted for publication, 2009.
- [32] E. Jerndal, T. Mattisson, and A. Lyngfelt. Thermal analysis of chemical-looping combustion. *Chemical Engineering Research and Design*, 84(A9):795–806, 2006.
- [33] J. Adánez, L. F. de Diego, F. García-Labiano, P. Gayán, and A. Abad. Selection of oxygen carriers for chemical-looping combustion. *Energy & Fuels*, 18:371–377, 2004.
- [34] Marcus Johansson, Tobias Mattisson, and Anders Lyngfelt. Investigation of  $\text{Fe}_2\text{O}_3$  with  $\text{MgAl}_2\text{O}_4$  for chemical-looping combustion. *Industrial & Engineering Chemistry Research*, 43:6978–6987, 2004.
- [35] P. Cho, T. Mattisson, and A. Lyngfelt. Defluidization conditions for a fluidized bed of iron oxide-, nickel oxide-, and manganese oxide-containing oxygen carriers for chemical-looping combustion. *Industrial & Engineering Chemistry Research*, 45(3):968–977, 2006.
- [36] Marcus Johansson. *Screening of oxygen-carrier particles based on iron-, manganese-, copper- and nickel oxides for use in chemical-looping technologies*. PhD thesis, Chalmers University of Technology, Göteborg, Sweden, 2007.
- [37] Nicolas Berguerand and Anders Lyngfelt. Design and operation of a 10 kW<sub>th</sub> chemical-looping combustor for solid fuels – Testing with South African coal. *Fuel*, 87:2713–2726, 2008.

## **A. Reactor cross-section with gas inlets and measuring points**



○ ... pressure sensor if not labeled otherwise

## **B. Measured particle levels and properties during and after the experiment sets**

## B.1: Particle properties after 31h (2009/03/27)

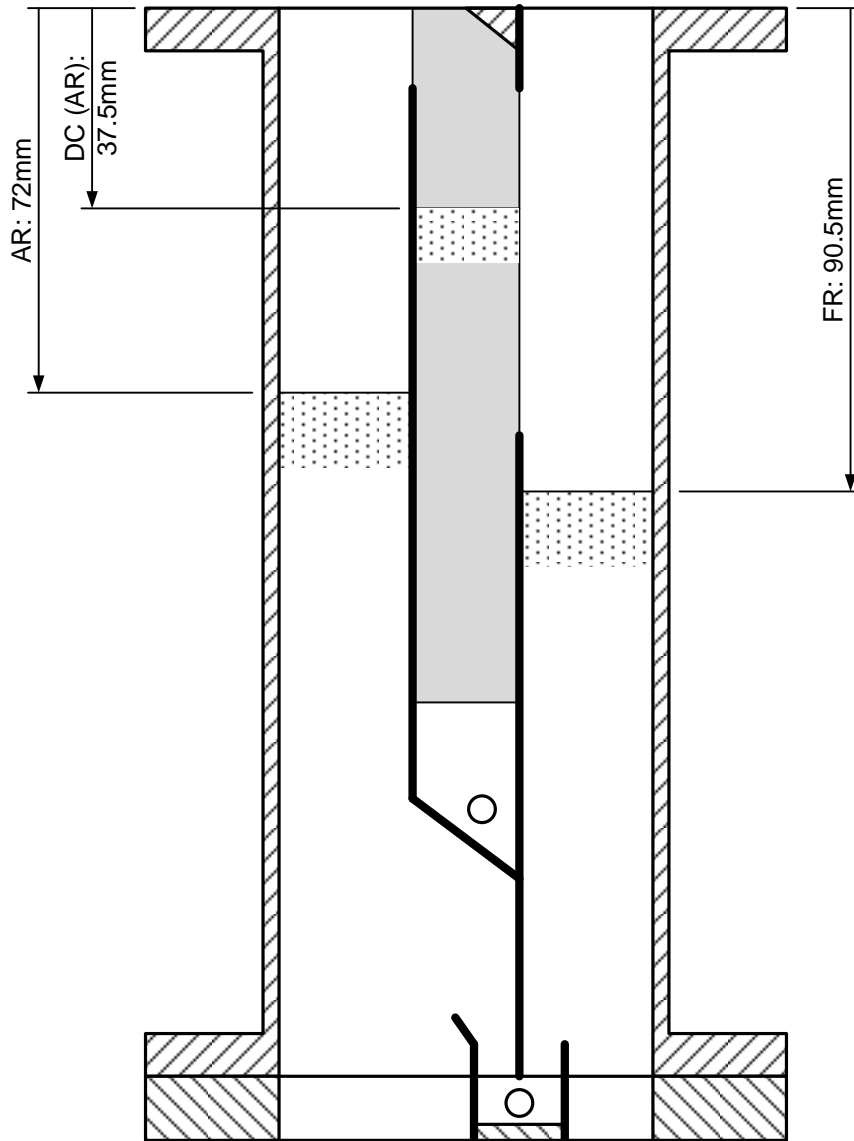
Material: Ilmenite

Initial mass: 270g (partly oxidized)

Initial bulk density:  $2.40\text{g/cm}^3$

Current mass: 264g (fully oxidized)

Current bulk density:  $1.22\text{g/cm}^3$



## B.2: Particle properties after 81h (2009/05/06)

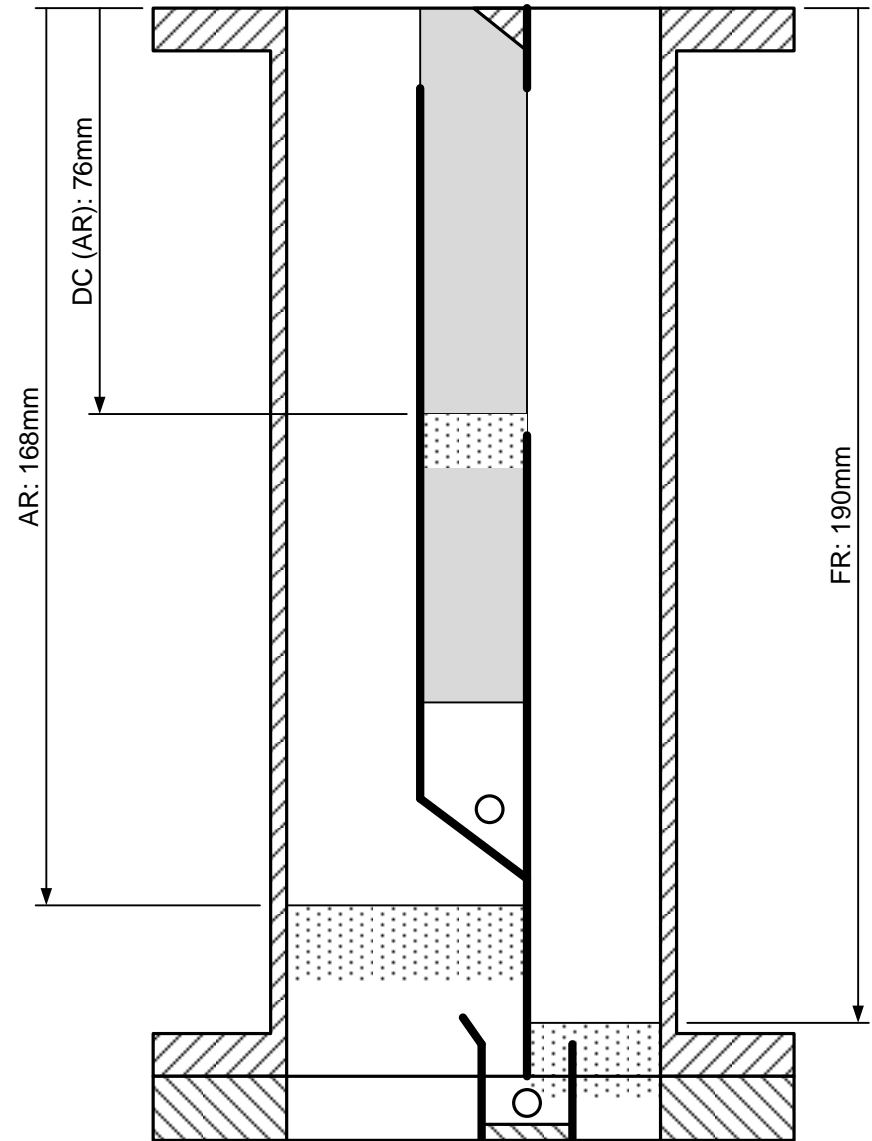
Material: Ilmenite

Initial mass: 130g (fully oxidized)

Initial bulk density:  $1.22\text{g/cm}^3$

Current mass: 130,5g (fully oxidized)

Current bulk density:  $1.54\text{g/cm}^3$



### B.3: Particle properties after 5h (2009/05/21)

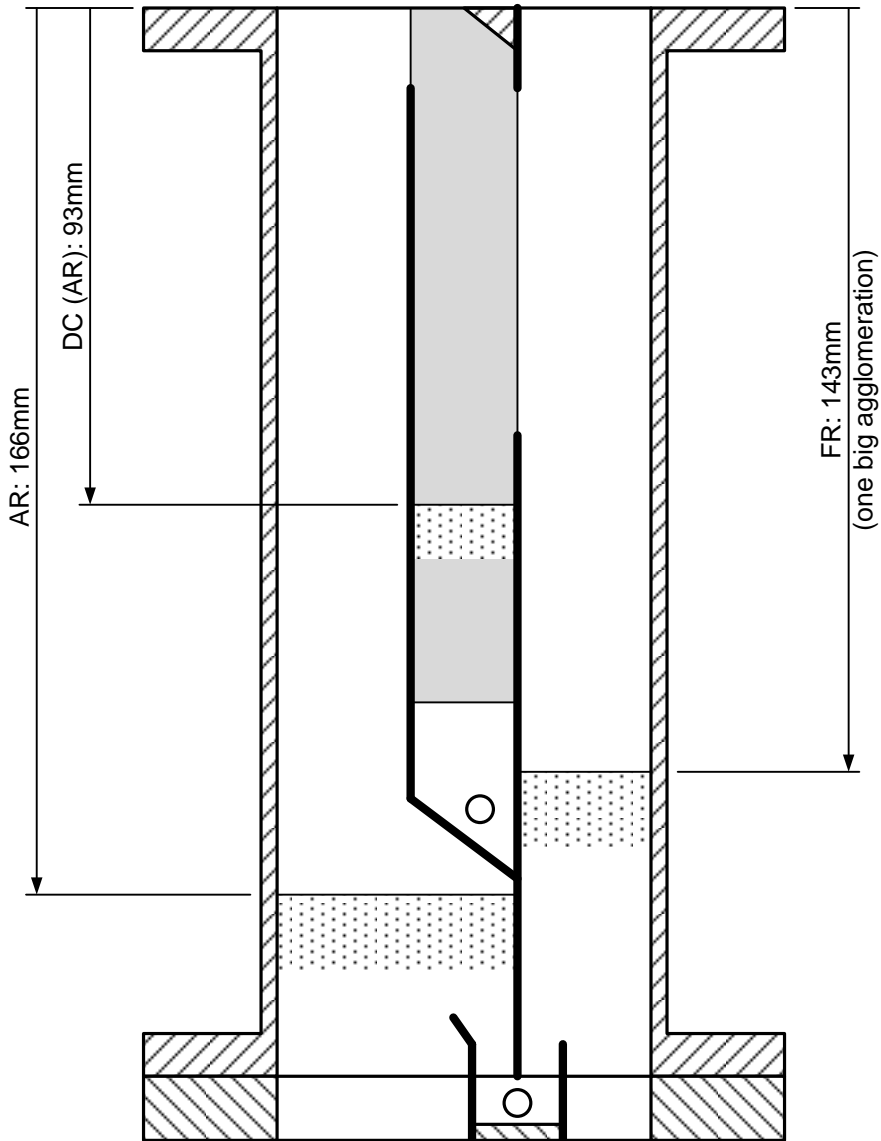
Material: Glödskal

Initial mass: 270g

Initial bulk density: 2,28g/cm<sup>3</sup>

Current mass: 238g (158g loose + 80g agglomerations)

Current bulk density: 2.36g/cm<sup>3</sup>



### B.4: Particle properties after 18.5h (2009/06/01)

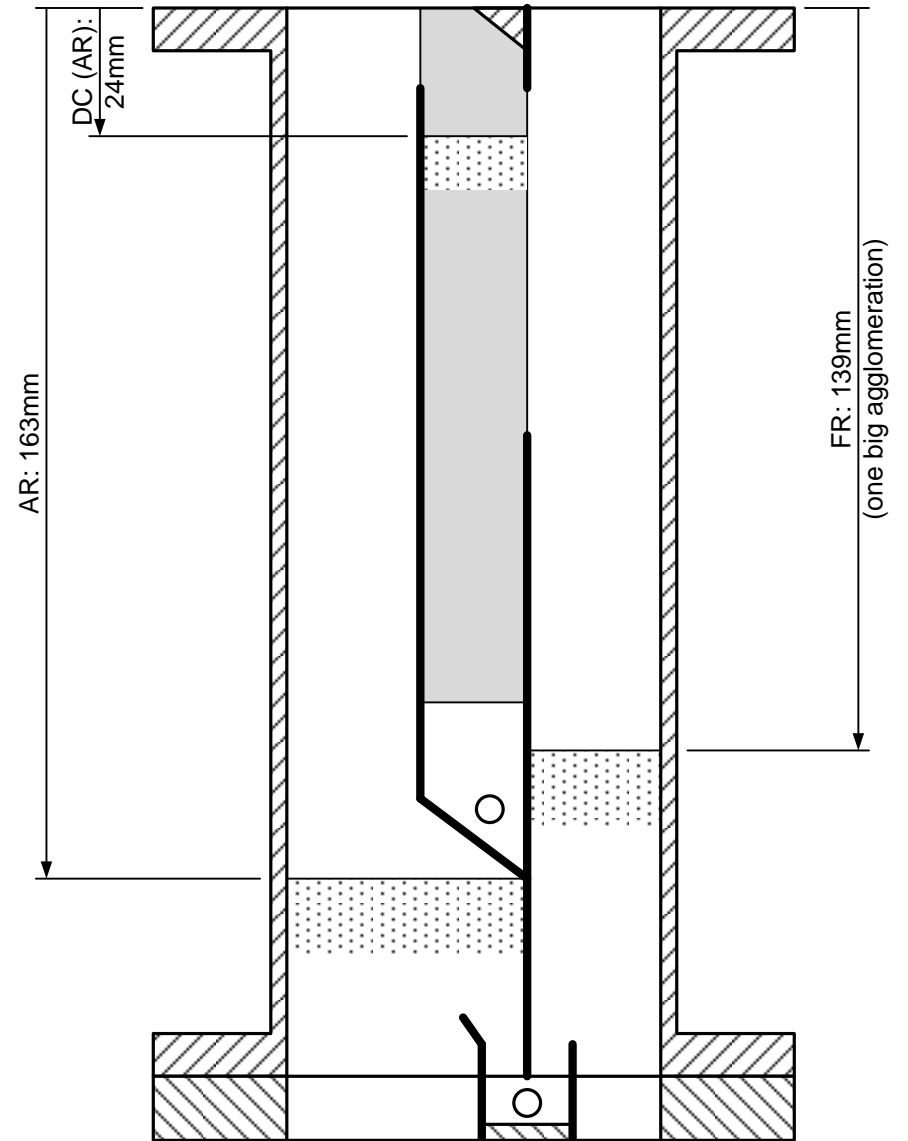
Material: Glödskal

Initial mass: 270g

Initial bulk density: 2,26g/cm<sup>3</sup>

Current mass: 253.1g (198.9g loose + 54.2g agglomerations)

Current bulk density: 2.48g/cm<sup>3</sup>



# B.5: Particle properties after 37h (2009/06/12)

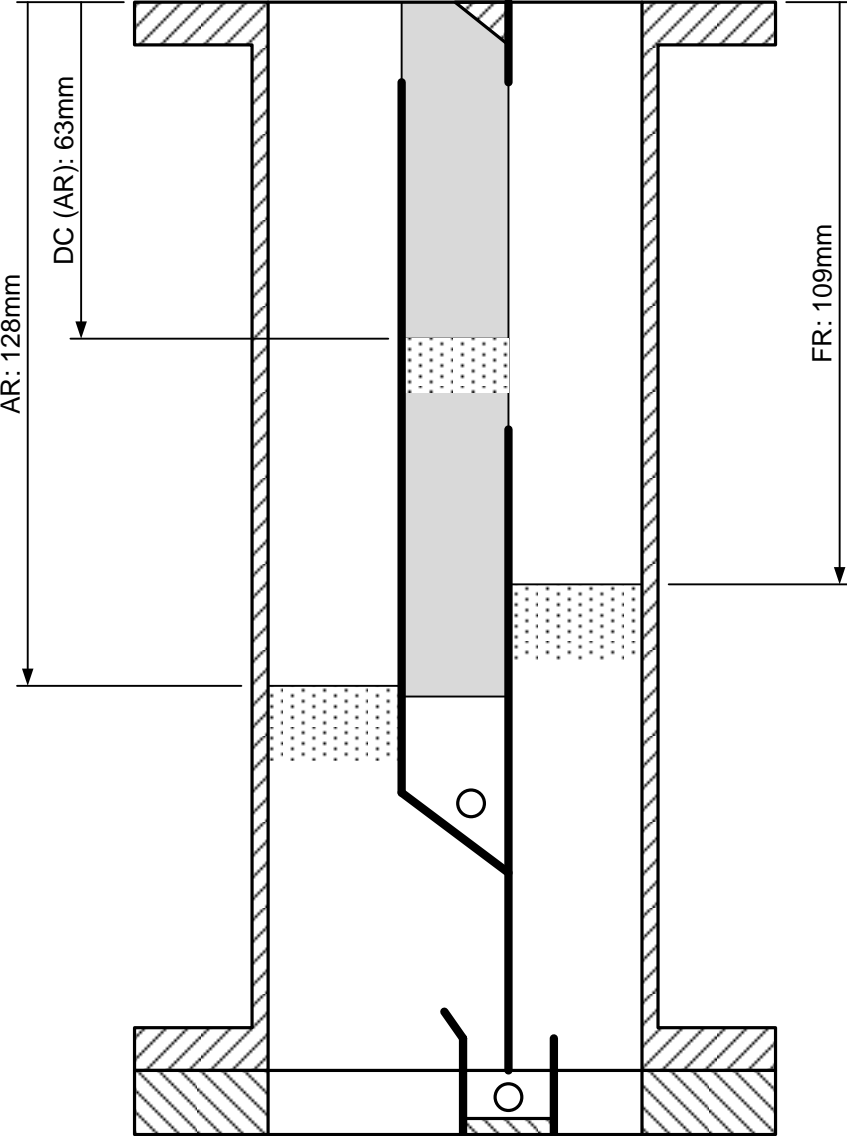
Material: Glödskal

Initial mass: 270g

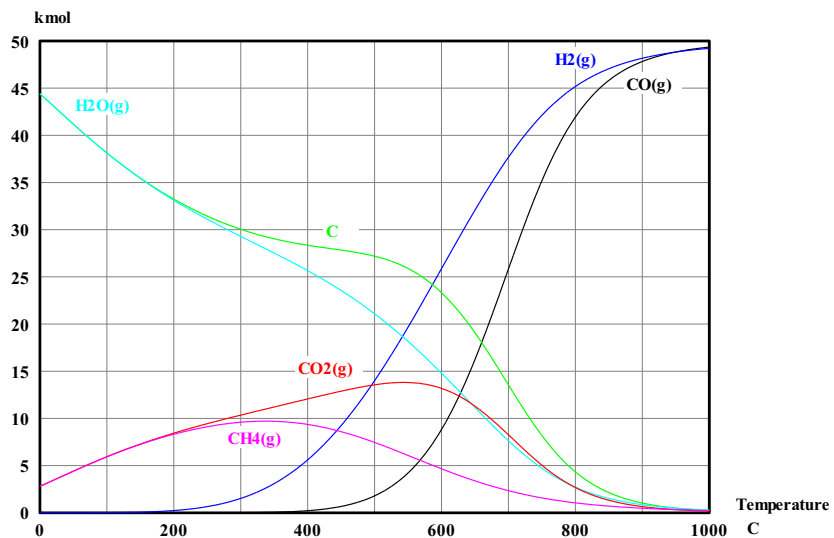
Initial bulk density: 2,51g/cm<sup>3</sup>

Current mass: 245,4g (237,8g loose + 7,6g agglomerations)

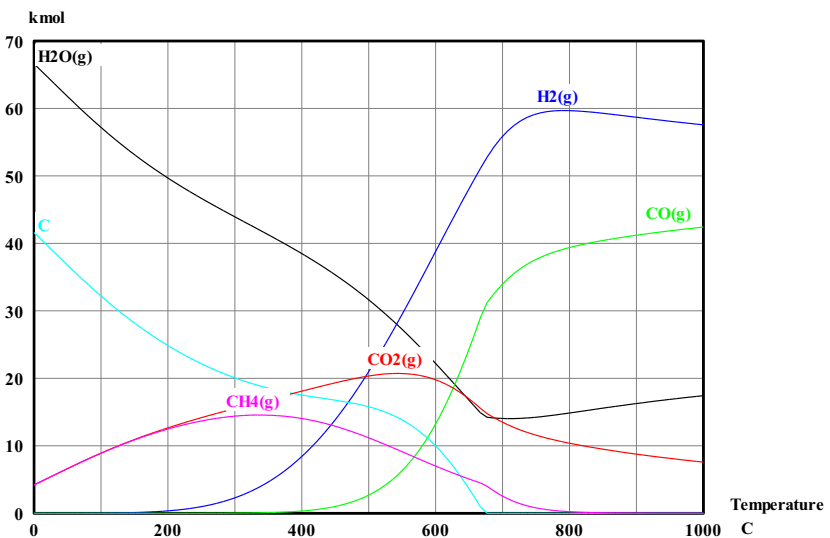
Current bulk density: 1.60g/cm<sup>3</sup>



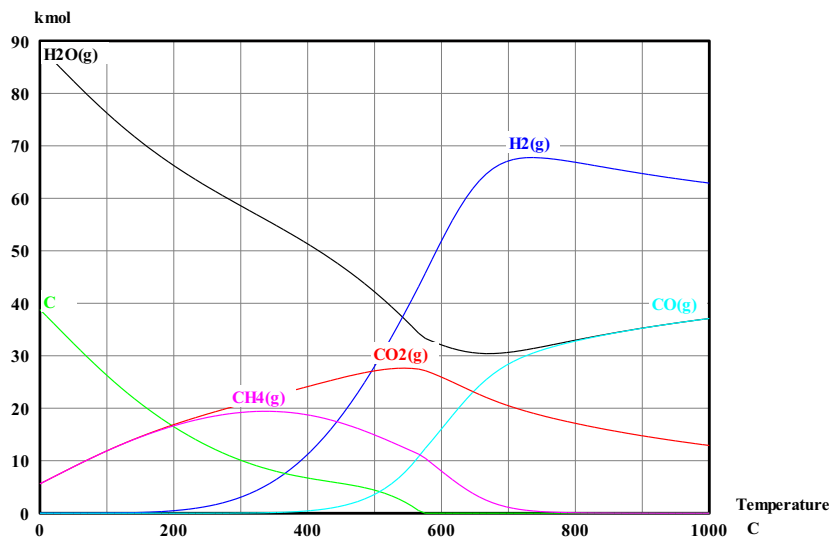
## **C. Chemical equilibria of syngas with different amounts of added steam**



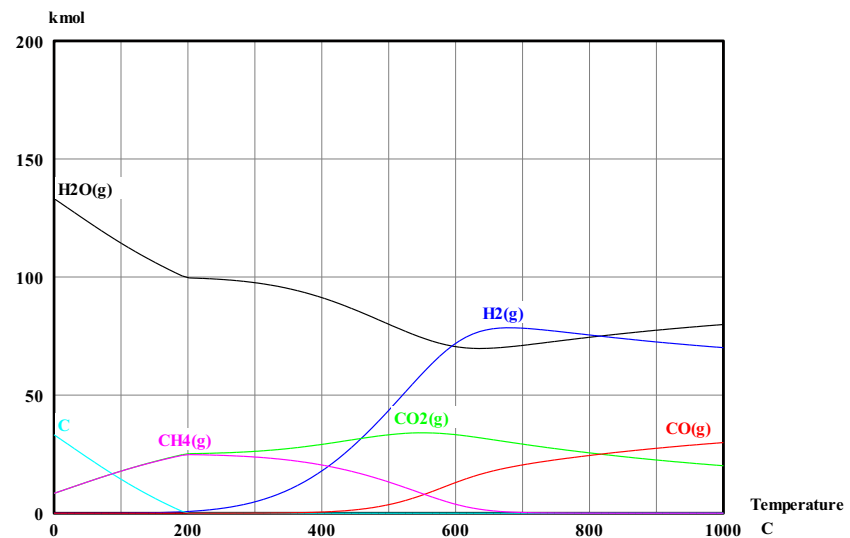
C.1: Syngas 50/50 without steam



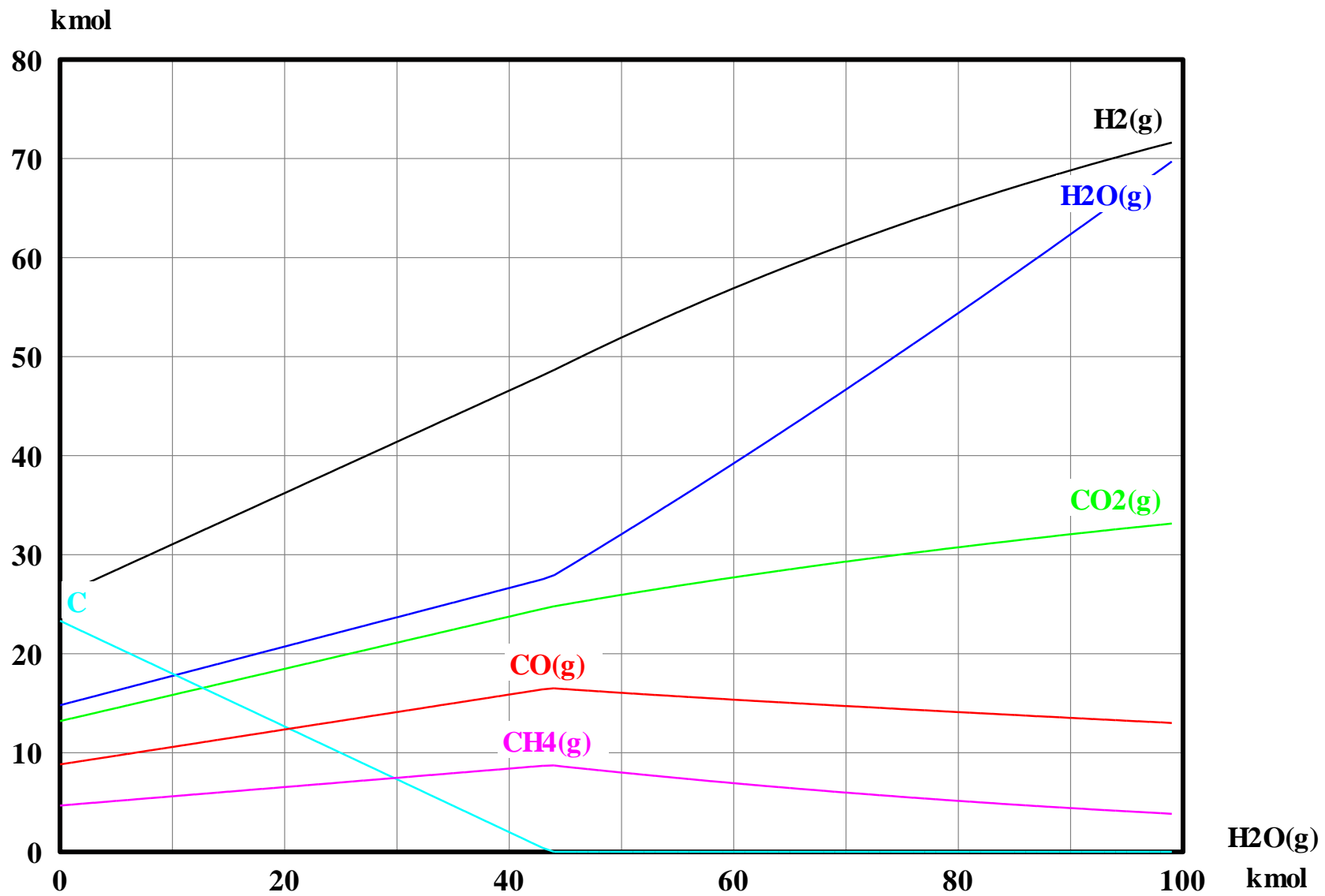
C.2: Syngas 50/50 with 20% steam



C.3: Syngas 50/50 with 33% steam



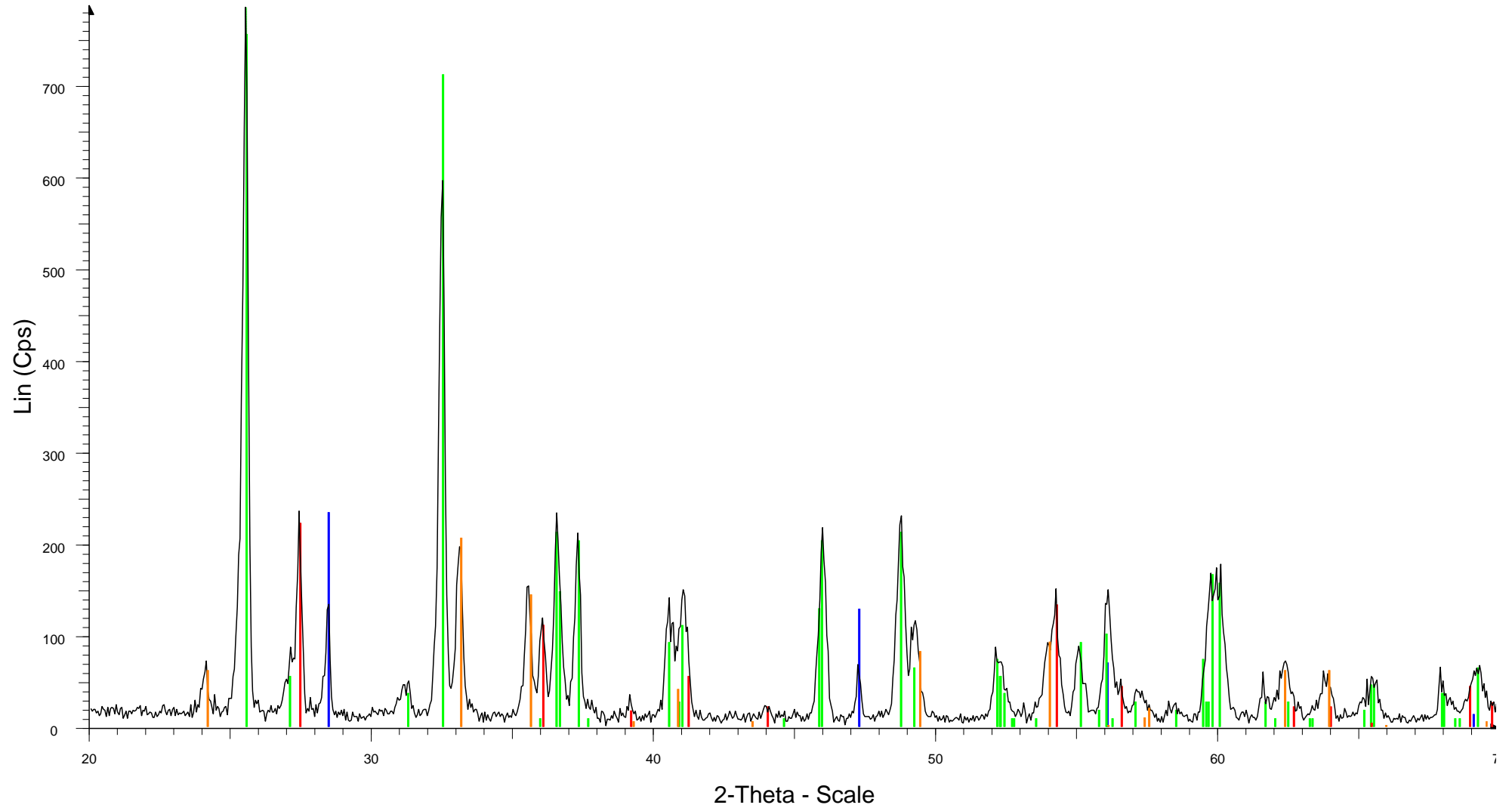
C.4: Syngas 50/50 with 50% steam



C.5: Syngas 50/50 at 600°C as function of steam addition

## D. XRD Analysis

# ilmenite30h

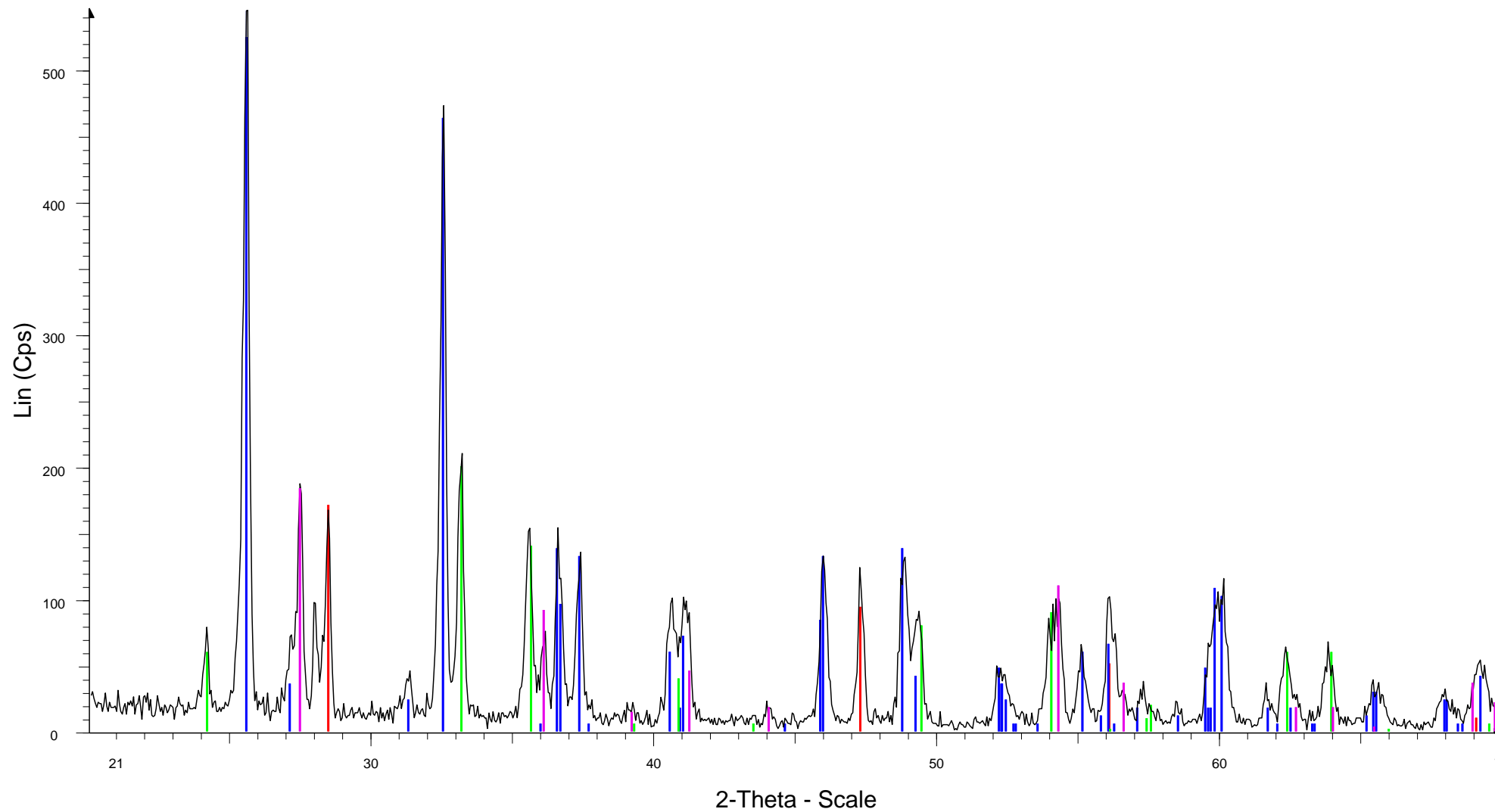


ilmenite30h - File: ilmenite30h.raw - Type: 2Th alone - Step: 0.050 ° - Step time: 1. s - Creation: 2009-06-25 13:30:19

Operations: Displacement 0.000 | Import

- 00-027-1402 (\*) - Silicon, syn - Si - Cubic -
- 00-041-1432 (\*) - Pseudobrookite, syn - Fe<sub>2</sub>TiO<sub>5</sub> - Orthorhombic -
- 00-033-0664 (\*) - Hematite, syn - Fe<sub>2</sub>O<sub>3</sub> - Rhombo.H.axes -
- 00-021-1276 (\*) - Rutile, syn - TiO<sub>2</sub> - Tetragonal -

# ilmenite80h

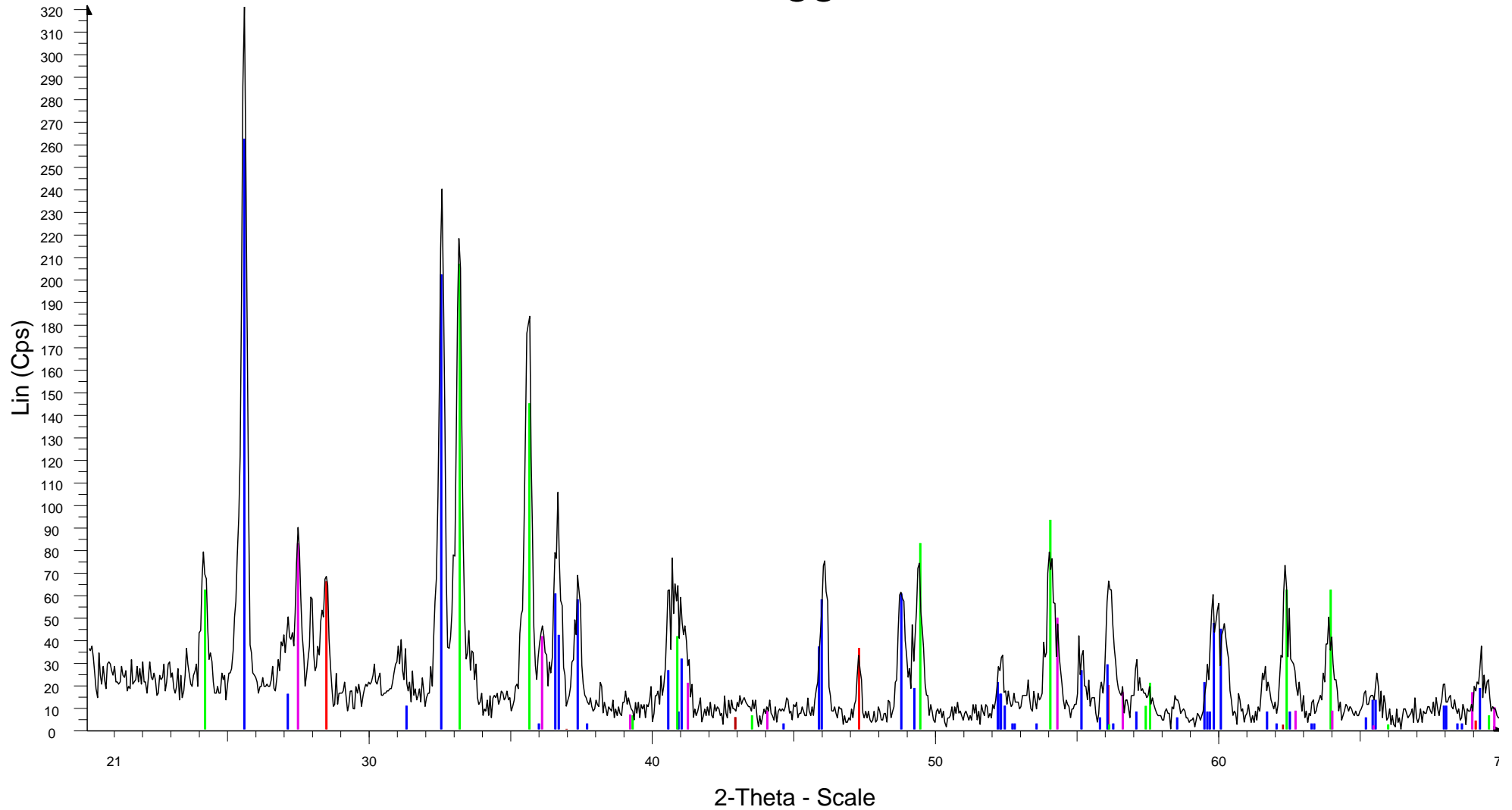


ilmenite80h - File: ilmenite80h.raw - Type: 2Th alone - Step: 0.050 ° - Step time: 1. s - Creation: 2009-06-25 14:26:25

Operations: Displacement -0.073 | Import

- 00-027-1402 (\*) - Silicon, syn - Si - Cubic -
- 00-041-1432 (\*) - Pseudobrookite, syn - Fe<sub>2</sub>TiO<sub>5</sub> - Orthorhombic -
- 00-033-0664 (\*) - Hematite, syn - Fe<sub>2</sub>O<sub>3</sub> - Rhombo.H.axes -
- 00-021-1276 (\*) - Rutile, syn - TiO<sub>2</sub> - Tetragonal -

# ilmenite\_agg\_80h

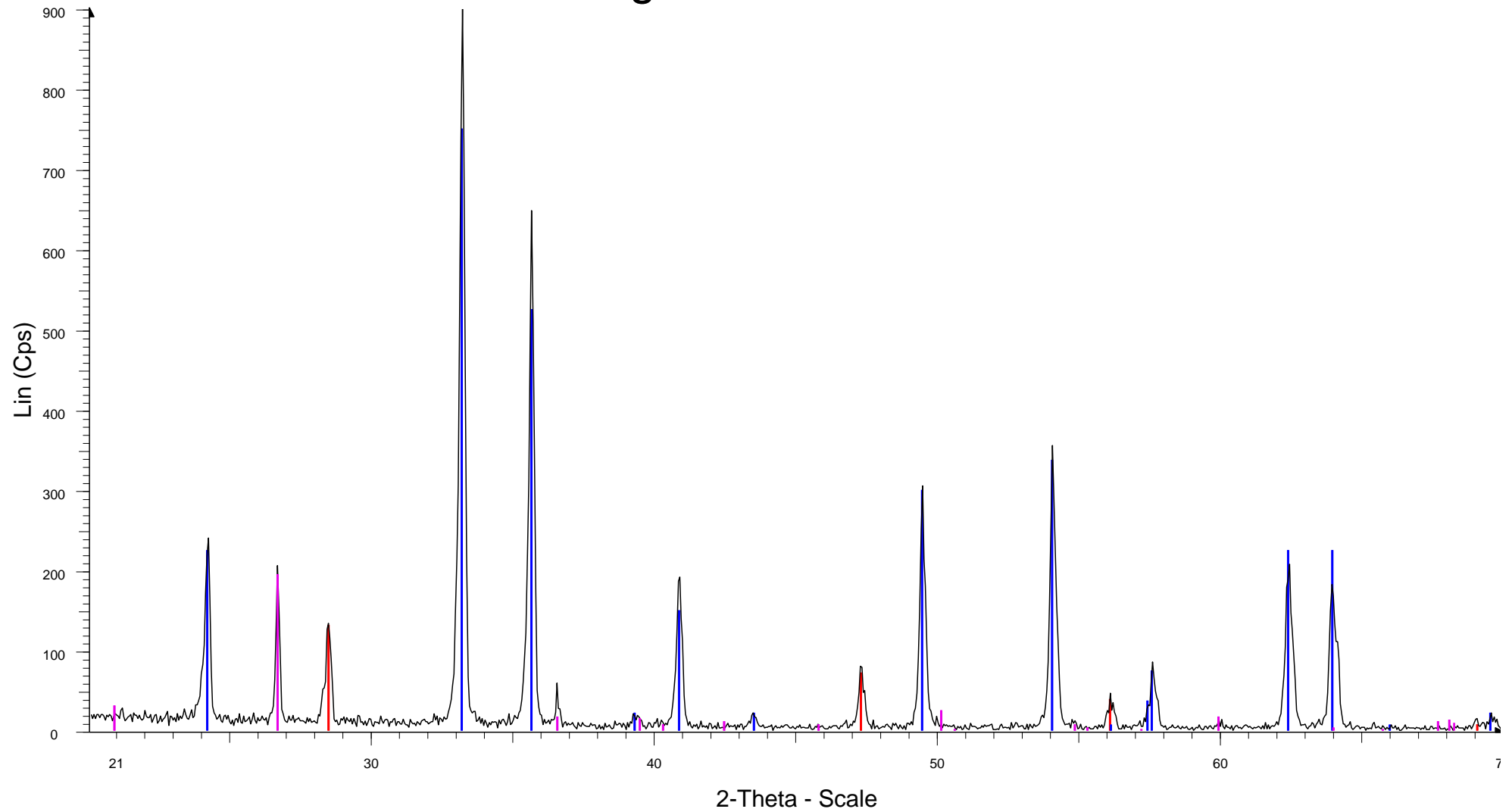


ilmenite\_agg\_80h - File: ilmenite\_agg\_80h.raw - Type: 2Th alone - Step: 0.050 ° - Step time: 1. s - Creation: 2009-06-25 13:51:13

Operations: Displacement -0.073 | Import

- 00-027-1402 (\*) - Silicon, syn - Si - Cubic -
- 00-041-1432 (\*) - Pseudobrookite, syn - Fe<sub>2</sub>TiO<sub>5</sub> - Orthorhombic -
- 00-033-0664 (\*) - Hematite, syn - Fe<sub>2</sub>O<sub>3</sub> - Rhombo.H.axes -
- 00-021-1276 (\*) - Rutile, syn - TiO<sub>2</sub> - Tetragonal -
- 00-045-0946 (\*) - Periclase, syn - MgO - Cubic -

# glödskal35h

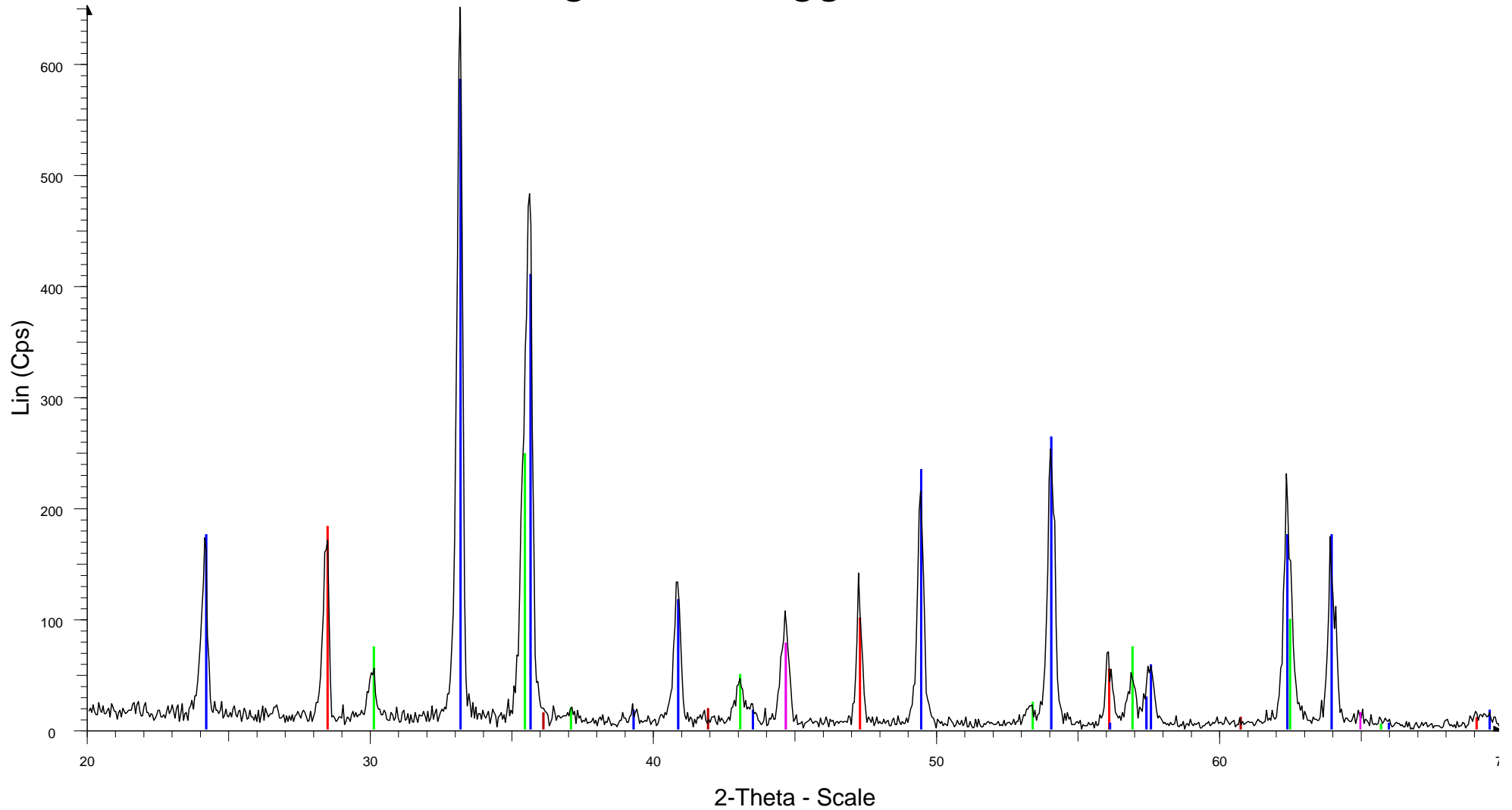


glödskal35h - File: glödskal35h.raw - Type: 2Th alone - Step: 0.050 ° - Step time: 1. s - Creation: 2009-06-25 15:15:24

Operations: Displacement -0.073 | Import

- 00-027-1402 (\*) - Silicon, syn - Si - Cubic - S-Q 7.0 %
- 00-033-0664 (\*) - Hematite, syn - Fe<sub>2</sub>O<sub>3</sub> - Rhombo.H.axes - S-Q 78.6 %
- 00-046-1045 (\*) - Quartz, syn - SiO<sub>2</sub> - Hexagonal - S-Q 14.4 %

# glödskal\_agg\_35h



glödskal\_agg\_35h - File: glödskal\_agg\_35h.raw - Type: 2Th alone - Step: 0.050 ° - Step time: 1. s - Creation: 2009-06-25 14:55:55

Operations: Import

- 00-027-1402 (\*) - Silicon, syn - Si - Cubic -
- 00-033-0664 (\*) - Hematite, syn - Fe<sub>2</sub>O<sub>3</sub> - Rhombo.H.axes -
- 00-019-0629 (\*) - Magnetite, syn - Fe<sub>3</sub>O<sub>4</sub> - Cubic -
- 00-006-0696 (\*) - Iron, syn - Fe - Cubic -
- 00-006-0615 (I) - Wustite, syn - FeO - Cubic -